

**THEORETICAL INVESTIGATION ON THE DEVELOPMENT OF
FUNCTIONAL ORGANIC MATERIALS AND APPLICATION**



RATTANAWALEE RATTANAWAN

**A THESIS SUBMITTED IN PARTIAL FULFILLMENT OF THE
REQUIREMENTS FOR THE DEGREE OF DOCTOR OF PHILOSOPHY
MAJOR IN CHEMISTRY
FACULTY OF SCIENCE
UBON RATCHATHANI UNIVERSITY
ACADEMIC YEAR 2016
COPYRIGHT OF UBON RATCHATHANI UNIVERSITY**



UBON RATCHATHANI UNIVERSITY
THESIS APPROVAL
DOCTOR OF PHILOSOPHY
MAJOR IN CHEMISTRY FACULTY OF SCIENCE

TITLE THEORETICAL INVESTIGATION ON THE DEVELOPMENT OF
FUNCTIONAL ORGANIC MATERIALS AND APPLICATION

AUTHOR MISS RATTANAWALEE RATTANAWAN

EXAMINATION COMMITTEE

DR. SUPAWADEE NAMUAGRUK	CHAIRPERSON
ASSOC.PROF.DR SIRIPORN JUNGSUTTIWONG	MEMBER
ASST.PROF.DR.CHAN INNTAM	MEMBER

ADVISOR

Siriporn Jungsutthiwong
.....
(ASSOC.PROF.DR SIRIPORN JUNGSUTTIWONG)

<i>Utith Inprasit</i> (ASSOC.PROF.DR.UTITH INPRASIT) DEAN, FACULTY OF SCIENCE	<i>A. Onggrat</i> (ASSOC.PROF.DR.ARIYAPORN ONGRAT) VICE PRESIDENT FOR ACADEMIC AFFAIRS
--	--

COPYRIGHT OF UBON RATCHATHANI UNIVERSITY
ACADEMIC YEAR 2016

ACKNOWLEDGEMENTS

I would like to express my gratitude and appreciation to Assoc.Prof.Dr. Siriporn Jungsuttiwong, my thesis advisor and Asst.Prof.Dr.Chan inntam for excellent suggestions, supervision, and understanding throughout my study. I wish to acknowledge my co-advisor Dr. Supawadee Namuangruk for constructive comments and suggestion. I would also like to thank the many people who contributed their time, instrumentation, and advice to my project. In particular, Prof.Dr. Vinich Promarak, Asst.Prof.Dr.Taweesak Sudyoadsuk and Asst.Prof.Dr.Tinnakorn keawin for the experimental data. I wish to acknowledge Thailand Graduate Institute of Science and Technology (TGIST), National science and technology development agency Thailand (NSTDA) and Ubon Ratchathani University for financial support.

I am very thankful to the Department of Chemistry and Excellent Center for Innovation in Chemistry, Faculty of Science, Ubon Ratchathani University for providing a wonderful academic environment during the course of research. I also wish to thank all the staff of the Department of Chemistry. Especially, I feel grateful to the member of in Computational and Theoretical Chemistry Ubon Ratchathani University and Center for Organic Electronic and Alternative Energy.

Finally, I truly thank to my beloved family who has provided me their love and support everything during my study.



Rattanawalee Rattanawan

Reseacher

บทคัดย่อ

เรื่อง : การศึกษาทางทฤษฎีในการพัฒนาโมเลกุลสารอินทรีย์และการประยุกต์ใช้
 ผู้วิจัย : รัตนาวลี รัตนวัน
 ชื่อปริญญา : ปรัชญาดุษฎีบัณฑิต
 สาขาวิชา : เคมี
 อาจารย์ที่ปรึกษา : รองศาสตราจารย์ ดร. ศิริพร จิงสุทธิวงษ์
 คำสำคัญ : เคนซิติฟังก์ชันแนล, สารเรืองแสงอินทรีย์, เซลล์แสงอาทิตย์ชนิดสีย้อมไวแสง

ในงานวิจัยนี้ ได้ทำการศึกษาชุดของสารเรืองซึ่งมีอนุพันธ์ของคาร์บาโซล-ไตรฟีนิลเอมีนและอนุพันธ์ของแนพทาลิไมด์เป็นโครงสร้างหลัก โดยศึกษาสมบัติทางโครงสร้าง ระดับพลังงาน การดูดกลืนแสงและการคายแสง ทำการคำนวณโดยใช้ระเบียบวิธีเคนซิติฟังก์ชันแนล (DFT) และโทม์ตีเพนเด็นต์-เคนซิติฟังก์ชันแนล (TDDFT) ที่ระดับความถูกต้อง B3LYP/6-31G(d,p) ซึ่งการคำนวณทั้งหมดใช้โปรแกรม Gaussian 09 ผลจากการคำนวณพบว่า พลังงานแถบช่องว่างที่ได้จากวิธี TDDFT มีค่าลดลง เมื่อเติมหมู่ที่มีความสามารถในการดึงอิเล็กตรอน ส่งผลให้สเปกตรัมการดูดกลืนแสงและสเปกตรัมการคายแสงเกิดการ red-shift จากการคำนวณค่าพลังงานไอออไนเซชัน (IP) แสดงให้เห็นว่าโมเลกุลเป้าหมายมีความสามารถส่งผ่านประจุบวกที่มีประสิทธิภาพ ผลจากการศึกษาพบว่าโมเลกุลเป้าหมายแสดงคุณสมบัติเป็นทั้งสารเรืองแสงและสารส่งผ่านประจุบวกซึ่งสามารถนำไปประยุกต์ใช้ในอุปกรณ์ไดโอดเรืองแสงอินทรีย์

นอกจากนั้น ผู้วิจัยได้ศึกษาสมบัติทางโครงสร้างและค่าพลังงานของโมเลกุลสีย้อมไวแสงซึ่งเป็นอนุพันธ์ของพอร์ไฟรินและคูมารินโดยใช้ระเบียบวิธีทางเคมีควอนตัม โดยใช้ระเบียบวิธีที่ระดับความถูกต้องเดียวกันกับชุดสารเรืองแสง ทำการศึกษาคำนวณโครงสร้างที่สถานะพื้น สมบัติในการส่งผ่านอิเล็กตรอนภายในโมเลกุลสีย้อมไวแสง ค่าพลังงานกระตุ้น รวมทั้งผลของหมู่ให้อิเล็กตรอน หมู่เชื่อมต่อและหมู่รับอิเล็กตรอนที่แตกต่างกัน ผลการคำนวณแสดงให้เห็นว่ามี การส่งผ่านประจุภายในโมเลกุลซึ่งสอดคล้องกับการส่งผ่านอิเล็กตรอนจากระดับพลังงาน HOMO ไปยังระดับพลังงาน LUMO นอกจากนี้ยังได้เปรียบเทียบผลที่ได้จากการคำนวณและผลที่ได้จากการทดลอง พบว่าผลที่ได้จากการคำนวณมีแนวโน้มที่สอดคล้องกับการทดลอง โดยการปรับเปลี่ยนโครงสร้างของโมเลกุลสีย้อมอินทรีย์โดยใช้หมู่เชื่อมต่อที่แตกต่างกันสามารถปรับปรุงสมบัติการกักเก็บแสงของโมเลกุลสีย้อมได้ แสดงให้เห็นว่าการคำนวณโดยระเบียบวิธี DFT และ TDDFT ทำให้ได้ข้อมูลสมบัติทางโครงสร้างและพลังงานของโมเลกุลสีย้อมไวแสงในเซลล์เพื่อนำไปใช้ในการออกแบบโมเลกุลสีย้อมชนิดใหม่เพื่อใช้ในอุปกรณ์เซลล์แสงอาทิตย์ชนิดสีย้อมไวแสงได้

ABSTRACT

TITLE : THEORETICAL INVESTIGATION ON THE DEVELOPMENT OF
FUNCTIONAL ORGANIC MATERIALS AND APPLICATION

AUTHOR : RATNAWALEE RATTANAWAN

DEGREE : DOCTOR OF PHILOSOPHY

MAJOR : CHEMISTRY

ADVISOR : ASSOC. PROF. SIRIPORN JUNGSUTTIWONG, Ph.D.

KEYWORDS : DENSITY FUNCTIONAL THEORY, ORGANIC LIGHT-
EMITTING DIODE, DYE-SENSITIZED SOLAR CELL

In this work, a series of new organic emitting materials based on carbazole-triphenylamine and naphthalimide derivative were investigated. The structural, energy level, absorption and emission properties were calculated by using density functional theory (DFT) and time-dependent density functional theory (TDDFT) method with B3LYP/6-31G(d,p) as implemented in Gaussian 09. The TDDFT calculated results revealed that the energy gaps were decreased when the strong electron withdrawing group were incorporated resulting in red-shifted of absorption and emission wavelengths. The calculated ionization potential (IP) reveals that target molecules can provided the efficient hole generating molecules. The results showed that the molecules can be used as multifunctional properties as the hole-transporting and emitting materials for application in OLEDs device.

Moreover, we have also studied the conformations, electronic and optical properties of porphyrin and coumarin dyes by using quantum chemistry with the same level of theory for the calculation of organic emitting material. The ground state structures, the intramolecular charge transfer (ICT) properties, the excitation energy were calculated. The effects of different donors, different linkers and different acceptors are included in this research. Our calculated results show that the ICT character involves primarily the promotion of an electron from the HOMOs to the LUMOs. The calculation results were compared with the experimental data. We also found that the calculation results are good agreement with experimental results. The modification of organic dye by using different linker can improve light harvesting

CONTENTS

	PAGE
ACKNOWLEDGEMENTS	I
THAI ABSTRACT	II
ENGLISH ABSTRACT	III
CONTENTS	V
LIST OF TABLES	VI
LIST OF FIGURES	VII
LIST OF ABBREVIATIONS	XI
CHAPTER 1 INTRODUCTION	
1.1 General introduction	1
1.2 Organic light-emitting diodes (OLEDs)	1
1.3 Dye sensitized solar cells (DSCs)	5
1.4 Photochemistry	9
1.5 Computation chemistry	12
1.6 Objectives	21
CHAPTER 2 LITERATURE REVIEWS	
2.1 Organic light-emitting diodes (OLEDs)	24
2.2 Dye sensitized solar cells (DSSCs)	31
CHAPTER 3 THEORETICAL INVESTIGATION OF ORGANIC COMPOUND FOR OLED APPLICATION	
3.1 Triphenylamine derivatives for OLEDs	39
3.2 Naphthimide derivatives for OLEDs	50
CHAPTER 4 THEORETICAL INVESTIGATION OF ORGANIC COMPOUND FOR DSCs APPLICATION	
4.1 Porphyrin derivatives for DSCs	58
4.2 Coumarin derivatives for DSCs	74
CHAPTER 5 CONCLUSION	87
REFERENCES	90
CURRICULUM VITAE	97

LIST OF TABLES

TABLE		PAGE
3.1	The selected important inter-ring distances (r , Å) and dihedral angle (Φ , °) of BCPA-Ar calculated by B3LYP/6-31G(d,p) calculations	42
3.2	HOMO and LUMO energies, IP and EA for BCPA-Ar with the B3LYP/6-31G (d,p) functional (in eV)	45
3.3	The absorption spectra of BCPA-Ar with the B3LYP/6-31G(d,p) functional	47
3.4	Fluorescence energies (E_{flu}) BCPA-Ar series	49
3.5	The selected important inter-ring distances (r , Å) and dihedral angle (Φ , °) of naphthlimide derivatives calculated by B3LYP/6-31G(d,p) calculations	52
3.6	HOMO and LUMO energies, IP and EA for NP, NA, NT and NTBT2A with the B3LYP/6-31G (d,p) functional (in eV)	54
3.7	The absorption spectra of naphthlimide derivatives	55
3.8	Fluorescence energies (E_{flu}) naphthlimide derivatives	56
4.1	The selected important inter-ring distances (r , Å) and dihedral angle (Φ , °) of porphyrin dye calculated by B3LYP/6-31G(d,p) calculations	61
4.2	Summarizes the Energies and Character of Frontier Orbitals of porphyrin dye Calculated by B3LYP/6-31G (d, p)	66
4.3	The excitation energies, oscillator strengths, and molecular compositions for the 2 lowest states of porphyrin by PBE0/6-31G(d,p)	69
4.4	Selected bond distances (r , Angstroms) and dihedral angles (Φ , degrees) for coumarin dyes, calculated using B3LYP/6-31G(d,p)	77
4.5	Calculated HOMO, LUMO, and HOMO-LUMO orbital energies, and energy gap (Δ_{H-L}) for coumarin dyes	79

LIST OF TABLES (CONTINUED)

TABLE		PAGE
4.6	Excitation energy, oscillator strength, and molecular composition for various electronic coumarin dye transition states by TDCAM-B3LYP/6-31G(d,p) (C-PCM model)	83
4.7	Selected bond lengths (Å) and adsorption energies (kcal/mol) of coumarin complexes calculated using Dmol ³	84

LIST OF FIGURES

FIGURE		PAGE
1.1	Schematic overview of organic light emitting diodes	2
1.2	Schematic single-layer OLED	3
1.3	Schematic multi-layer OLED	5
1.4	Simple energy level diagram for DSCs	7
1.5	The Jablonski Diagram	9
1.6	Franck-Condon energy level diagram	11
1.7	Structure of carbazole target molecule	22
1.8	Structure of naphthalimide target molecule	22
1.9	Structure of Porphyrin target molecule	23
2.0	Structure of coumarin dye target molecule	23
2.1	The chemical structure of TPA-Cz compound	24
2.2	The chemical structure of carbazole derivatives	25
2.3	The molecular structure of TPA-BZP and CzP-BZP emitters	26
2.4	A series of bis(3,6-di-tert-butylcarbazol-9-ylphenyl)aniline end-capped oligoarylenes	26
2.5	The molecular structure of 1,8-naphthalimide derivatives	27
2.6	A series of N-butyl-1,8-naphthalimide derivatives	28
2.7	A series of D- π -A star-shaped small molecules with 1,8-naphthalimide	29
2.8	Molecular structures of NIM, Nap1, Nap2 and Nap3	30
2.9	A series of D-A naphthalimide-substituted fluorene derivatives	30
2.10	A series of porphyrin dyes with an electron-donating group (EDG)	31
2.11	A series of zinc porphyrin dyes YD22–YD28	32
2.12	Chemical structures of ID7-ID9 and reference dye	33
2.13	Structures of the phenothiazine-modified porphyrin dyes	34
2.14	The designing of novel D- π -A porphyrins	35
2.15	The molecular design of coumarin dyes	36

LIST OF FIGURES (CONTINUED)

FIGURE		PAGE
3.11	Emission spectra of BCTA by TDCAM-B3LYP/6-31G(d,p) level in CH ₂ Cl ₂ solvent (C-PCM model)	58
4.1	Sketch map of porphyrin derivatives	60
4.2	Optimized structures and HOMO (left) LUMO (middle) of porphyrin target molecule	62
4.3	Molecular orbital energy diagram of porphyrin target molecule	65
4.4	Frontier molecular orbital of porphyrin target molecule	67
4.5	Absorption spectra of porphyrin target molecule	70
4.6	The distance between the edge of the porphyrin core and the surface	72
4.7	Frontier molecular orbital of porphyrin dye adsorbed on TiO ₂ in gas phase calculated by CAM-B3LYP/6-31G(d,p) on Dmol ₃ geometry	73
4.8	Structures of the D- π -A, D-A- π -A, and D- π -A- π -A dyes	75
4.9	Optimized structures of the D- π -A, D-A- π -A, and D- π -A- π -A dyes	78
4.8	Frontier molecular orbitals for (a) D- π -A and (b) D-A- π -A, calculated using CAM-B3LYP/6-31G(d,p)	79
4.10	HOMO and LUMO of D- π -A and D-A- π -A calculated using B3LYP/6-31G(d,p)	80
4.11	Calculated absorption spectra of D- π -A and D-A- π -A, calculated using TDCAM-B3LYP/6-31G(d,p)	81
4.11	Frontier molecular orbitals for NKX-2510@TiO ₂ and NCTBTA@TiO ₂ in the gas phase, calculated by CAM-B3LYP/6-31G(d,p) using Dmol ³	86

LIST OF ABBREVIATIONS

ABBREVIATIONS	FULL WORD
Å	Augstrom
λ_{abs}	Absorption wavelength
λ_{em}	Emission wavelength
B3LYP	Becke's three parameter hybrid functional and Lee-Yang-Parr gradient-corrected correlation functional
r	Bond distance
CAM-B3LYP	Coulomb-attenuating method of B3LYP
CB	Conduction band
CPCM	Conductor-like Polarizable Continuum Model
DSCs	Dye-sensitized solar cells
D-A	Donor-acceptor
D- π -A	Donor- π -acceptor
D-A- π -A	Donor-acceptor- π -acceptor
D- π -A- π -A	Donor- π -acceptor- π -acceptor
DFT	Density functional theory
°	Degree of angle
Φ	Dihedral angle
DFT	Density functional theory
E_{g}	Lowest excitation energy
$\Delta_{\text{H-L}}$	HOMO-LUMO gap
GGA	Generalized Gradient Approximation
HF	Hartree Fock
HOMO	Highest occupied molecular orbital
LUMO	Lowest unoccupied molecular orbital
I/I_3^-	Iodide / triiodide redox couple

LIST OF ABBREVIATIONS (CONTINUED)

ABBREVIATIONS	FULL WORD
J_{sc}	The photocurrent density measured at short circuit
KS	Kohn sham
LDA	Local Density Approximation
LHE	Light harvesting efficiency
nm	Nanometer
OLEDs	Organic Light Emitting Diodes
PCM	Polarizable continuum model
Ru	Ruthenium
STO	Slater type orbital
TDDFT	Time dependent density functional theory
TiO ₂	Titanium dioxide
V_{oc}	The open circuit photo-voltage
η	Conversion efficiency
Ψ	Wave function
E	Energy
\hat{H}	Hamiltonian operator
ρ	Electron density
f	Oscillator strengths

CHAPTER 1

INTRODUCTION

1.1 General introduction

Organic electronic materials have received great attention over the past two decades due to their optical and electronic properties which can serve as organics semiconductor in optoelectronics applications such as sensor, light-emitting diodes, solar cells and many others. Interestingly, the electroluminescence properties in organic materials allow their being used in organic light emitting diodes (OLEDs). Furthermore the conjugated molecules are employed for converting sunlight to electric in dye sensitized solar cells (DSCs). The electronics properties can be modified by the degree of conjugation of the individual systems in the organic molecule, which opens various possibilities for improving the performance of organic electronic materials. The molecular structure, the electronics properties and the optoelectronic properties should be modify for suitable properties in optoelectronics device.

1.2 Organic light-emitting diodes (OLEDs)

The research in OLEDs has become one of the most interesting topics because of their potential utilization in display technologies. The structural arrangement of an OLED, first proposed by Tang and Van Slyke, consists of three layers: a hole-transporting layer (HTL), an emissive layer (EL) and an electron-transporting layer (ETL) which is essentially organic sandwiched between two electrodes usually with indium tin-oxide (ITO) serving as an anode and a low work function metal or alloy as a cathode. OLEDs exhibit many attractive features as OLED displays [1]. Compared to LCDs, today's dominant flat panel display technology, OLEDs are capable for providing better performance features

Other than thinner, lighter and more attractive, OLEDs offer much faster response times, wider viewing angles, higher contrast ratios and brighter, more saturated colors for a more enjoyable viewing experience. The OLEDs products have provided variety electronics applications during the period. In order to generate the material with high light emitting efficiencies, high thermal stability, and good amorphous film formation property, highly efficient red, green and blue (RGB) emitting materials are required. A schematic shown in Figure 1.1 is an organic light emitting diodes. The OLEDs structure is including an emitting layer between an anode and a cathode. Holes and electrons are injected from the anode and cathode, respectively [2, 3]. The device performance of OLEDs depends on the charge balance of the injected holes and electrons as well as the exciton limitation in a device. The holes and electrons meet in the emissive layer in equal quantities need to control the excitons (electron and hole pairs) that is the key point to operate OLEDs. Usually, the structure includes charge transport layer, an ETL and/or a HTL, which are favorable for injection holes from the anode to emissive layer. The ETL is used to inject electrons from the cathode to the emitting layer (EML). Thus, the efficient OLEDs can be achieved by the balancing of electron hole pairs for generate the exciton in the devices.

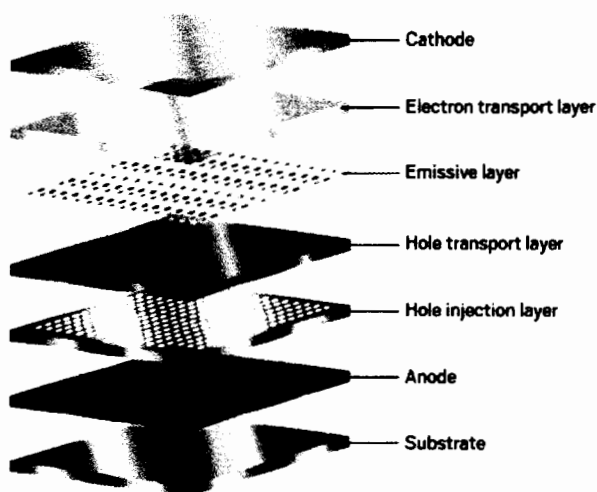


Figure 1.1 Schematic overview of organic light emitting diodes

1.2.1 Typical structure of OLEDs

The typical structure of OLEDs consists of single or multiple layers of organic thin films sandwiched normally between the transparent indium tin oxide (ITO) coated glass and vacuum-evaporated metals with low work function such as magnesium/ silver (Mg/Ag) or aluminum (Al).

1.2.1.1 Single layer devices

The single-layer OLEDs consists of a thin film of an organic electroluminescent material sandwiched between two conducting electrodes upon a substrate shown in Figure 1.2. A high work-function material is used as the anode while the cathode is usually made from Al. The transparent material ITO is chosen as the anode. When the current is applied across the device, electrons are injected into the light emitting material near to the cathode to form radical anions. Material near the anode is oxidized, giving radical cations, this is the hole was generated. These charges move across the device under the applied electric field where they recombine forming an exciton. The exciton is formed either as a singlet or a triplet spin state, the singlet being the same as the singlet excited state involved in photoluminescence. The radiative transition process of singlet excitons from the singlet excited state (S1 state) to the ground state (S0 state) can be utilized for emitting light. The efficiency of the device is reduced by a non-radiative pathway due to the resultant heating may cause breakdown of the device and reduce its working lifetime.

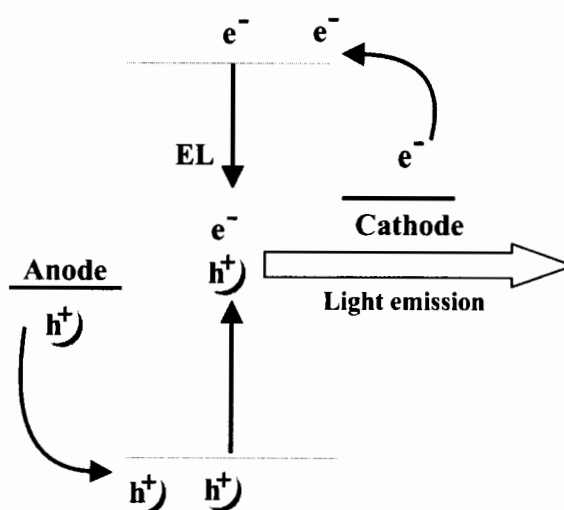


Figure 1.2 Schematic single-layer OLED

1.2.1.2 Multi-layer devices

The engineering of OLED is important factor for efficient injection and transport of charge carriers and the design of the electron-hole balance in OLED devices. The introduction charge transport materials in addition to the emitter layer that can provide the efficient way to controlling charge injection, transport, and recombination in OLEDs. For organic electroluminescent materials, HTL act as the transporting holes and blocking electrons, thus preventing electrons from reaching the opposite electrode without recombining with holes. Moreover, the hole injection layer HIL material is incorporate which reduces the energy barrier between anode/hole HTL as shown in Figure 1.3. Thus, power efficiency of the device is improved due to enhancing charge injection at the interfaces [4]. One of the widely used polymers for promoting the hole injection is poly (3,4-ethylenedioxythiophene)-poly (styrene) known as the PEDOT:PSS which has been found to be useful in a hybrid. In order to achieve high power efficiency (PE) in OLEDs, effective and balanced charge injection and transport is necessary. HTL and ETL layers are commonly used to improve the charge injection from anode and cathode, respectively. Many ETL/HTL materials designed for the thermal evaporation process are also solution process. However, since these materials and EML materials have similar solubility in common organic solvents used for solution processing, such as chlorobenzene or p-xylene, the interface mixing/erosion becomes a severe problem. Therefore, the fabrication of well define multilayer OLED devices through solution processing is a key challenge. Currently there are two ways to address this problem: the first one is to develop cross-linkable materials, making the already processed cross-linked layer invulnerable to solvent erosion from the new layer. The second way is to develop water/alcohol soluble materials, so that adjacent layers can be processed by orthogonal solvents, thus eliminating the interface mixing problem. In the single-layer OLED, one base material is designed for multiple roles in the device and, with a phosphorescent emitter, can achieve nearly quantitative electro-optical conversion for the luminescence.

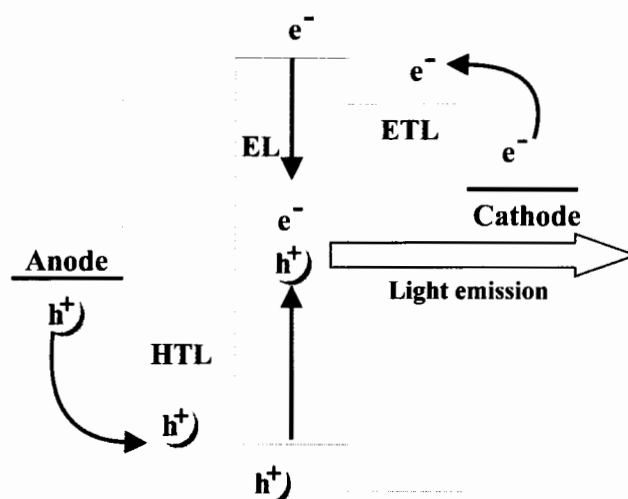


Figure 1.3 Schematic multi-layer OLED

1.3 Dye sensitized solar cells (DSCs)

The development of DSCs have been employed as an alternative to the silicon solar cell because of their advantages such as high power conversion efficiency, environmentally friendly photovoltaic device and inexpensive. The noble metal complex photo-sensitizers, **N3** and **N719** compounds, have power conversion efficiency about 10% on average [5]. However, the limitation of Ruthenium complex dyes is a rare and expensive metal which are not suitable for the DSCs application of these complexes. Recently, the synthetic porphyrins have attracted much interest as novel sensitizer in DSCs due to their efficient harvesting sun light and tunable the photophysical properties via optimizing the β -or *meso*-substituents of the porphyrin core. The high performance of porphyrin-based sensitizer is a zinc porphyrin sensitizer, namely **GY50** using a cobalt-based electrolyte shows an overall conversion efficiency of 12.75% under standard AM 1.5 one-sun irradiation [6]. The typical DSCs consists of three main components: (i) organic sensitizer coating with wide band gap semiconductor which is placed in contact with a redox electrolyte, the material of choice has been TiO_2 (anatase) although alternative wide band gap oxides such as ZnO have also been investigated, (ii) an electrolyte solution containing redox couple such as iodide/tri-iodide (I^-/I_3^-), the regeneration of the sensitizer by iodide intercepts the recapture of the conduction band electron by the oxidized dye and (iii) a counter electrode which is a platinized conductive glass substrate. The iodide is regenerated by

the reduction of I_3^- at the counter-electrode the circuit being completed via electron migration through the external load. The voltage generated under illumination corresponds to the difference between the Fermi level of the electron in the solid and the redox potential of the electrolyte. Overall the device generates electric power from light without suffering any permanent chemical transformation. As show in Figure 1.4, The DSCs process is initiated by dye absorb photons, which excites the dye molecule from the ground stated to the excited state, and the resultant excited dye molecule injects an electron to the conduction band (CB) of TiO_2 . The resultant oxidized dye molecule is quickly reduced to its original state by I^- ions in the electrolyte. While, I^- is oxidized to its oxidized form, I_3^- , and the latter is reduced back to I^- through accepting electrons at the counter electrode, and thus the electric circuit is completed by diffusion of I^- and I_3^- from and to the counter electrode, respectively. The power conversion efficiency can be increased by improving the photophysical properties for highly efficient dye. The modification of sensitizer must be designed to absorb most of the radiation of sun light invisible to near-IR region to generate a large photocurrent response. Moreover, the energy level of HOMO and LUMO orbital of the dye are required to match with potential of electrolyte system and conduction band edge level of the TiO_2 semiconductor respectively. These organic compounds based on electron donor, π -conjugated and acceptor (D- π -A) system have been found to possess photo induced intramolecular charge transfer (ICT) properties. Currently, molecular modeling techniques and especially quantum chemistry offer a competitive alternative for the interpretation of the experimental data. The theoretical investigations of the physical properties of dye sensitizers can provide the detail of the structural and the electronic properties which is benefit to develop the novel organic sensitizers with high efficient.

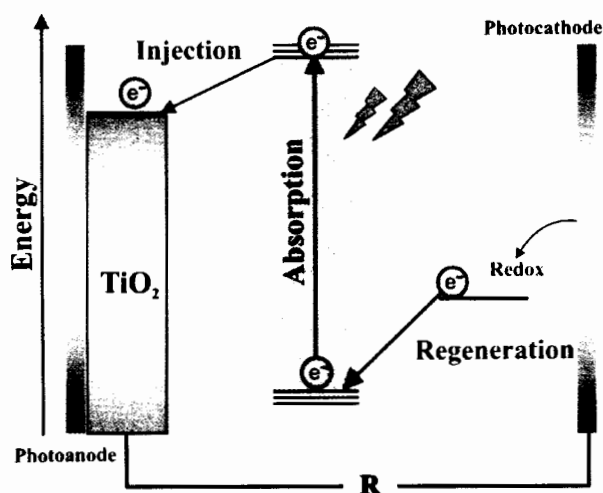


Figure 1.4 Typical of dye sensitized solar cells

1.3.1 Ruthenium complex

The sensitizer is one of the key components in achieving high efficiency and durability of DSCs devices. The extensively used charge-transfer sensitizers employed so far in such cells are ruthenium complex producing solar energy-to-electricity conversion efficiencies of 11%. Although, Ruthenium complexes have shown very good efficiency, there are certain limitations in the practical application of these complexes for DSCs. The first problem is the rarity of the ruthenium metal as a result, it is very expensive. Secondly, these complexes have a lack of absorption in the red region of the visible spectrum and also relatively low molar extinction coefficients. The third drawback is that the metal complex-based sensitizers involve careful synthesis and tricky purification steps. A new class of compounds such as metal-free organic dye was developed. Organic sensitizer is indeed possible to tune the absorption and electrochemical properties in a desired manner through suitable molecular design strategies. More interestingly, the high molar extinction coefficient of these metal-free sensitizers is particularly attractive because they enhance the conversion efficiency.

1.3.2 Metal-free organic sensitizer

The ideal of sensitizer for DSCs converting standard global A.M 1.5 sunlight to electricity should absorb all light below a wavelength of about 920 nm. In addition, it must also carry attachment groups such as carboxylate to the

semiconductor oxide surface. The energy level of the excited state should be well matched to the lower bound of the conduction band of the oxide to minimize energetic losses during the electron transfer reaction. Its redox potential should be sufficiently positive that it can be regenerated via electron donation from the redox electrolyte. Thereafter, much effort has been put in to improve the power conversion efficiency. Moreover, it did not take much time for the scientific community to prove the DSCs are alternatives to the conventional first- and second-generation silicon solar cells. In fact, the DSCs technology works well, even in diffused light conditions, unlike the first and second-generation photovoltaic devices. The D- π -A system is the basic structure for designing the metal-free dyes due to the effective photo induced ICT properties. Most of the organic sensitizers applied in DSCs have three important parts: the electron donor, the electron acceptor and the linker units for the π -conjugation to enhance the molar absorption coefficient. Thus, it is interesting to study the influence of the electron donor, the electron acceptor, and the linker separately in metal-free dyes with a general structure D- π -A.

1.3.3 Porphyrin sensitizer

The novel sensitizer, push-pull Zinc porphyrin system, has considerable attention because of their light harvesting ability which can enhance the power conversion efficiency of DSCs. The push-pull porphyrin dyes were designed and sensitized with containing a strongly electron-donating triphenylamine moiety as the electron donor. With the employing strong electron donating group, the light-harvesting properties of porphyrin dye possess better in terms of significantly red-shifted and high intensity of Q-band absorption. The conversion efficiencies for push-pull porphyrin dyes are reaching to 9-10% owing to large J_{SC} . Additionally, the porphyrin sensitizers functionalized with various π -spacers were developing to enhanced charge transfer character from the porphyrin ring to the anchoring group. The push-pull porphyrin with the strong electron withdrawing moiety can be adsorbed on the TiO₂ surface with the strong electronic coupling and would be more favorable for electron injection into the TiO₂ surface. The presence of strong donating and strong withdrawing for D- π -A structure was reported with efficiency of 10%. Therefore, the effect of spacer length and anchoring significantly to improve the efficiency

in push-pull ability of porphyrin dye, which are very useful to make efficient future development DSCs.

1.4 Photochemistry

Photochemistry is the study of chemical reaction that proceeds with the absorption of light by atom or molecule. Chemical reactions occur when a molecule is provided the activation energy. In case of photochemical reactions light provides the activation energy. Simplistically, light is one mechanism for providing the activation energy that required for many reactions. The absorption of a photon of light by a reactant molecule may also permit a reaction to occur not just by bringing the molecule to the necessary activation energy, but also by changing the symmetry of the molecule's electronic configuration, enabling an otherwise inaccessible reaction path. Photochemical reactions involve electronic reorganization initiated by electromagnetic radiation. The reactions are several orders of magnitude faster than thermal reactions; reactions as fast as 10^{-9} seconds and associated processes as fast as 10^{-15} seconds are often observed. The ease of electronic transition from the ground to a higher excited state dictates whether the observed wavelength is in the ultraviolet (UV) or visible (VIS) region. The UV and VIS spectra offer valuable information for identifying compounds, especially by the use of their emission. The photoabsorption properties of a D- π -A dye are associated with ICT excitation from the donor to the acceptor moiety of the dye, resulting in efficient electron transfer through the acceptor moiety from the excited dye into the semiconductor CB.

1.4.1 The Jablonski Diagram

The energy gained by a molecule when it absorbs a photon causes an electron to be promoted to a higher electronic energy level. As show in Figure 1.5 illustrate, the principal photophysical radiative and non-radiative processes displayed by organic molecules in solution. The horizontal lines represent the vibrational levels of each electronic state. Straight arrows indicate radiative transitions, and curly arrows indicate non -radiative transitions. The boxes detail the electronic spins in each orbital, with electrons shown as up and down arrows, to distinguish their spin. Note that all transitions from one electronic state to another originate from the lowest vibrational level of the initial electronic state. For example, fluorescence occurs only from S_1 ,

because the higher singlet states (S_2 , etc.) decay so rapidly by internal conversion that fluorescence from these states cannot compete.

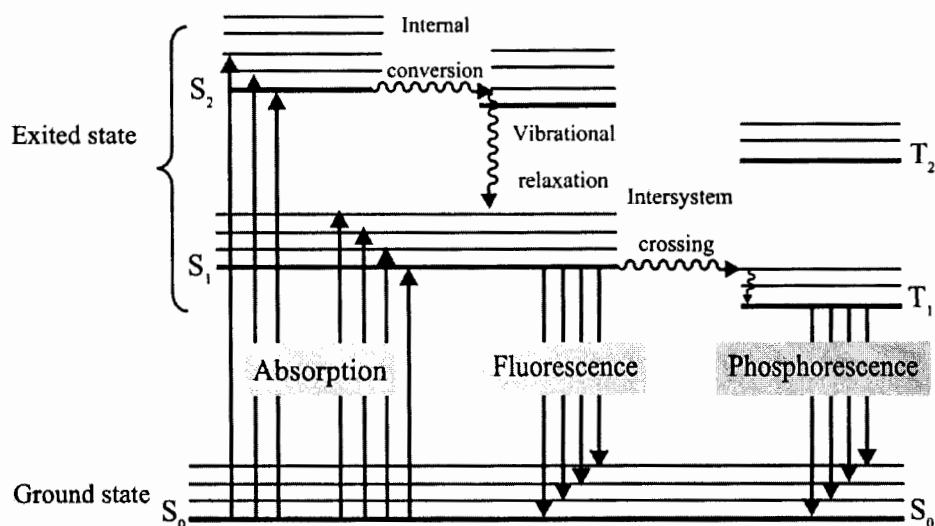


Figure 1.5 The Jablonski Diagram

1.4.2 Electronically Excited States

The absorption of a UV or visible photon by a molecule produces an electronically excited state. Electron excitation is the movement of an electron to a higher energy state. This can either be done by photoexcitation (PE), where the original electron absorbs the photon and gains all the photon's energy or by electrical excitation (EE), where the original electron absorbs the energy of another, energetic electron. Within a semiconductor crystal lattice, thermal excitation is a process where lattice vibrations provide enough energy to move electrons to a higher energy band. When an excited electron falls back to a lower energy state again, it is called electron relaxation. This can be done by radiation of a photon or giving the energy to a third spectator particle as well. In physics there is a specific technical definition for energy level which is often associated with an atom being excited to an excited state. The excited state, in general, is in relation to the ground state, where the excited state is at a higher energy level than the ground state.

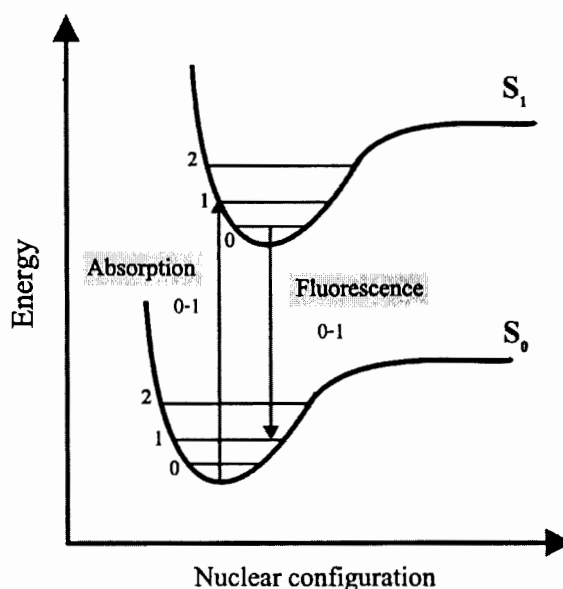


Figure 1.6 Franck-Condon energy level diagram

One way to view the properties of molecular excited states is shown by the potential energy diagram in Figure 1.6. This diagram, known as a *Franck-Condon* energy level diagram, shows potential energy curves for S_0 state and S_1 singlet state of an organic molecule as a function of nuclear configuration. These curves are sometimes referred to as potential energy wells, because of their shape. The horizontal lines within each curve represent the vibrational levels of each electronic state. The lowest vibrational state for each energy level is designated as 0, and the levels above it are successively 1, 2, etc. The band assignments in brackets (*e.g.*, (0, 1)) indicate, respectively, the vibrational level of the initial state, and of the final state involved in a transition. The horizontal axis is the nuclear configuration, which can be thought of as the distance between nuclei. When considering two atoms bonded to each other, the bottom of the well corresponds to the equilibrium bond length. Because excitation involves the movement of charge density into an antibonding orbital, the equilibrium bond length in S_1 is generally longer than in S_0 . This is illustrated in Figure 1.6 by the displacement of the S_1 well to the right of the S_0 well. The absorption of light takes place on a much faster time scale ($\sim 10^{-15}$ s) hence the initially formed excited state must have the same nuclear configuration as the ground state. This transition is called the vertical or Franck-Condon transition, and results in the molecule having excess

vibrational energy. The excess vibrational energy can be dissipated through the process of vibrational relaxation, i.e., the process of internal conversion, which returns the molecule to the lowest vibrational level of S_1 . Fluorescence usually occurs from the lowest vibrational level of S_1 . Because these transitions occur at lower energies than absorption, fluorescence is observed at longer wavelengths than absorption (i.e., lower energy).

1.5 Computation chemistry

Nowadays, the computational chemistry has reached a consensus on a relatively well-defined range of computational methods suitable for studying electronic and optical properties of dyes used in DSCs. For this reason, calculations by different groups are often comparable in terms of accuracy and expected discrepancy from experiment. In practice, geometry optimization is performed using Density Functional Theory (DFT) and Time-Dependent Density Functional Theory (TDDFT) is used to describe the excited states and optical properties of the optimized molecules [7].

1.5.1 The Hartree-Fock Theory

The quantum chemical methods are based on finding solution to the Schrodinger wave equation on molecular orbital theory.

$$H\Psi = E\Psi \quad (1.1)$$

Where H is Hamiltonian operator which gives the kinetic and potential energies of the system. The Hamiltonian operator for many electrons system is

$$\hat{H} = -\sum_{i=1}^n \frac{1}{2} \nabla_i^2 - \sum_{A=1}^K \frac{1}{2M_A} \nabla_A^2 - \sum_{i=1}^n \sum_{A=1}^K \frac{Z_A}{r_{iA}} + \sum_{i=1}^n \sum_{j < i} \frac{Z_A}{r_{ij}} + \sum_{A=1}^K \sum_{B < A} \frac{Z_A Z_B}{R_{AB}} \quad (1.2)$$

The first and second term represent the kinetic energies of electron and nucleus, respectively. The third term is the electron-nucleus attraction. The fourth term corresponds to the electron-electron repulsion and the fifth the nuclear-nuclear repulsion.

The Born-Oppenheimer Approximation is central to quantum chemistry. Since nuclei are much heavier than the electron one can treat electrons as if they are moving in the field of fixed nuclei. With this approximation the five terms in Equation 1.2 can be reduced to three and the Schrodinger equation for nuclei and electron can be solved separately.

$$\hat{H} = -\sum_{i=1}^n \frac{1}{2} \nabla_i^2 - \sum_{i=1}^n \sum_{A=1}^K \frac{Z_A}{r_{iA}} + \sum_{i=1}^n \sum_{j<i}^n \frac{Z_A}{r_{ij}} \quad (1.3)$$

Within this approximation, the kinetic energy of the nuclei can be neglected to be constant. The remaining terms are called the electronic Hamiltonian describing the motion of N electrons in the field of M point charge.

$$\hat{H}_{elec} \psi_{elec} = E_{elec} \psi_{elec} \quad (1.4)$$

In the Hartree Approximation the n-electron wavefunction Ψ^{HP} is simply written as a product of one-electron wavefunctions ϕ_1 .

$$\psi^{HP}(x_1, x_2, \dots, x_n) = \phi_1(x_1) \phi_2(x_2) \dots \phi_n(x_n) \quad (1.5)$$

Such a many – electrons wavefunction is termed a Hartree product, with electron being described by the orbital ϕ_1 , electron –two being described by the orbital, ϕ_2 ect. Using the Hartree product, the energy is just the sum of orbital energies.

Hartree product Ψ^{HP} does not satisfy the asymmetry principle. That is the inter change of two electron coordinates dose not lead to change in sign of the wave function, in the Hartree-Fock theory the wavefunction is given by the slater determinants of N spin-orbital. A short hand notation for slater determinant is written using only the diagonal element.

$$\psi(x_1, x_2 \dots x_n) \equiv |\phi_1(x_1) \phi_2(x_2) \dots \phi_n(x_n)\rangle \quad (1.6)$$

By using Slater determinant the Pauli Exclusion Principle is automatically satisfied from the most important property of determinate, namely the determinant is zero if two rows or two columns of the determinant are exactly the same. In the other words, no two electrons are allowed to occupy the same spin orbital since this will lead to zero value of the wave function.

The Hartree-Fock method seeks to approximately solve the electronic Schrodinger equation and it assumes that the wavefunction can be approximated by a single Slater determinant made up of one spin orbital per electron. Since the energy expression is symmetric, the variational theorem holds, and so we know that the Slater determinant with the lowest energy is as close as we can get to the true wavefunction for the assumed functional form of a single Slater determinant.

$$\langle \tilde{\phi} | \hat{H} | \tilde{\phi} \rangle \geq E_0 \quad (1.7)$$

The equality holds only when $|\tilde{\phi}\rangle$ is identical to the exact wavefunction $|\phi\rangle$. The problem of minimizing a function subject to a constraint of normalization is solved by Lagrange's method of undetermined multipliers. According to the variational principle, the orbitals are those which minimize the electronic energy E , which is defined by

$$\begin{aligned} E &= \langle \psi | \hat{H} | \psi \rangle \\ &= \sum_a^N \langle \psi | \hat{H} | \psi \rangle + \frac{1}{2} \sum_{a,b}^N (\langle ab | ab \rangle - \langle ab | ba \rangle) \\ &= \sum_a^N h_{aa} + \frac{1}{2} (J_{ab} - K_{ab}) \end{aligned} \quad (1.8)$$

Where h_{aa} is a core Hamiltonian for an electron, describing its kinetic energy and potential energy in the field of the nuclei and J_{ab} and K_{ab} is the coulombic energy and exchange energy, respectively. By a linear variational method, the orbitals can be

systematically varied with the constraint that they remain orthonormal unit the energy E_0 is a minimum.

For a given single determinant $|\psi\rangle \equiv |\phi_1\phi_2 \dots \phi_a\phi_b \dots \phi_n\rangle$ the energy is a function of the orbital $\{\phi_i\}$. We need to minimized E with respect to the orbital, subject to the constants that the orbitals remain orthonormal,

$$\int dx(1)\phi_a^*(1)\phi_b(1) = \langle \phi_a | \phi_b \rangle = \delta_{ab} \quad (1.9)$$

The Coulomb operator, corresponding to the classical electronic interaction, is defined by

$$\hat{J}_{ab}(1)\phi_a(1) = \left[\int dx_2\phi_b^*(2)r_{12}^{-1}\phi_b(2) \right] \phi_a(1) \quad (1.10)$$

And the non-local potential operator describing the exchange term interaction, is

$$\hat{K}_{ab}(1)\phi_a(1) = \left[\int dx_2\phi_b^*(2)r_{12}^{-1}\phi_b(2) \right] \phi_b(1) \quad (1.11)$$

The Fock equation can be written in a short form of

$$\hat{F}|\phi_a\rangle = \sum_{b=1}^N \epsilon_{ab} |\phi_b\rangle \quad (1.12)$$

The Fock operator, \hat{F} , is an effective one electron operator, describing the kinetic energy of an electron, the attraction of all the nuclei and the repulsion of all the outer electrons (via \hat{J} and \hat{K}) called the Fock operator, of the form

$$\hat{F}(1) = \hat{h}(1) + \sum_{b=1}^N \hat{J}_b(1) - \hat{K}_{ab}(1) \quad (1.13)$$

Since the Fock operator has function dependence, through the Coulomb and exchange operators, on the solution of $\{\phi_i\}$. The pseudo-eigenvalue equation, thus the Hartree-Fock equations are really nonlinear equations and will need to be solved by iterative procedures.

1.5.2 Density functional theory

The DFT methods ultimately derive from quantum mechanics research from the 1920's, especially the Thomas-Fermi-Dirac model. The DFT approach is based on a strategy of modeling electron correlation via general functionals of the electron density

1.5.2.1 Hohenberg-Kohn theorems

Such methods owe their modern origins to Hohenberg-Kohn theorem, published in 1964, which demonstrated the existence of a unique functional which determines the ground state energy and density exactly. In the quantum mechanics Hamiltonian, the kinetic energy of electron and electron-electron interaction (V_{ee}) adjusts themselves to the external potential (V_{ex}) to get the lowest total energy. Thus, the external potential can be uniquely determined from knowledge of the electron density. The Hohenberg-kohn theorem states that if N interacting electrons move in an external potential V_{ext} , the ground state electron density $\rho(r)$ minimized the functional

$$E[\rho] = F[\rho] + \int \rho(r) V_{ext}(r) dr \quad (1.14)$$

Where $F[\rho]$ is a universal functional of $\rho(r)$ and the minimum value of the functional E is E_0 , the exact ground-state electronic energy.

$$\hat{F} = \hat{T}_e + \hat{V}_{ee} = \sum_i -\frac{1}{2} \nabla_i^2 + \sum_{i \neq j} \frac{1}{|r_i - r_j|} \quad (1.15)$$

And by using the variation principle, the density can be obtained.

1.5.2.1 The Kohn-sham Equation

Kohn and Sham (1965) introduce a method based on the Hohenberg-Kohn theorem that allows one to minimize the functional $E[n(r)]$ by varying $\rho(r)$ over all the densities containing N electron. They derived a coupled set of differential equations enabling the ground state density $\rho(r)$ to be found. Kohn and Sham separated $F[\rho(r)]$ in Equation into three distinct parts, so that the functional becomes.

$$E[\rho] = T_s[\rho(r)] + \frac{1}{2} \iint \frac{\rho(r)\rho(r')}{|r_i - r_j|} dr dr' + E_{xc}\rho(r) + \int \rho(r)V_{ext}(r)dr \quad (1.16)$$

Where $T_s[\rho(r)]$ is defined as the kinetic energy of non-interacting electron gas with density $\rho(r)$,

$$T_s[\rho(r)] = -\frac{1}{2} \sum_i \psi_i^*(r) \nabla^2 \psi_i(r) dr \quad (1.17)$$

And $E_{XC_s}[\rho(r)]$ is the exchange-correlation energy functional. Introducing a normalization constraint on the electron density, $\int \rho(r) dr = N$, by the Lagrange's method of undetermined multiplier, we obtain

$$\delta \left\{ E[\rho(r)] - \mu \left[\int \rho(r) dr - N \right] \right\} = 0 \quad (1.18)$$

When μ is an undetermined Lagrang multiplier. The number of electrons in the system is constant so $\delta N = 0$ then equation is reduced to

$$\delta E[\rho(r)] - \mu \delta \left(\int \rho(r) dr \right) = 0 \quad (1.19)$$

Equation 1.19 may now be rewritten in terms of an effective potential, $V_{eff}(r)$,

$$\frac{\delta T_s[\rho(r)]}{\delta \rho(r)} + V_{eff}(r) = \mu \quad (1.20)$$

Where

$$V_{eff}(r) = V_{ext}(r) + \int \frac{\rho(r')}{|r-r'|} + V_{xc}(r) \quad (1.21)$$

And

$$V_{xc}(r) = \frac{\delta E_{xc}[\rho(r)]}{\rho(r) dr} \quad (1.22)$$

1.5.4 Exchange and correlation

Hohenberk and Kohn demonstrated that E_{xc} is determined entirely by the electron density. In practice, E_{xc} is usually approximated as an integral involving only the spin densities and possibly their gradient. E_{xc} is usually divided into separate part, referred to as the exchange and correlation part, but actually corresponding to the same-spin and mixed-spin interaction, respectively:

$$E_{xc}[\rho] = E_x[\rho] + E_c[\rho] \quad (1.23)$$

All three term are again functionals of the electron density, and functional defining the two components on the right side of equation are termed exchange functional and correlation functional, respectively. The form of E_{xc} is in general unknown and its exact value has been calculated for only a few very simple systems. In the density functional theory, the exchange functional is always defined as follow

$$E_x[\rho] = \langle \phi[\rho] | \hat{V}_{ex} | \phi[\rho] \rangle - U[\rho] \quad (1.24)$$

When $U[\rho]$ is the Hartree value of the coulombic potential. The correlation term is defined as the remaining unknown value of the energy:

$$E_C[\rho] = F[\rho] - T_s[\rho] - U[\rho] - E_x[\rho] \quad (1.25)$$

1.5.5 Hybrid Functionals

There is an exactn connection between the non-interacting density functional system and the fully interacting many body system via integration of the work done in gradually turning on the electron electron interaction. The adiabatic connection approach allow the exact functional to be formally written as

$$E_{xc}[\rho] = \frac{1}{2} \int d\vec{r} d\vec{r}' \int_{\lambda=0}^1 d\lambda \frac{\lambda e^2}{|\vec{r} - \vec{r}'|} \left[\langle \rho(\vec{r}) \rho(\vec{r}') \rangle_{\rho, \lambda} - \rho(\vec{r}) \delta(\vec{r} - \vec{r}') \right] \quad (1.26)$$

Where the expectation value $\langle \dots \rangle_{\rho, \lambda}$ is the density-density correlation functional and is computed at density $\rho(r)$ for a system described by effective potential;

$$V_{eff} = V_{en} + \sum_{i \neq j} \frac{\lambda e^2}{|\vec{r} - \vec{r}'|} \quad (1.27)$$

Thus the exact energy could be computed if one knew the variation of density density correlation function with the coupling constant, λ . The LDA is recovered by replacing the pair correlation function with that for the homogeneous electron gas. The adiabatic integration approach suggests a difference approximation for the exchange-correlation functional. At $\lambda=0$ the non-interacting system corresponds identically to Hartree-Fock, while the LDA and GGA functional are constructed to be excellent approximations for the fully interacting homogeneous electron gas-that is, a system with $\lambda=0$ It is therefore not unreasonable to approximate the integral over the coupling constant as a weighted sum of the end point that is, we might set:

$$E_{XC} \approx aE_{Fock} + aE_{EX}^{GGA} \quad (1.28)$$

With the coefficients are to be determined by reference to a system for which the exact result is known. Becke adopted this approach in the definition of a functional with coefficients determined by a fit to the observe atomization energies, ionization potential, proton affinities and total atomic energies for a number of small molecule. Hybrid functional of this type is now very widely used in chemical applications with the B3LYP functional being the most notable. Computed binding energies, geometries and frequencies are systematically more reliable than the best GGA functional. A Becke – style three- parameter functional may be defined via the following expression:

$$E_{XC}^{B3LYP} = (1-a)E_{XC}^{LCD} + aE_{XC}^{\lambda=0} + bE_X^{B88} + cE_C^{LYP} + (1-c)E_C^{LCD} \quad (1.29)$$

Here, the parameter C_0 allows any any admixture of Hartree-Fock and LDA local exchange to be used. In addition, Becke's gradient correction to LDA exchange is also included, scaled by the parameter c_X . Similarly, the VWN3 local correlation functional is used and it used, and it may be optionally corrected by the LYP correction via the parameter the parameter c_C . In B3LYP functional, the parameters values are those specified by Becke, which he determined by fitting to the atomization energies, ionization potential, proton affinities and first – row atomic energies in the G1 molecule set: $c_0=0.20$, $c_X=0.72$ and $c_C=0.81$. Note that Beck used the Perdew-Wang 1991 correlation functional in his original work rather than VWN3 and LYP. The fact that the same coefficients work well with different functional reflects the underlying physical justification for using such a mixture of Hartree – Fock and DFT exchange first pointed out by Becke.

1.5.6 Time-dependent density functional theory

The TDDFT has become the method of choice. This is due to it's the accuracy coupled with its reasonable scaling with the systems dimensions. TDDFT can be as accurate as correlated ab initio techniques for the description of excited states, displaying a much lower computational cost. TDDFT is still limited to excited state having a single-excitation character and various problems of current XC

functional have been highlighted for long-range charge transfer excitations in which the starting and arriving orbitals of given transition do not overlap significantly. Nevertheless, TDDFT is currently successfully applied to study of organic molecule and systems containing transition metal centers. Considering the ground state geometry the excited state geometry, TDDFT can simulate absorption spectra. This opens the way to calculations of emission spectra and excited state dynamics. Furthermore, efficient procedures for calculations of dense spectra have recently been reported.

The DFT in its usual time-independent form is essentially a ground state theory and, as such, excludes the interaction of matter with time-dependent fields. There is generally no rigorous way, for example, to calculate electronic excitation energies due to photoabsorption. Standard DFT can be extended to excited states representing the lowest state of a given space-spin symmetry. The description of time-dependent phenomena, including photoexcitation, was incorporated properly into DFT by Runge and Gross who generalized the Hohenberg-Kohn theorem to time-dependent densities and potentials. It makes sense to distinguish between two main types of TDDFT calculations. The overwhelming majority of applications deal with relatively weak electric fields, e.g. photoabsorption spectra, which can be treated as a small perturbation within linear response theory. The other branch solves the TDDFT equations in the time domain to dynamically propagate electrons and nuclei. In the present article we will limit the discussion to the linear response aspect, the particular focus being on electronic excitation.

1.6 Objectives

1.6.1 To study the ground state conformation, energy gap, absorption, and emission properties of emitting material using DFT and TDDFT method.

1.6.2 To improve and enhance the electronic and optical properties of target organic materials using the combined theoretical and experimental studies.

1.6.3 To study the ground state conformation, energy gap, absorption, and emission properties of organic sensitizer by using DFT and TDDFT method.

1.6.4 To develop and design new OLED materials and organic sensitizer using the electronic and optical properties from our known target molecules

1.6.5 To improve and enhance light harvesting efficiency of organic sensitizer sensitizer using the combined theoretical and experimental studies.

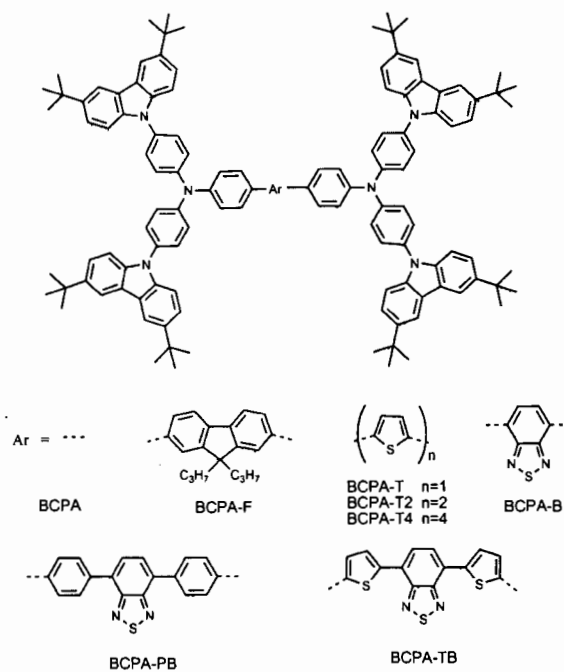


Figure 1.7 Structure of carbazole target molecule

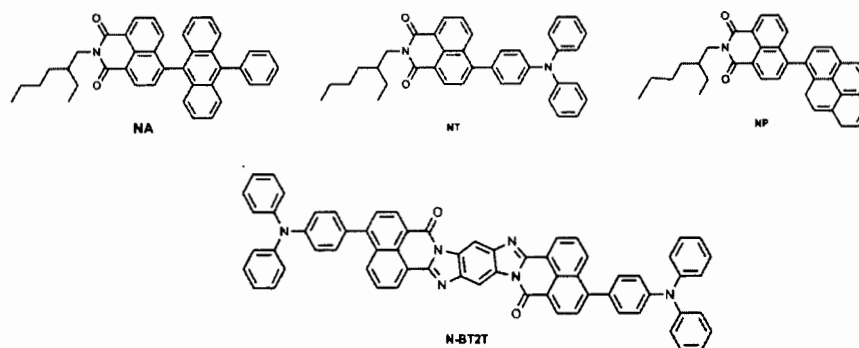


Figure 1.8 Structure of naphthalimide target molecule

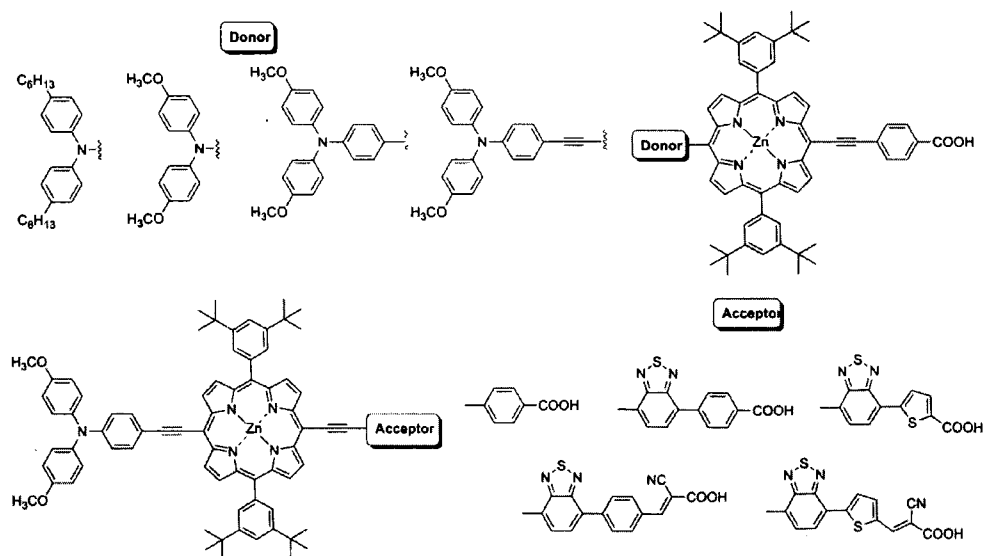


Figure 1.9 Structure of porphyrin target molecule

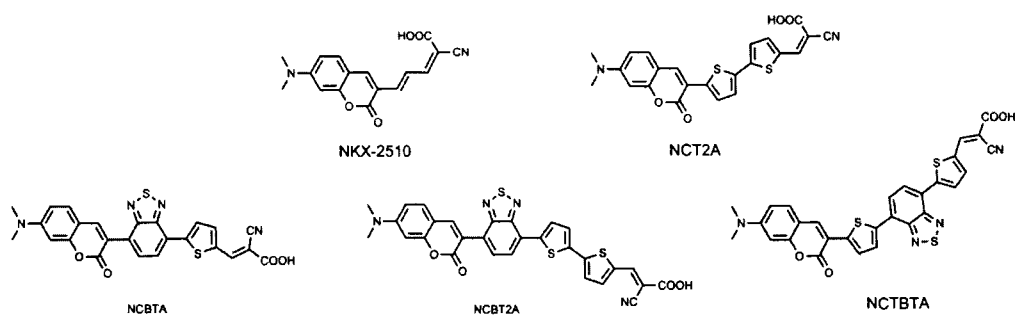


Figure 1.10 Structure of coumarin dye target molecule

CHAPTER 2

LITERATURE REVIEWS

2.1 Organic light-emitting diodes (OLEDs)

Gobal Singh and coworker have developed the organic molecule with a good hole transporting ability to improve thermal and morphological stability of carbazole-triphenyl derivatives. Figure 2.1 shows the chemical structure of TPA-Cz compound was designed and synthesized with triphenylamine as core and carbazole as peripheral group and investigated its photophysical properties. This compound show the excellent thermal and morphological stabilities, good solution-processability, and low oxidation potential, highly stable amorphous phase and high transparency to visible light. Furthermore, the electrochemical stability behavior with high HOMO level, which is more close to the work function of ITO than the conventional HTMs material. Thus, carbazole-triphenyl derivatives were expected to enhance device efficiency by improving charge injection and transport [8].

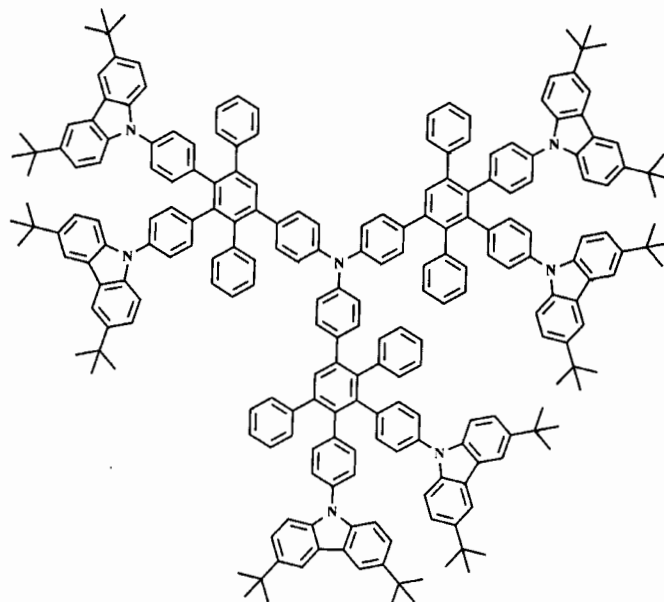


Figure 2.1 The chemical structure of TPA-Cz compound

As shown in Figure 2.2 new organic luminescent materials containing carbazole and benzimidazole chromophores were synthesized by incorporating with thiophene or phenyl spacer. Both 3,6- and 2,7-disubstitutions were explored. The photophysical, electrochemical, thermal and electroluminescence properties of the new materials were analyzed. The thiophene containing dyes showed red-shifted absorption and emission profiles than that of the phenyl analogs due to effective electronic delocalization in the former. Moreover, the thiophene-based dyes exhibited low oxidation potentials than that of the phenyl analogs attributable to electron richness. Electroluminescence devices were fabricated using these dyes as emitting layer or dopant in a multi-layered configuration. The devices containing thiophene-based dyes showed relatively low turn-on voltage in the neat devices due to the favorable alignment of energy levels, which facilitated balanced charge transport [9].

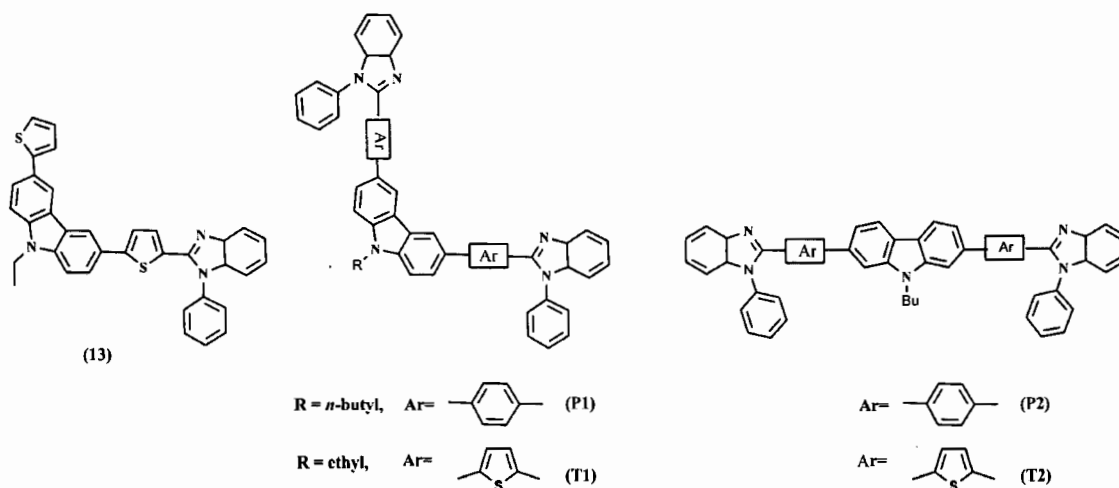


Figure 2.2 The chemical structure of carbazole derivatives

C. Wang and co-worker have reported an efficient combination that was achieved through two concepts of hybridized local and charge-transfer (CT) state (HLCT) and “hot exciton”. The former is responsible for high photo luminescent (PL) efficiency while the latter contributes to high exciton utilization. Figure 2.3 illustrates the molecular structure of donor acceptor molecule (D-A). On the basis of a tiny chemical modification in **TPA-BZP**, a green-light D-A molecule, **CzP-BZP** were synthesized with the efficient combination of high PL efficiency of $\eta_{\text{PL}} = 75\%$ in the solid state and

maximal exciton utilization efficiency up to 48% in OLED. This combined HLCT state and “hot exciton” strategy should be a practical way to design next-generation, low-cost, high efficiency fluorescent OLED materials [10].

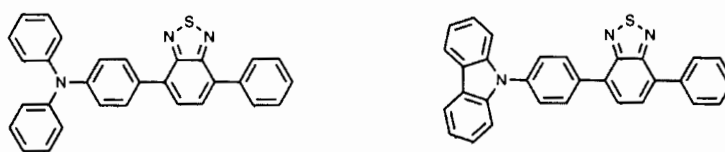


Figure 2.3 The molecular structure of TPA-BZP and CzP-BZP emitters

In 2013 T. Khanasa *et al* synthesized a series of bis(3,6-di-tert-butylcarbazol-9-ylphenyl)aniline end-capped oligoarylenes, **BCPA-Ars** shown in Figure 2.4. The optical and electrochemical properties in this studies show that their HOMOs, LUMOs, and energy gaps can be easily modified or fine-tuned by either varying the degree of π -conjugation or using electron affinities of the aryl cores which include fluorene, oligothiophenes, 2,1,3-benzothiadiazole, 4,7-diphenyl-4-yl-2,1,3-benzothiadiazole, and 4,7-dithien-2-yl-2,1,3-benzothiadiazole. The results show that their emission spectra can cover the full UV-vis spectrum (426-644 nm). This report offers a practical approach for tuning their emission colors to be suitable for applications in nondoped and solution processable full-color emission OLEDs [11].

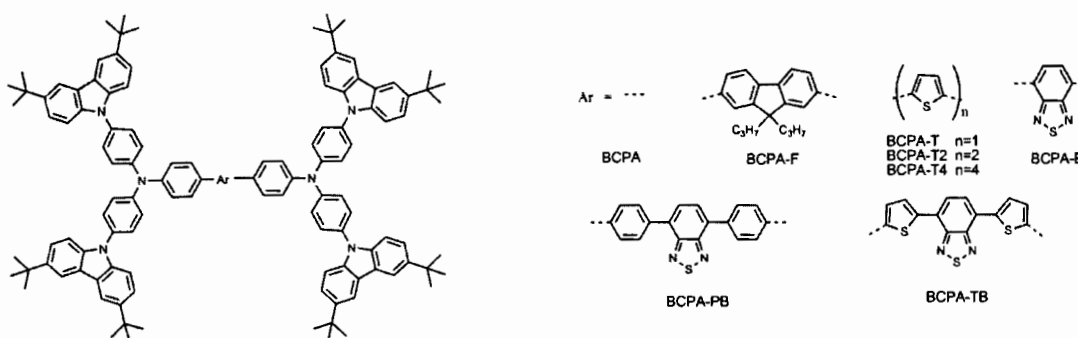


Figure 2.4 A series of bis(3,6-di-tert-butylcarbazol-9-ylphenyl)aniline end-capped oligoarylenes

The structure properties relationship of new D-A organic molecules with triphenylamine (TPA) fragment as core and 1,8-naphthalimide fragments as arms

which were reported. The molecular structures of D-A organic molecules are presented in Figure 2.5. The presence of double bond linkage between TPA and 1,8-naphthalimide fragments was expected to extend the absorption of these molecules due to intramolecular charge transfer between the donor and the acceptor units. The synthesized compounds show strong absorption peaks in the visible wavelength range from 400 to 550 nm, which can be ascribed to the intramolecular charge transfer. DFT calculations show that HOMO and LUMO orbitals are almost entirely localized on the donor and acceptor moieties, respectively. The charge-transporting properties of the synthesized materials were studied. The differences in the hole mobilities between the three synthesized compounds are discussed by comparing the reorganization energy and electronic coupling parameters [12].

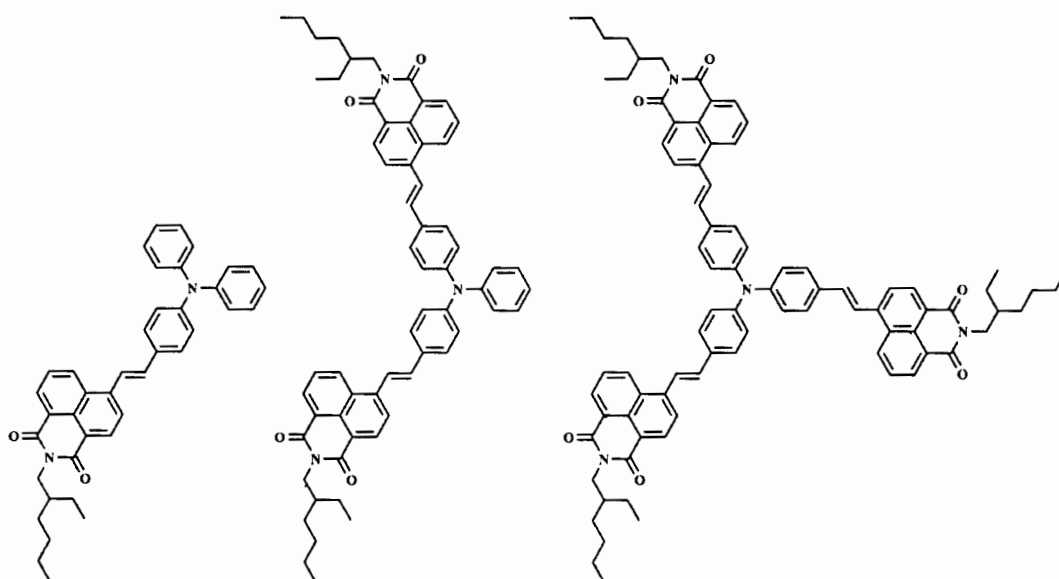


Figure 2.5 The molecular structure of 1,8-naphthalimide derivatives

In 2014, a series of N-butyl-1,8-naphthalimide derivatives have been designed to explore their optical, electronic, and charge transport properties as charge transport and/or luminescent materials for OLEDs. The molecular structures of N-butyl-1,8-naphthalimide derivatives are shown in Figure 2.6. The introduction of different aromatic substituent groups in the 4-position of N-butyl-1,8-naphthalimides was studied to describe in more detail about their charge transporting and optical properties. Furthermore, this D-A molecule structure extended the conjugation

systems to favor absorption and emission. The calculated results show that their optical and electronic properties are affected by their substituent groups in 4-position of N-butyl-1,8-naphthalimide. The study of substituent effects suggest that the λ_{abs} and λ_{fl} of 1-8 compound show bathochromic shifts compared with those of the reference compound. Furthermore, 1-8 compounds have large fluorescent intensity and they are promising luminescent materials for OLEDs, particularly for 1–3 and 5 compound [13].

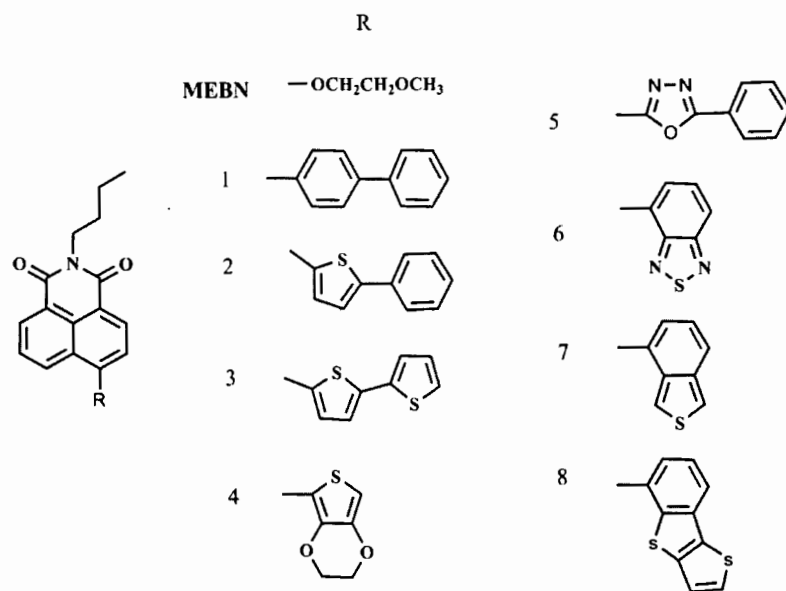


Figure 2.6 A series of N-butyl-1,8-naphthalimide derivatives

In 2015, a series of D- π -A star-shaped small molecules with 1,8-naphthalimide fragments as core and different electron-rich aromatic heterocycles as end groups have been designed to explore their optical, electronic, and charge transport properties as OLED. As shown in Figure 2.7, the molecular structures of D- π -A star-shaped 1,8-naphthalimide derivatives. The frontier molecular orbitals analysis has turned out that the molecules can lower the material band gap and extend the absorption spectrum toward longer wavelengths. The calculated results showed that their optical and electronic properties are affected by the different end groups and π -bridges. The results reveal that the molecules under investigation can serve as luminescent

materials for OLEDs. In addition, they are expected to be promising candidates for hole and/or electron transport materials [14].

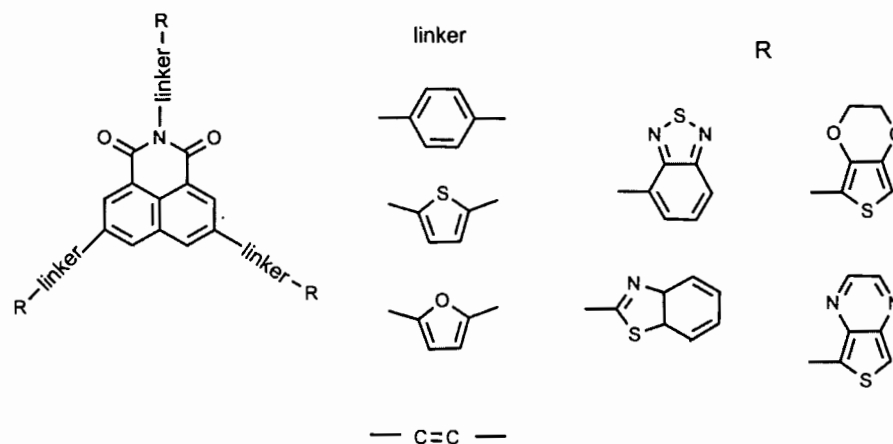


Figure 2.7 A series of D- π -A star-shaped small molecules with 1,8-naphthalimide

Shuai. Luo and co-worker have designed and synthesized three red-emissive D- π -A-structured fluorophores with an aromatic amine as the donor, ethene-1,2-diyl as the π -bridge, and 1,8-naphthalimide as the acceptor subunit, namely, **Nap1**, **Nap2** and **Nap3** shown in Figure 2.8. In-depth investigations on the correlations between their molecular structures and photophysical characteristics revealed that the presence of an electron-rich 4-dimethylaminophenyl donor moiety in compound **Nap1** could endow it with a red emission moreover, the replacement of the n-hexyl group of **Nap1** bonding to the imide nitrogen atom for a more bulky 2,6-di(isopropyl)phenyl one would result in compound **Nap2**. Alteration of the 4-(dimethylamino)phenyl donor subunit of **Nap2** into a more electron-donating 1,1,7,7-tetramethyljulolidin-9-yl substituent would render compound **Nap3** with more improved chromaticity. Consequently, **Nap3** could not only emit standard-red fluorescence with satisfactory chromaticity, but it also showed suppressed intermolecular interactions. All these results indicated that 1,8-naphthalimide derivatives could act as quite promising standard-red light-emitting materials for OLED applications [15].

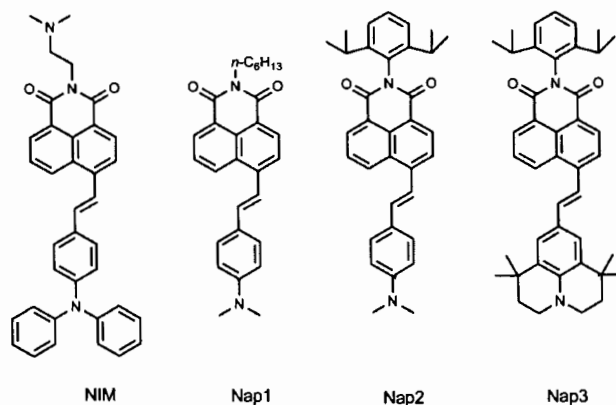


Figure 2.8 Molecular structures of NIM, Nap1, Nap2 and Nap3

A series of D-A naphthalimide-substituted fluorene derivatives were designed and synthesized. The molecular structures of naphthalimide derivatives are present in Figure 2.8. Their optical, electronic, and charge transport properties as charge transport and/or luminescent materials for OLEDs were demonstrated. The frontier molecular orbitals (FMOs) analysis turned out that the vertical electronic transitions of absorption and emission are described as ICT. The calculated results show that their optical and electronic properties are affected by the substituent groups in fluorene moieties. The results suggest that all selected candidates are promising as luminescent materials for OLEDs. In addition, naphthalimide-substituted fluorene derivatives can be used as promising hole and electron transport materials while derivatives with benzothiophene fragment can be used as the hole transporting material only for OLEDs [16].

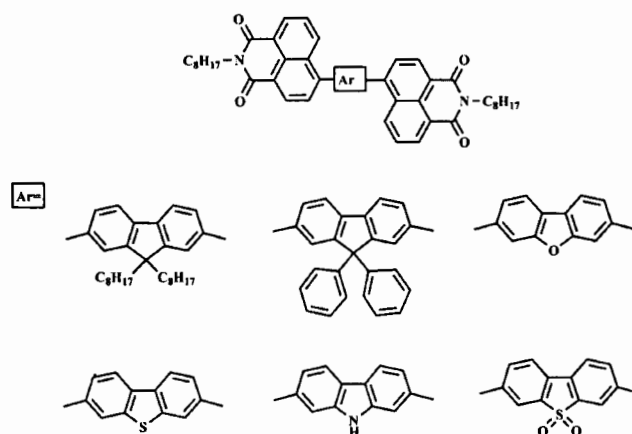


Figure 2.9 A series of D-A naphthalimide-substituted fluorene derivatives

2.2 Dye sensitized solar cells (DSCs)

A series of porphyrin dyes with an electron-donating group (EDG) attached at a meso-position (**YD-YD8**) have been designed and synthesized for use as sensitizers in dye-sensitized solar cells. The molecular structures of porphyrin substituted EDG are shown in Figure 2.10. The tuning of the HOMO-LUMO energy gap, thus the optical and electrochemical properties, is achievable on varying the structure of the donor group. Upon introduction of an EDG at the meso-position, the potential for the first oxidation alters significantly to the negative whereas that for the first reduction changes inappreciably, indicating a decreased HOMO-LUMO gap. The results reveal that direct attachment of an alkyl-substituted diarylamino group to the porphyrin ring results in significant improvement in solar-to-electrical conversion efficiency. The porphyrin dye with long alkyl-substituted diarylamino group is better performance than porphyrin with the strong EDG group due to decreasing of the tendency of aggregation [17].

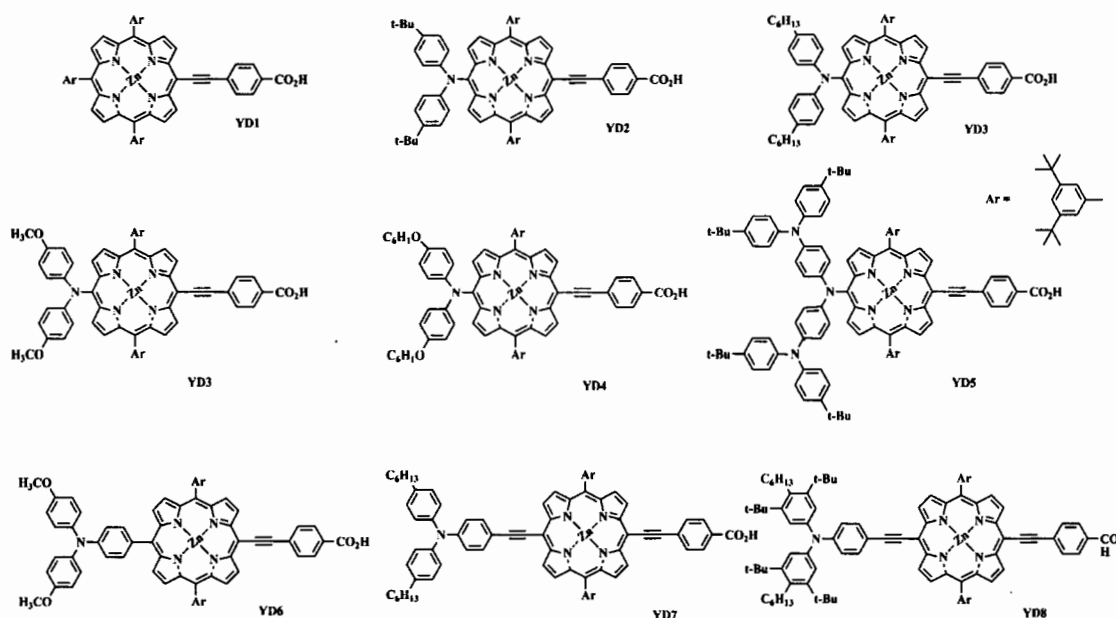


Figure 2.10 A series of porphyrin dyes with an electron-donating group (EDG)

A series of zinc porphyrin dyes **YD22-YD28** were synthesized and used for dye-sensitized solar cells as shown in Figure 2.11. Dyes **YD26-YD28** consist of zinc porphyrin (ZnP) as core unit, arylamine (Am) as electron-donating group, and

p-ethynylbenzoic acid (EBA) as an electron-withdrawing/-anchoring group. The dyes **YD22-YD25** contain additional phenylethynylene group (PE) bridged between Am and ZnP units. The influences of the PE unit on molecular properties as well as photovoltaic performances were investigated via photophysical and electrochemical studies and density functional calculations. With the insertion of PE unit, the dyes **YD22-YD25** possess better light-harvesting properties in terms of significantly red-shifted Q-band absorption. The conversion efficiencies for dyes **YD22-YD25** are better than those of dyes **YD26-YD28** owing to larger photocurrent density (J_{SC}) output. The results indicated that insertion of additional PE unit is beneficial to higher J_{SC} by means of improved light-harvesting property due to broadened and red-shifted absorption [18].

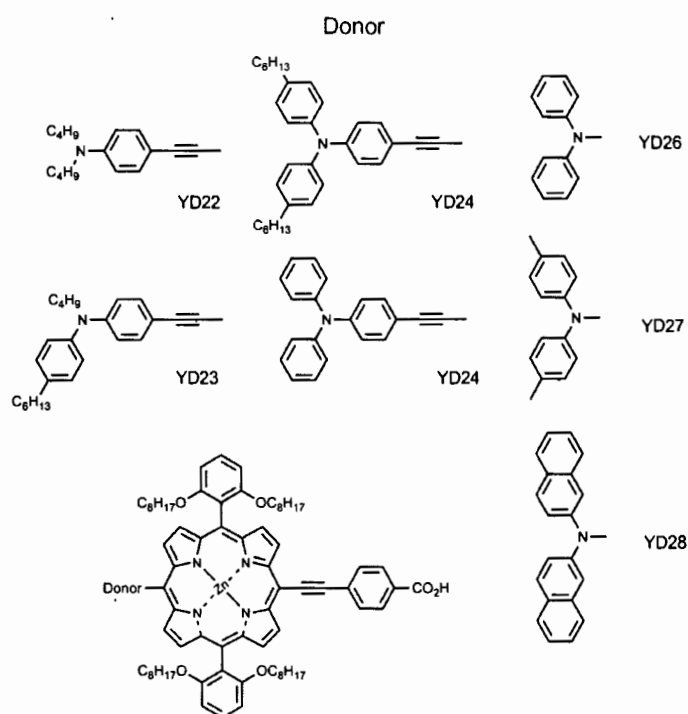


Figure 2.11 A series of zinc porphyrin dyes **YD22–YD28**

In 2016 Metalloporphyrin assemblies such as Zn-porphyrins are significant photoactive compounds with a number of applications including molecular devices and DSCs. In the present study, TDDFT is employed to simulate the ultraviolet-visible (UV-vis) spectra of the new photoactive compounds through chemical modifications of the donor (D) and π -bridge of a high performing reference Zn-porphyrin

(Pzn-EDOT) dye in DSCs. The Chemical structures of ID7-ID9 and reference dye are presented in Figure 2.12. It is found that substitutions with electron donating groups such as $-\text{NH}_2$, $-\text{OCH}_3$ and $-\text{N}(\text{CH}_3)_2$ at the meso positions of the D of the dye reduce the highest occupied molecular orbital (HOMO) - lowest unoccupied molecular orbital (LUMO) energy gap by lifting up the occupied frontier orbitals; whereas chemical modification of the π -bridge with dyad monomers such as pyrimidine (Py), thiophene (Th_n) and EDOT reduces the HOMO-LUMO energy gap by lowering the frontier virtual orbitals. The new dye compounds exhibit the predicted changes to the UV-vis spectra, with a splitting of the Soret band and a distinct red-shift of the Q-bands. The study demonstrates that modification of the π -bridge is an attractive approach for tuning Zn-porphyrin assemblies for DSC applications. The present study provides a rationale to design new architectures of molecular devices and for the improvement of metalloporphyrin assemblies [19].

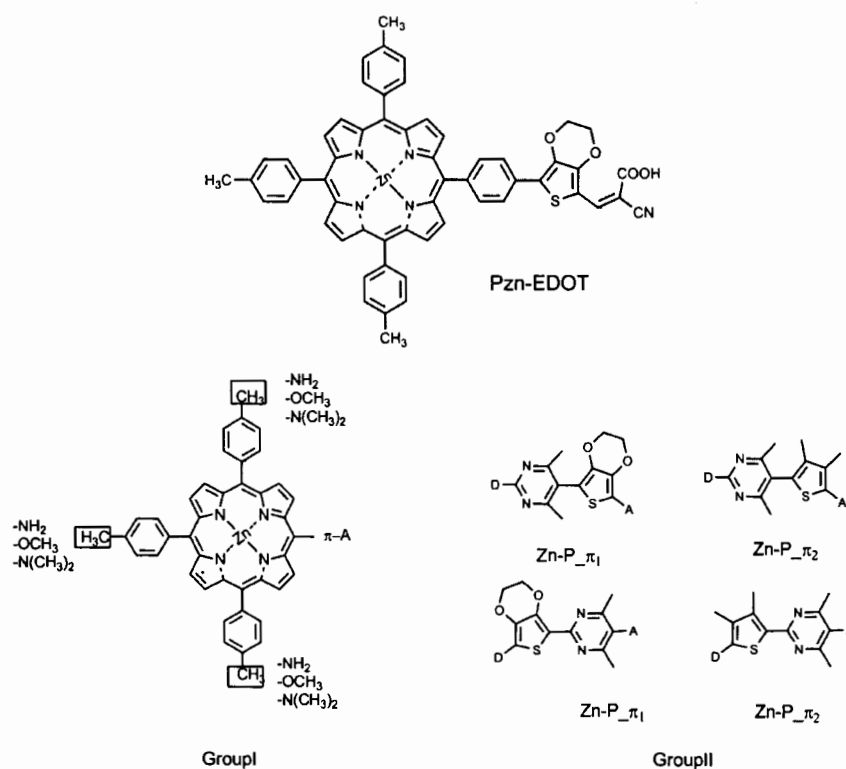


Figure 2.12 Chemical structures of ID7-ID9 and reference dye

A series of zinc porphyrin dyes (JY24-27) featured phenothiazine moieties have been synthesized and applied as photosensitizers in DSCs as displayed in Figure 2.13.

The phenothiazine donors were directly attached to the meso-position of porphyrins, and different π -linkers (benzene, thiophene and ethynyl benzene) and acceptor groups (carboxylic acid and cyanoacrylic acid) were applied to tune the photoelectric properties of these push-pull porphyrin dyes. The photophysical, electrochemical and theoretical studies revealed that the synthesized porphyrin dyes were all capable of being used as photosensitizer. The dye **JY27** with an extended conjugation by introducing ethynyl group exhibited a broader absorption region and more significantly improved IPCE values between 550 and 750 nm than the other three dyes, which ensured a good light-harvesting ability and a high short-circuit current density of 15.3 mA cm^{-2} . Finally, **JY27**-based cell achieved a high efficiency of 6.25% under standard simulated irradiation [20].

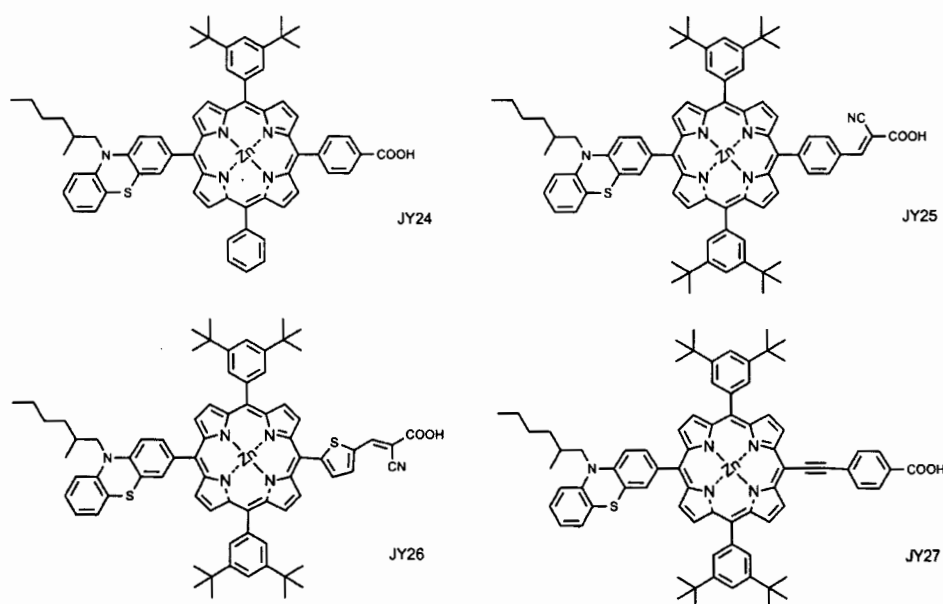


Figure 2.13 Structures of the pheno-thiazine-modified porphyrin dyes

The designing of novel porphyrins based sensitizers is essential to resolve the current existing issues. The seven D- π -A porphyrin dyes (**LG1-LG7**) engineered with 3-ethynyl phenothiazine tethered at the meso-position and different π -spacers were incorporated between porphyrin macrocycle and anchoring group are exhibited in Figure 2.14. The introduction of secondary π -spacer alters the electronic properties of the porphyrin sensitizers resulting in both soret and Q-band absorption red-shifted with onset extending up to 850 nm in **LG5**. The light harvesting efficiency of

porphyrin dye with 4-ethynylthiophene (**LG5**) is shift to near-infrared region resulting in the highest efficiency of 10.20% among other derivatives. Furthermore, DFT and TD-DFT studies showed that HOMO spread over the donor and porphyrin π -spacer, LUMO spread over the π -spacer, and anchoring carboxylic acid groups are suitable for dye-sensitized solar cell applications [21]

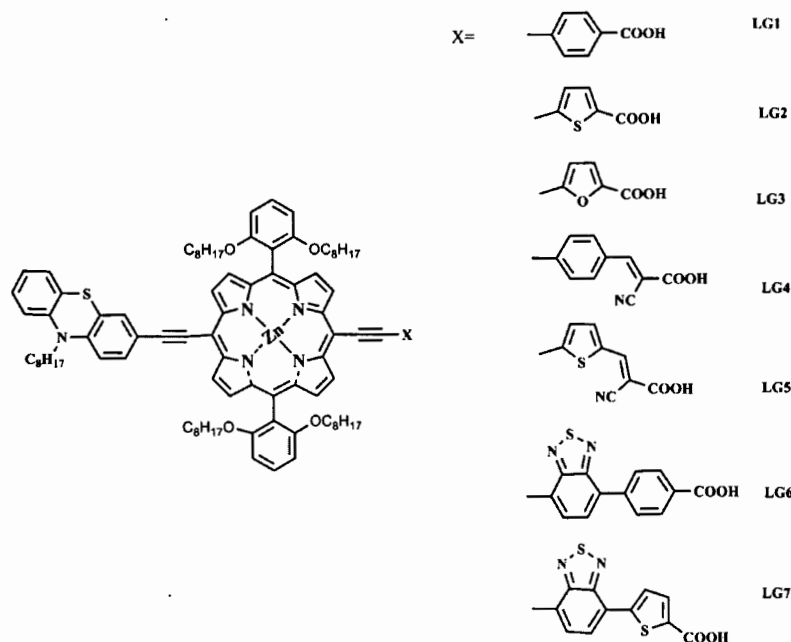


Figure 2.14 The designing of novel D- π -A porphyrins

The metal-free photosensitizers have been also used as photosensitizers for DSCs. There are several advantages as of these organic materials such as the larger absorption coefficients than metal-complex photosensitizers that lead to efficient light-harvesting properties; their easier modified structural for molecular design, and; there are no concerns about resource limitations. The molecular design of coumarin dyes with includes their photoelectrochemical properties and their performance in DSCs was reported. The molecular design of coumarin dyes are presented in Figure 2.15. Introduction of a methine unit (-CH=CH-) connecting the anchoring groups into the coumarin framework expanded the π conjugation in the dye and thus resulted in a wide absorption in the visible region. The maximum 6.0% was achieved by optimization under AM 1.5 with a DSC based on NKX-2311. From these results strongly support the prospects for successful application of DSCs based on organic-

dye photosensitizers and indicate the importance of molecular structure design for tuning photosensitizers to produce highly efficient DSCs [22].

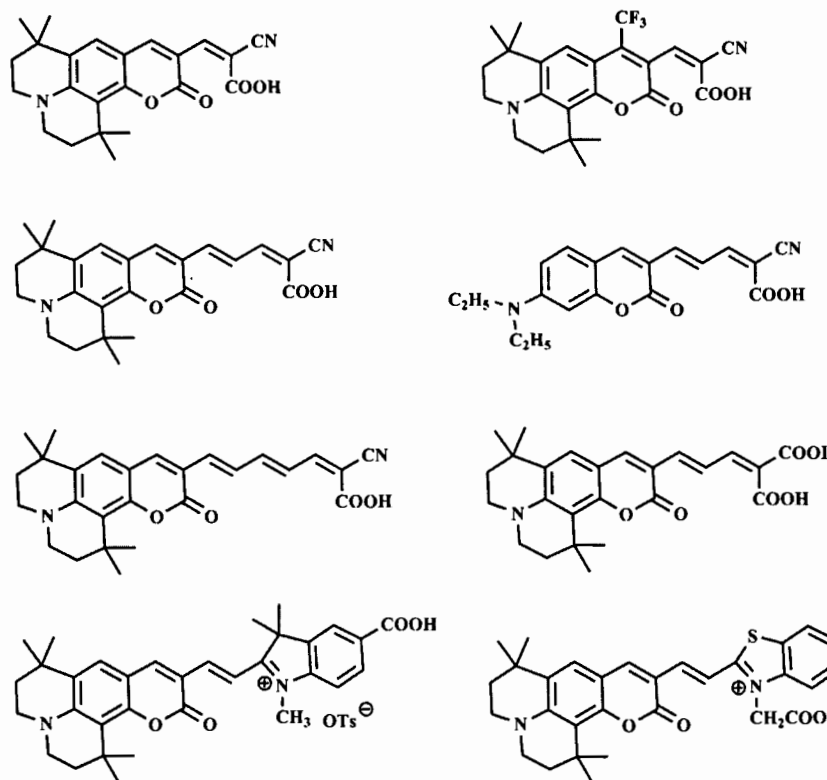


Figure 2.15 The molecular design of coumarin dyes

In 2015, a group of dyes derived from coumarin was studied, which consisted of nine molecules for DSCs as present in Figure 2.16. In this research, it was observed that the π -bridge had an important effect on the properties of the dyes. When the conjugation of the π -bridge was extended, the dye presents a good ICT and the LUMO energy is closer to the TiO_2 conduction band. The above parameters have a good correlation with the experimental efficiency parameters [23].

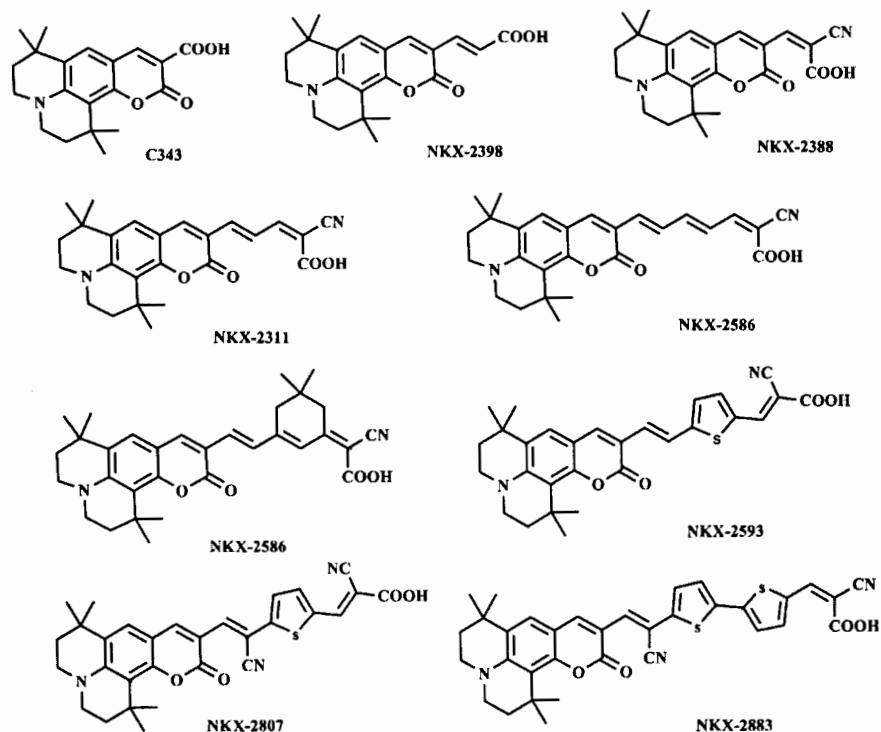


Figure 2.16 A group of coumarin dyes

Ethynyl group has been widely employed in DSCs as an efficient π -spacer to prolong the conjugation and promote electronic coupling at the interface of TiO_2 films. However, the systematic study of ethynyl position on non-ruthenium sensitizers remains relatively blank. This report suggesting that triple bond was introduced to indoline-based organic dyes in different position of D-A- π -A featured organic dyes presented in Figure 2.17. Based on the reference dye **D1**, an ethynyl unit in either the left or right side of benzothiadiazole was insert to construct two novel dyes **D2** and **D3**. Interestingly, **D2** and **D3** display better photovoltaic performance with respect to **D1**. Especially, **D3** exhibits an over 90 mV enhanced open-circuit voltage (V_{OC}) than **D2** owing to longer electron lifetime and slower charge recombination. With this incredible increase of V_{OC} , The organic sensitizer, **D3**, show the higher efficiency about 7.13% with respect to **D1** and **D2**. This work has paved a useful and practical way for molecular engineering in D-A- π -A featured metal-free organic dyes [24].

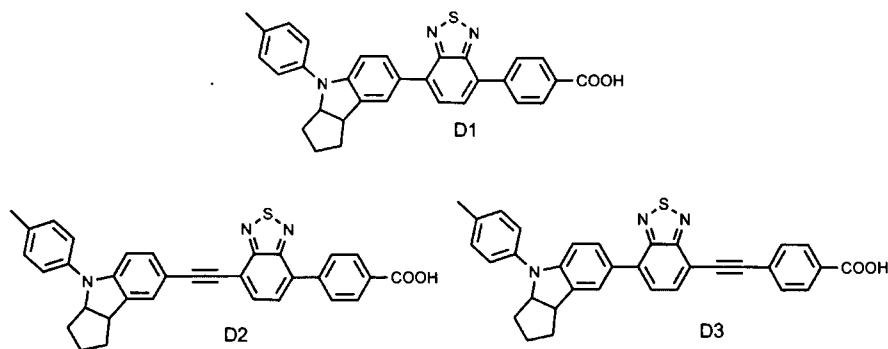


Figure 2.17 The indoline-based dyes in different position of D-A- π -A

New D- π -A- π -A type organic dyes were synthesized and characterized as sensitizers for DSCs. Chemical structures of dyes D- π -A- π -A were displayed in Figure 2.18. These dyes showed wide absorption spectra (300–625 nm) and high molar extinction coefficients. As dye sensitizers in DSCs, the D- π -A- π -A dye having a cyano-acrylic acid as an acceptor gave the best cell performance with a J_{sc} of 7.14 mA/cm², V_{oc} of 0.62 V, and a fill factor (FF) of 0.72, corresponding to an overall conversion efficiency of 3.19% [25].

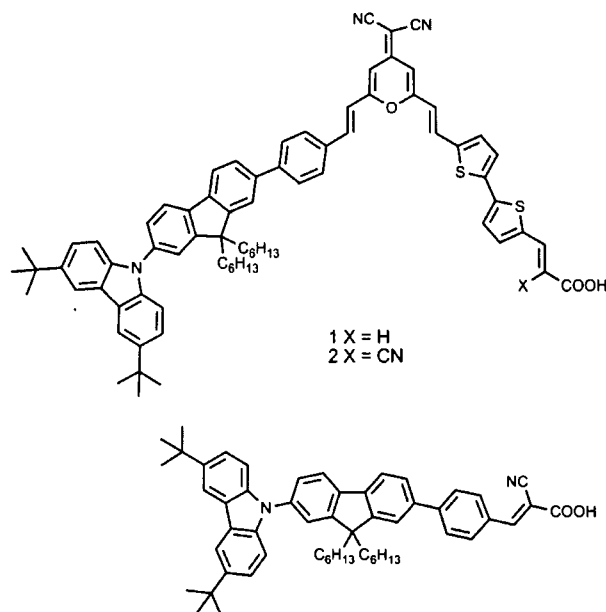


Figure 2.18 The New D- π -A- π -A type organic dyes

CHAPTER 3

THEORETICAL INVESTIGATION OF ORGANIC COMPOUND FOR OLED APPLICATION

3.1 Triphenylamine derivatives for OLEDs

The research in organic light-emitting diodes (OLEDs) has become one of the most interesting topics due to their potential for utilization in next-generation display technologies and light application. During the past decade, triphenylamine (TPA) is a unique star molecule possessing useful function such as redox activity, fluorescence and transport positive charge via the radical cation species. To our best knowledge, fluorene derivatives are well-known as highly fluorescent compounds because of their excellent chemical, thermal, photochemical stabilities as well as the possibility of structure tuning to adjust the electronic and morphological properties of desired compounds via the substitution on the C-9 position, offering the prospect of controlling the polymer solubility and other physical properties. The advantages of oligothiophenes are that their physical properties can be easily tuned to the desired properties by changing the structure, for example, solubilizing chains, terminal groups, and different oligomer lengths. Benzothiadiazole is red fluorophore which is showing red emission. It can be extended π -conjugation. The luminescent properties are closely related to the electronic structures of the emitting molecules, especially those of the excited states. The excited states have a short life time, which are not easy to describe directly by experimental observation. The theoretical investigation of the electronic structures of emitting materials used in OLED is important for a better understanding of the photoelectronic process, as well as for the design of new analogues with improved performances. At present, a number of papers have been proposed the theoretical studies of the adsorption and emission properties of emitting material for OLED using different calculation methods. In particular, the TDDFT method was developed and widely used as a powerful tool for the excited-state investigation.

Many previous works focused on TDDFT electronic properties related to the ground state geometry, while the properties based on the excited state have not been widely investigated. Some research groups have used CIS method to obtain the excited state structure; however, the limitation of CIS method is a controversial issue. Therefore, calculation of electronic structure of excited states is still very challenging. Currently, molecular modeling techniques and especially quantum chemistry offer a competitive alternative for the interpretation of the experimental data. So the theoretical investigations of the physical properties of organic materials are very important in order to disclose the relationship among the performance, structures and the properties, it is also helpful to design and synthesis novel organic materials with higher performance. Herein, bis(3,6-di-tert-butylcarbazol-9-ylphenyl)aniline (**BCPA**) derivatives were designed and synthesized by incorporating different aromatic ring to investigate the impact of optical, electrochemical properties of organic material for applied as emitters and also hole-transporting material. Moreover, the DFT/TDDFT calculations were investigated to provide a detailed characterization of the structural, electronic and optical properties of these materials.

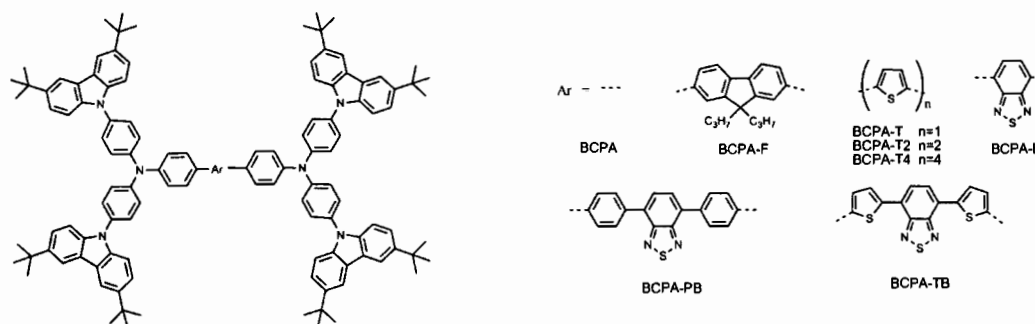


Figure 3.1 Sketch map of triphenylamine derivative

3.1.1 Computational details

In this research, we perform DFT and TDDFT calculations on the ground state of organic material. This computational procedure allows us to provide a detailed assignment of the excited state involved in the absorption process. The geometries in the gas phase were optimized by the DFT method using the B3LYP exchange-correlation function, with 6-31G(d,p) basis set in the Gaussian 09 program package. Electronic population of the HOMO and LUMO were calculated to show the position

of localization of electron populations along with the calculated molecular orbital energy diagram. The electronic absorption spectra require calculation of the allowed excitation and oscillator strengths. These calculations were carried out using TDDFT with the same basis set and exchange-correlation functional. The energy gap has been estimated from two ways, namely, HOMO–LUMO energy gap and the first excitation energies. Based on the excited geometries, the first excitation energy (E_g) and the maximal absorption wavelength of all molecules have been performed by using the TDDFT at the same level based on the optimized geometries. The solvent effect for dichloromethane (DCM) solution was implicitly accounted using conductor-like polarizable continuum model (C-PCM). In addition, we calculated the lowest singlet-singlet electronic transitions. Subsequently, the absorption properties calculated by TDDFT method were imported into the Gausssum program to visualize the absorption profiles.

3.1.2 Results and discussion

3.1.2.1 Ground-state geometries of triphenylamine

The ground state structure of target molecules were optimized by the DFT method using the B3LYP exchange–correlation function with 6-31G (d,p) basis set. The optimized geometries in the gas phase shown in Figure 3.1. Their distance and dihedral angle parameters are shown in Table 2.1. The target molecules were designed involved the use of BCPA as an end-capping group and the different oligoarylene as the fluorescent core. The use of fluorene and thiophene as a core will be useful to extend π -conjugation length of the molecule, while benzothiadiazole moiety will improve intramolecular charge transfer properties of organic materials which impacts on the emission behavior of organic materials. In addition, variation the effect of aromatic ring affected the dihedral angle between Ar and Ar is changed. The dihedral angle between Ar and Ar in **BCPA-Th1**, **BCPA-Th1** and **BCPA-Th4** were calculated to be about 12.09°-18.50° indicating that dihedral angle between Ar and Ar are decrease by extend pi-conjugation lengths of aromatic ring. For **BCPA-PB**, the dihedral angle between Ar and Ar were calculated to be about -34.14° to -35.52° which is larger than dihedral angle of **BCPA-TB** because of its repulsion interaction. The optimized structures reveal that the **BCPA** moieties attached to the end of the molecules adopt a bulky conformation creating nonplanar geometry around the planar

oligoarylene cores, which could help to prevent the close π - π contact between molecules. This would facilitate the formation of amorphous materials for a simple solution processed hole-transporting non-doped emitter for OLED application.

Table 3.1 The selected important inter-ring distances (r , Å) and dihedral angle (Φ , °) calculated by B3LYP/6-31G(d,p) calculations

Molecule	Distances (r , Å) and dihedral angle (Φ , °)				
	D-Ar1 (ϕ 1)	Ar-D (ϕ 2)	Ar1- Ar2 (ϕ 3)	Ar2-Ar3 (ϕ 4)	Ar3-Ar4 (ϕ 5)
BCPA	-33.88	-	-	-	-
	1.48	-	-	-	-
BCPA-F	-36.84	35.88	-	-	-
	1.48	1.48	-	-	-
BCPA-T1	25.62	-23.57	-	-	-
	1.46	1.46	-	-	-
BCPA-T2	-24.09	-23.38	18.50	-	-
	1.46	1.46	1.45	-	-
BCPA-T4	41.41	-24.01	15.37	-12.09	15.42
	1.46	1.46	1.44	1.44	1.44
BCPA-B	-35.53	-35.52	-	-	-
	1.48	1.48	-	-	-
BCPA-PB	-34.14	-34.69	-35.38	-35.52	-
	1.48	1.48	1.48	1.48	-
BCPA-TB	-18.94	-18.94	-11.14	-11.15	-
	1.46	1.46	1.45	1.45	-

D = bis(carbazol-9-yl)triphenylamine, Ar = Aromatic ring

3.1.2.2 Electronic properties of triphenylamine derivative

Electronic population of the HOMO and LUMO were calculated to show the position of localization of electron populations along with the calculated molecular orbital energy diagram. The frontier molecular orbitals of all target molecules are shown in Figure 3.2 and Figure 3.3. In the HOMO of all molecules, π -electrons are delocalized over the entire oligoarylene core and triphenylamine moieties. In the LUMOs of **BCPA-F**, having fluorene as cores, the excited electrons delocalize over the fluorene moiety. For **BCPA-T1**, **BCPA-T2** and **BCPA-T4** having oligothiophenes as cores, the LUMO is a delocalized π^* orbital over the thiophene

unit. In the LUMO orbitals of **BCPA-B**, **BCPA-PB** and **BCPA-TB**, the excited electrons delocalized over the strong electron withdrawing group, creating a donor-acceptor characteristic. This suggests that substitution of different fluorescent core with BCPA bulky conformation significantly affect the distribution patterns of LUMO level for organic molecules while has little effect on the HOMO level of these molecules. From these results suggesting that different LUMO energies should be then expected for these compounds affect to optical properties. The ICT transition in **BCPA-B**, **BCPA-PB** and **BCPA-TB** molecules becomes much easier after introducing of different donor groups, resulting in the large bathochromic shift in their absorption and fluorescence spectra.

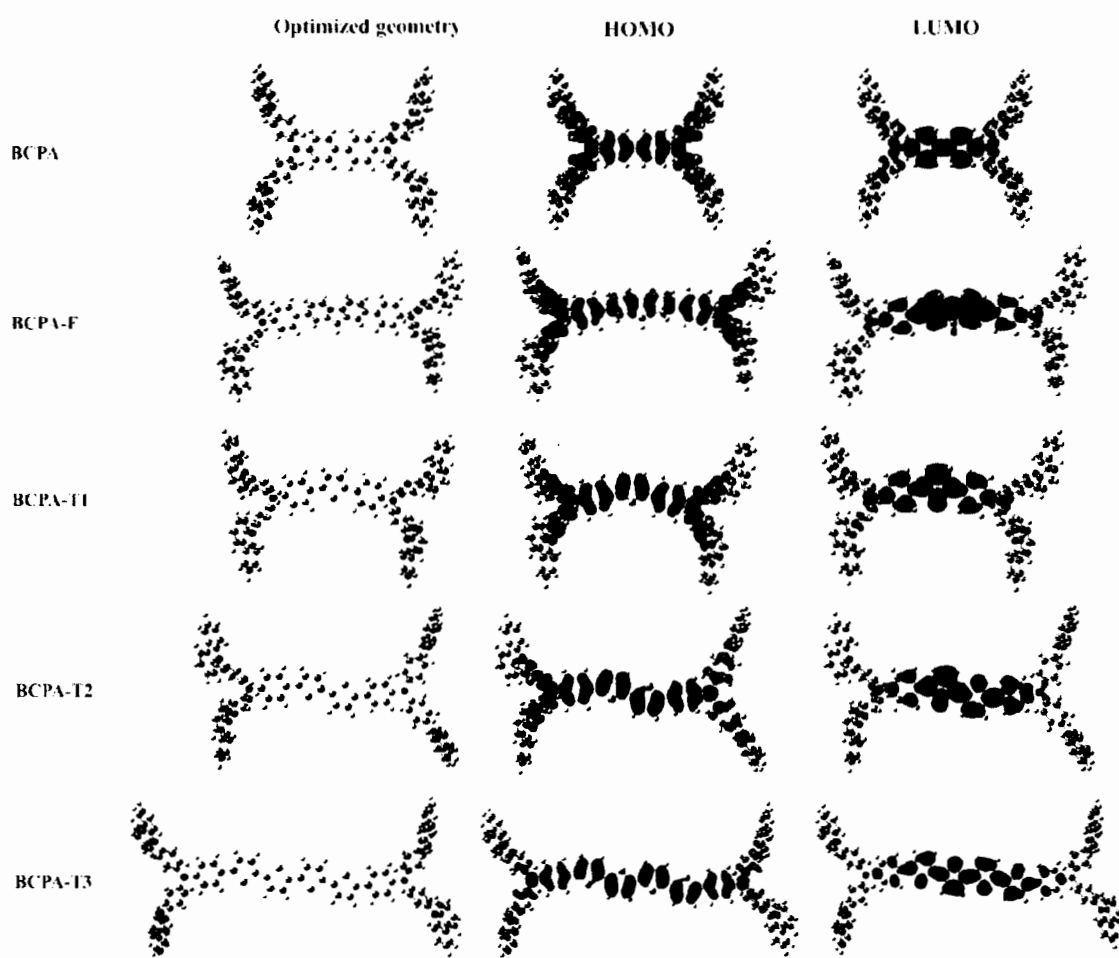


Figure 3.2 Optimized structures (left), HOMO (middle) and LUMO (right) of **BCPA**, **BCPA-F**, **BCPA-T1**, **BCPA-T2** and **BCPA-T3** target molecule

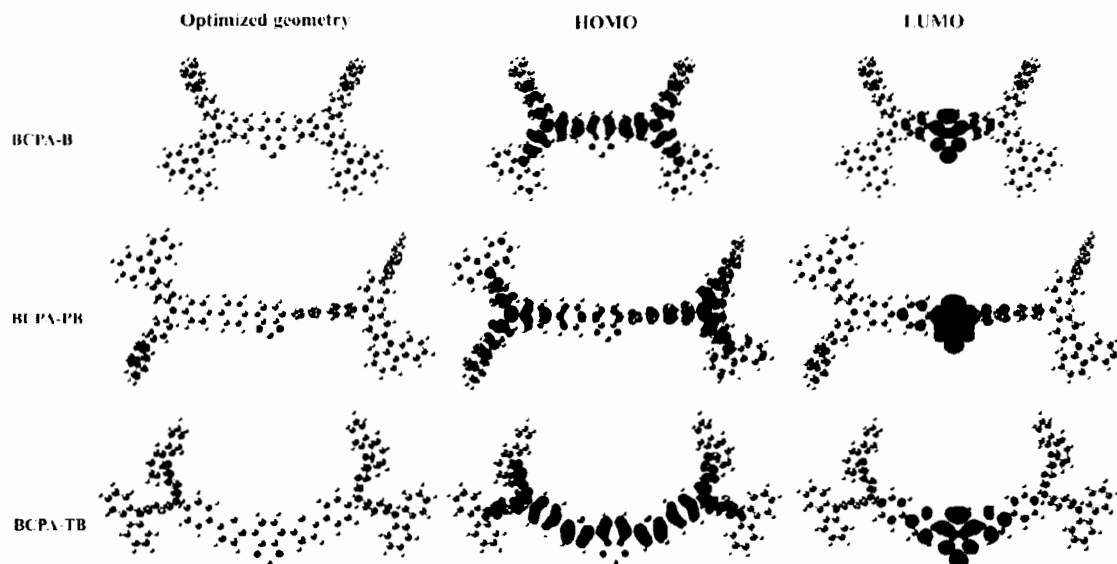


Figure 3.3 Optimized structures and HOMO (left) LUMO (middle) of BCPA-B BCPA-PB and BCPA-TB target molecule

The HOMO–LUMO energy gaps of **BCPA-Ar** series were calculated and the values (2.14–3.74 eV). These results show the accepting electron efficiency of the oxidized dye from the electrolyte system. As shown in Figure 3.4 and Figure 3.5, the HOMO levels of **BCPA-Ar** series are increased with increasing π -conjugation length approaching the redox potential of the electrolyte system.

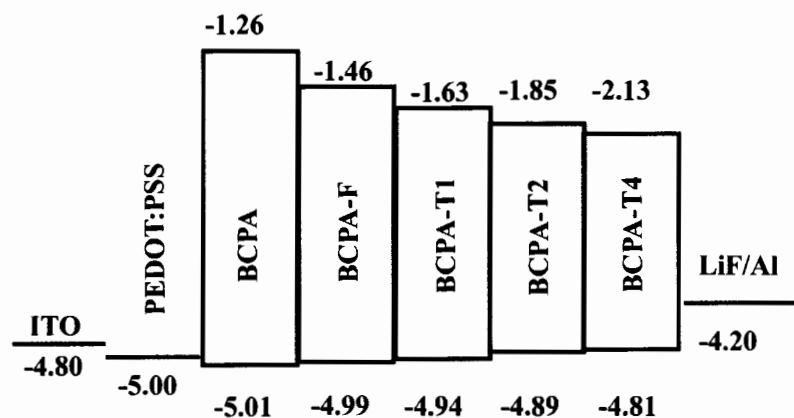


Figure 3.4 Energy diagram of of BCPA, BCPAF, BCPAT1, BCPAT2 and BCPAT4 target molecule

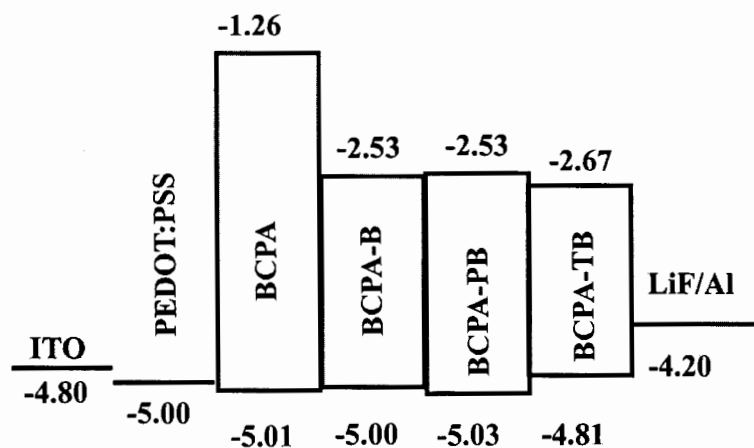


Figure 3.4 Energy diagram of BCPA-B, BCPA-PB and BCPA-TB target molecule

3.1.2.3 Ionization potential and electron affinity energies

The device performance of OLEDs depends on the charge injection, transfer, and balance as well as the exciton confinement in a device. Thus, the IP and EA are important to investigate which can be used to evaluate the energy barrier for the injection of holes and electrons, and the charge transfer rate and balance. The DFT calculated IP and EA values of **BCPA-Ar** target molecule are listed in Table 3.2.

Table 3.2 HOMO and LUMO energies, IP and EA for BCPA-Ar with the B3LYP/6-31G (d,p) functional (in eV)

Molecules	E_{HOMO}	E_{LUMO}	IP	EA
BCPA	-5.01	-1.26	5.68	0.63
BCPA-F	-4.99	-1.46	5.61	0.86
BCPA-T1	-4.94	-1.63	5.58	1.04
BCPA-T2	-4.89	-1.85	5.51	1.26
BCPA-T4	-4.81	-2.13	5.41	1.55
BCPA-B	-5.00	-2.53	5.64	1.62
BCPA-PB	-5.03	-2.53	5.60	1.59
BCPA-TB	-4.81	-2.67	-	-

The IP and EA energy can be adiabatic excitations (optimized structure for both the neutral and charged molecule). The ionization potential of molecule may be computed as: $E(\text{cation}^+) - E(\text{neutral})$, the electron affinity of molecule may be computed as: $E(\text{neutral}) - E(\text{anion}^-)$. The IP and EA are approximate from this below equation.

$$\text{IP} = (E_{\text{total}}(\text{cationic}) + \text{ZPE}(\text{cationic})) - (E_{\text{total}}(\text{neutral}) + \text{ZPE}(\text{neutral}))$$

$$\text{EA} = (E_{\text{total}}(\text{neutral}) + \text{ZPE}(\text{neutral})) - (E_{\text{total}}(\text{anionic}) + \text{ZPE}(\text{anionic}))$$

It can be seen that the IP values decrease with increasing of thiophene units. In addition, the order of the IP of the series is observed following: **BCPA > BCPA-F > BCPA-T1 > BCPA-T2 > BCPA-T4**, suggesting that the hole injection and transportation of **BCPA-T4** are expected to be easier than the others. While the EA values increase significantly from 0.63 to 1.60 eV when incorporated the different core.

3.1.2.4 Absorption spectra of organic sensitizers

The absorption spectra of these molecules have been studied by TD-B3LYP/6-31G(d,p) level in the CH_2Cl_2 solvent. Comparison of the theoretically calculated wavelength with experimental data has been performed. The corresponding simulated absorption spectra of **BCPA-Ar** are shown in Figure 3.6. The electronic properties, oscillator strengths, conjugations of the orbitals, and the maximum wavelength in the solvent phase of all organic sensitizers are shown in Table 3.3. Their UV-vis absorption spectra of **BCPA**, **BCPA-F**, **BCPA-T1**, **BCPA-T2** and **BCPA-T4** were calculated to be 381, 400, 436, 479 and 547 nm, respectively. The characteristic absorption peaks is ascribing to the $\pi-\pi^*$ transition from HOMO– LUMO. It is found that the calculated data have similar tendencies with the experiment. The trend of maximum absorption wavelength exhibits red-shift and the absorption intensity increases with the increase conjugation length of organic emitters.

Table 3.3 The absorption spectra of BCPA-Ar with the B3LYP/6-31G (d,p) functional

Dyes	State	Excitation	Oscillator	Character	Assignment	exp
		Energy (nm)	strength (<i>f</i>)			
BCPA	$S_0 \rightarrow S_1$	381	1.3715	$\pi-\pi^*$	HOMO \rightarrow LUMO	349
BCPA-F	$S_0 \rightarrow S_1$	400	1.9341	$\pi-\pi^*$	HOMO \rightarrow LUMO	373
BCPA-T1	$S_0 \rightarrow S_1$	436	1.6886	$\pi-\pi^*$	HOMO \rightarrow LUMO	396
BCPA-T2	$S_0 \rightarrow S_1$	479	2.0923	$\pi-\pi^*$	HOMO \rightarrow LUMO	418
BCPA-T4	$S_0 \rightarrow S_1$	547	2.7567	$\pi-\pi^*$	HOMO \rightarrow LUMO	450
BCPA-B	$S_0 \rightarrow S_1$	591	0.5577	ICT	HOMO \rightarrow LUMO	462
BCPA-PB	$S_0 \rightarrow S_1$	562	0.4673	ICT	HOMO \rightarrow LUMO	422
BCPA-TB	$S_0 \rightarrow S_1$	685	1.0509	ICT	HOMO \rightarrow LUMO	528

For **BCPA-B**, **BCPA-PB**, and **BCPA-TB**, the strongest absorption peak with the largest oscillator strength arises from $S_0 \rightarrow S_1$ transition and corresponds to the intramolecular charge transfer transition, which is primarily contributed from the HOMO to the LUMO. The ICT absorption peak of **BCPA-PB** (562 nm) is blue-shifted, while that of **BCPA-TB** (685 nm) is red-shifted compared with that of the reference compound **BCPA-B** (591 nm). These results suggest that introducing the thiophene link between BCPA bulky group and BTD core gives rise to more intense ICT interaction in **BCPA-TB** than that of **BCPA-PB**.

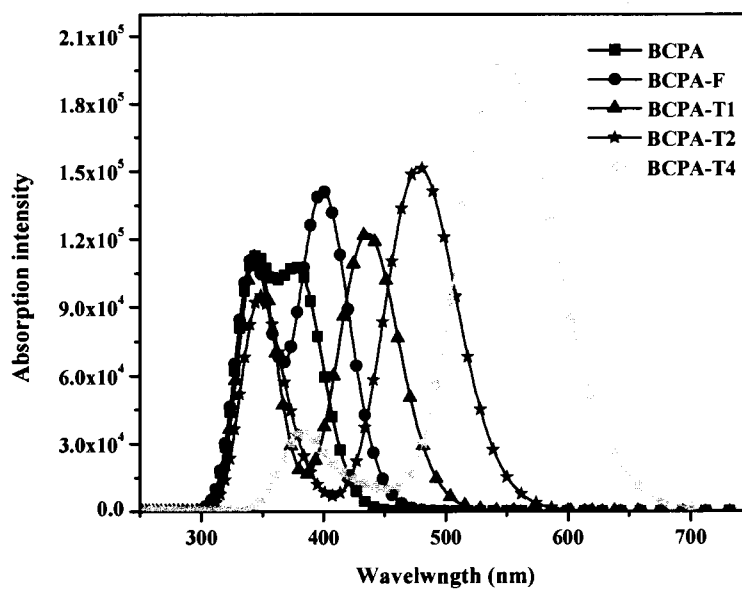


Figure 3.6 Absorption spectra of BCPA, BCPAF, BCPAT1, BCPAT2 and BCPAT4 target molecule by TD-B3LYP/6-31G(d,p) level in CH_2Cl_2 solvent (C-PCM model)

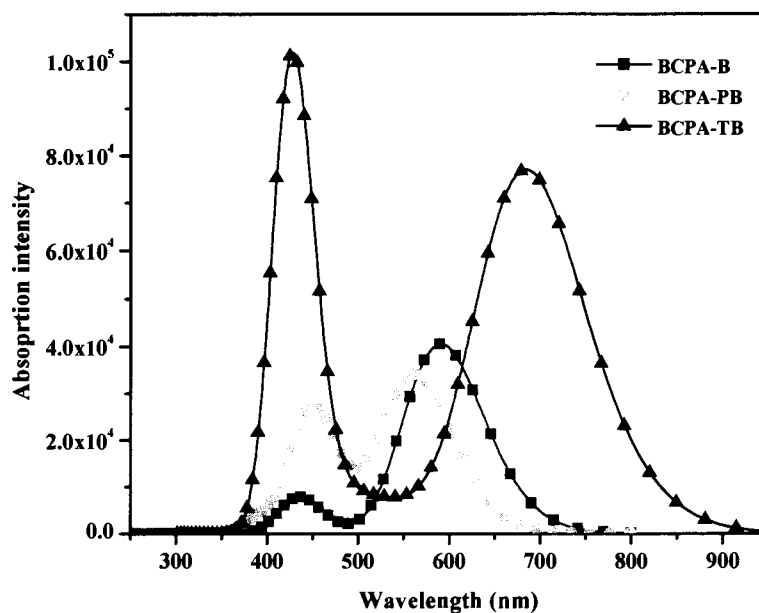


Figure 3.7 Absorption spectra of BCPA-B, BCPA-PB and BCPA-TB target molecule by TD-B3LYP/6-31G(d,p) level in CH_2Cl_2 solvent (C-PCM model)

3.1.2.5 Fluorescence energies

The geometries at the first excited state were optimized at the CIS/6-31G (d,p) level of theory. The important inter-ring distance and dihedral angle parameters are listed in Table 3.4. The emission wavelengths are also calculated by TDDFT method on the basis of optimized excited-state geometries by B3LYP/6-31G (d,p) level. The calculated values of the fluorescence spectra in the gas of **BCPA-Ar** are calculated to be 420, 440, 484, 527, 586, 635 and 593 nm, respectively. From the results indicate that are emission-wavelength are red-shifted with a longer π -conjugation length or stronger electron-withdrawing strength of the central core. Moreover, the emission colors range can be tune from deep blue to red upon illumination.

Table 3.4 Fluorescence energies (E_{flu}) BCPA-Ar series

Molecules	λ_{em} (nm) ^a	f	λ_{em} (nm) ^b
BCPA	420	1.6706	426
BCPA-F	440	2.5082	444
BCPA-T1	484	1.9693	488
BCPA-T2	527	2.3539	517
BCPA-T4	568	2.8869	545
BCPA-B	635	0.8989	601
BCPA-PB	593	0.9791	528

^aCalculated by TDDFT method

^bWavelength emission (λ_{em}) measured according to emission spectra in solution

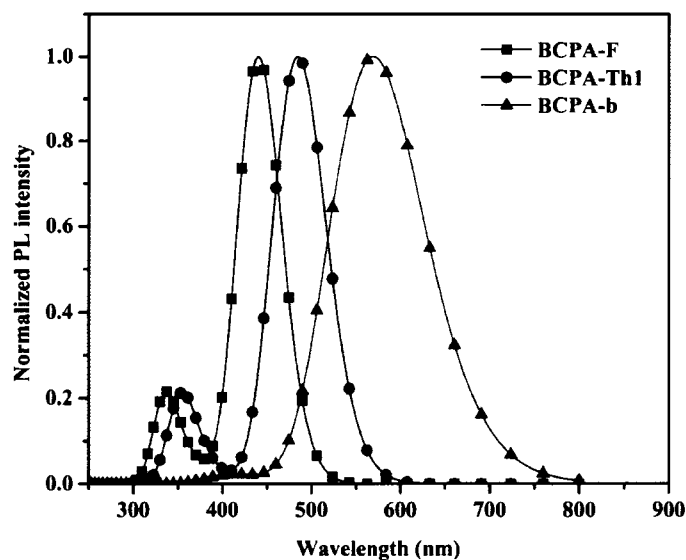


Figure 3.8 Emission spectra of BCPA-B, BCPA-PB and BCPA-TB target molecule

3.2 Naphthalimide derivatives for OLEDs

The development of organic light-emitting diodes (OLEDs) has become one of the most attention topics due to the efficiency of OLEDs need to be improve for their commercialization application. The donor-acceptor (D-A) molecules are promising class of multifunctional materials for OLEDs. The electronics properties of these molecules are closely related to the electronic structures of the emitting molecules, especially those of the excited states of organic compounds can be tune by introducing different fluorophore in the D-A organic materials. Among the various kinds of organic materials, 1,8-naphthalimide (NI) derivatives have been considered as building blocks owing to their chemical stability, a large stokes shift, and high photoluminescence quantum efficiency. Moreover, 1,8-naphthalimide derivatives can be used as electron-transporting or hole-blocking due to these orgainc materials have high electron affinity that are appropriate for balanced carrier injection in OLEDs. Recently, a flat aromatic molecule, pyrene core, has been used as blue emitter in OLEDs with the excellent fluorescence properties. The luminescence properties of the pyrene core might be modulated using the suitable functionalized. Anthracene derivatives have also been used blue light-emitting materials for OLED application due to its narrow band gap and rich electron. However, the substitution of a

fluorophore onto the anthracene core should prevent intermolecular packing which can affect to thermal and electrical stability. Organic molecules containing triphenylamine (TPA) units are of significant importance among the solution-processable amorphous organic molecular materials and have been intensively investigated for the applications in optoelectronic devices. Moreover, TPA derivatives have good optical properties and hole-transporting ability. The theoretical investigation of the electronic structures of emitting materials used in OLED is important for a better understanding of the photoelectronic process, as well as for the design of new analogues with improved performances.

3.2.1 Computational details

In this research, we perform DFT and TDDFT calculations on the ground state of organic material. This computational procedure allows us to provide a detailed assignment of the excited state involved in the absorption process. The geometries in the gas phase were optimized by the DFT method using the B3LYP exchange-correlation function, with 6-31G(d,p) basis set in the Gaussian 09 program package. Electronic population of the HOMO and LUMO were calculated to show the position of localization of electron populations along with the calculated molecular orbital energy diagram. The electronic absorption spectra require calculation of the allowed excitation and oscillator strengths. These calculations were carried out using TDDFT with the same basis set and exchange-correlation functional. The energy gap has been estimated from two ways, namely, HOMO-LUMO energy gap and the first excitation energies. Based on the excited geometries, the first excitation energy (E_g) and the maximal absorption wavelength of all molecules have been performed by using the TDDFT at the same level based on the optimized geometries. The solvent effect for DCM solution was implicitly accounted using conductor-like polarizable C-PCM. In addition, we calculated the lowest singlet-singlet electronic transitions. Subsequently, the absorption properties calculated by TDDFT method were imported into the guessum program to visualize the absorption profiles.

3.2.2 Results and discussion

3.2.2.1 Ground-state geometries of naphthlimide derivatives

The ground state structure of target molecules were optimized by the DFT method using the B3LYP exchange-correlation function with 6-31G (d,p)

basis set. The optimized geometries in the gas phase shown in Figure 3.9. The optimized structures reveal that the naphthimide moieties attached to the end of the molecules adopt a bulky conformation creating nonplanar geometry around the planar could help to prevent the close π - π contact between molecules.

Table 3.5 The selected important inter-ring distances (r , Å) and dihedral angle (Φ , °) of naphthimide derivatives calculated by B3LYP/6-31G(d,p) calculations

Molecule	Distances (r , Å) and dihedral angle (Φ , °)			
	NP	NA	NT	NTB2T
D-A	-71.80	91.48	52.22	-53.52
D-A-D	-	-	-	-53.53

D = Donor, Ar = Acceptor

The optimized structures of all the compounds revealed that the naphthimide moieties attached to donor molecule are nearly perpendicular with the plane of the donor moiety for NP and NA compound. Whereas the dihedral angle between donor and acceptor of NT compound was calculated to be 52° which is smaller than those NP and NA compound. Therefore, π -electron delocalization between those units will be performed smoothly Furthermore, the naphthimide-based material with D-A-D structure was calculated by DFT method. The results reveal that the dihedral angle between donor and acceptor were estimated around 53°. The non-planar geometry with the bulky conformation around the planar π -conjugate backbone could help to prevent the close π - π contact between molecules.

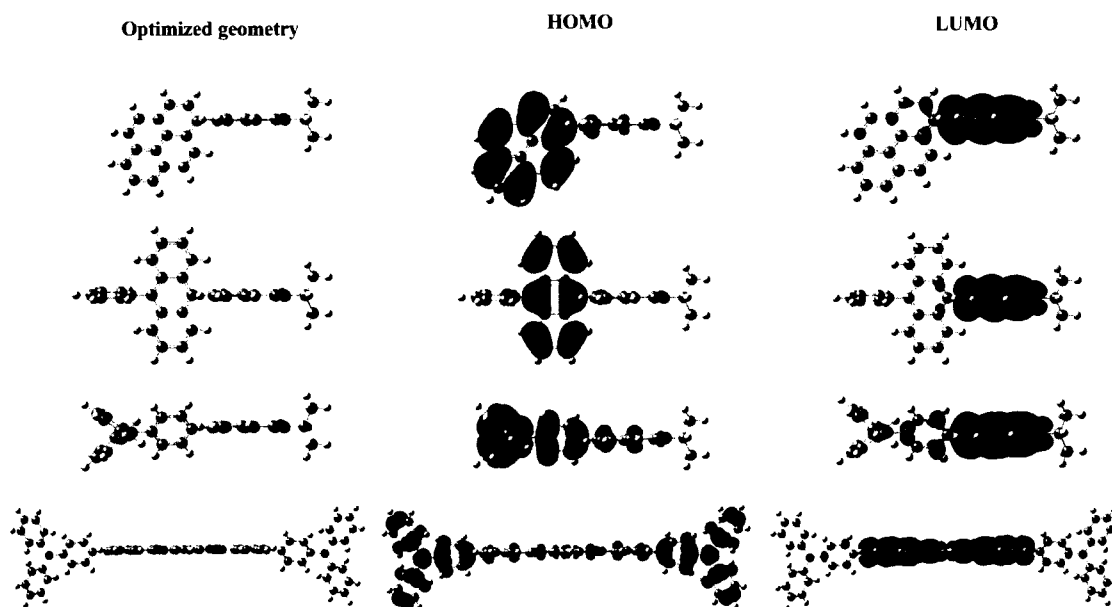


Figure 3.9 Optimized structures and HOMO (left) LUMO (middle) of TPA target molecule

3.2.2.2 Electronic properties naphthimide derivatives

Electronic population of the HOMO and LUMO were calculated to show the position of localization of electron populations along with the calculated molecular orbital energy diagram. The frontier molecular orbitals of all target molecules are shown in Figure 3.9. The electron contribution in their HOMO orbitals of NP, NA and NT are able to delocalize over the donor moieties. As shown in the LOMO orbitals, electrons are delocalized over the naphthimide moieties. As observed in the calculation results, π -electrons are delocalized over the donor, the excited electron transfer through the conjugate system of the naphthimide, which is attributed to the intramolecular charge transfer electronic transition. The HOMOs of the NTBT2 compounds are localized almost entirely on the TPA core. Similarly, only the 1,8-naphthalimide moieties are found to contribute to the LUMOs, As shown, the intramolecular charge transfer of the naphthimide can occur with increasing donor ability, which resulted in the energy gaps being in a sequence of the naphthimide. Therefore, the naphthimide with its narrow energy gap would be an efficient emitter to extend the absorption wavelengths of this organic material. The HOMO–LUMO energy gaps of NP, NA, NT and NTBT2A were determined and the values (2.70–3.20 eV). From these results, the HOMO levels of NP, NA, NT and NTBT2A series are

decrease with extended π -conjugation length which should be good for the hole transport through the molecules when naphthlimide are used as the hole-injecting/hole-transporting materials in the OLEDs.

3.2.2.3 Ionization potential and electron affinity energies

The device performance of OLEDs depends on the charge injection, transfer, and balance as well as the excitation confinement in a device. Thus, the IP and EA are important to investigate which can be used to evaluate the energy barrier for the injection of holes and electrons, and the charge transfer rate and balance. The DFT calculated IP and EA values of NP, NA, NT and NTBT2A target molecule are listed in Table 3.6.

Table 3.6 HOMO and LUMO energies, IP and EA for NP, NA, NT and NTBT2A with the B3LYP/6-31G (d,p) functional (in eV)

Molecules	E_{HOMO}	E_{LUMO}	IP	EA
NP	-5.57	-2.37	6.82	1.30
NA	-5.39	-2.35	6.62	1.25
NT	-5.21	-2.30	6.39	1.21
NTB2T	-5.13	-2.43	5.83	1.69

The IP and EA energy can be adiabatic excitations (optimized structure for both the neutral and charged molecule). The ionization potential of molecule may be computed as: $E(\text{cation}^+) - E(\text{neutral})$, the electron affinity of molecule may be computed as: $E(\text{neutral}) - E(\text{anion}^-)$. The IP and EA are approximate from this below equation.

$$\text{IP} = (E_{\text{total}}(\text{cationic}) + \text{ZPE}(\text{cationic})) - (E_{\text{total}}(\text{neutral}) + \text{ZPE}(\text{neutral}))$$

$$\text{EA} = (E_{\text{total}}(\text{neutral}) + \text{ZPE}(\text{neutral})) - (E_{\text{total}}(\text{anionic}) + \text{ZPE}(\text{anionic}))$$

It can be seen that the IP values of NP, NA, NT and NTBT2A were found to be 6.82, 6.62, 6.39 and 5.83 eV, respectively. The IP values decrease with introducing TPA units as donating group. From the results suggesting that the hole injection and transportation of BCPA-T4 are expected to be easier than the others.

3.2.2.4 Absorption spectra of organic sensitizers

The electronic absorption spectra were carried out using TDDFT method. Comparison of the theoretically calculated wavelength with experimental data has been performed. The corresponding simulated absorption spectra of the naphthlimide are shown in Figure 3.10. The electronic properties, oscillator strengths, conjugations of the orbitals, and the maximum wavelength in the solvent phase of all organic sensitizers are shown in Table 3.7. The strongest absorption peak with the largest oscillator strength arises from $S_0 \rightarrow S_1$ transition and corresponds to the intramolecular charge transfer transition, which is primarily contributed from the HOMO to the LUMO. Beside the good agreement between the calculation and experimental spectra proving the accuracy of the strategy, the calculations allow further insights into the electronic structure for the family of naphthlimide-based light emitting materials with D-A structure, especially the electronic and geometrical structures for the excited states.

Table 3.7 The absorption spectra of naphthlimide derivatives

Dyes	State	Excitation energy (nm)	Oscillator strength (f)	Character	Assignment
NP	$S_0 \rightarrow S_1$	346	0.5519	ICT	HOMO→LUMO
NA	$S_0 \rightarrow S_1$	363	0.4134	ICT	HOMO→LUMO
NT	$S_0 \rightarrow S_1$	365	0.7903	ICT	HOMO→LUMO
NTB2T	$S_0 \rightarrow S_1$	407	2.5383	ICT	HOMO→LUMO

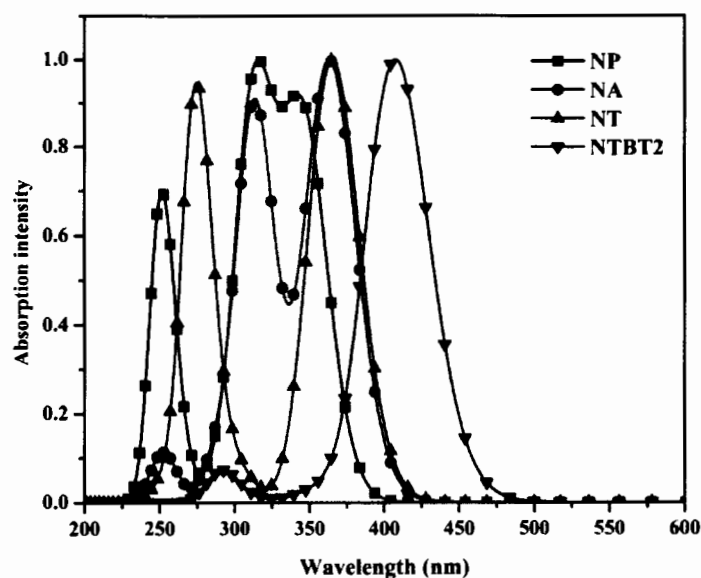


Figure 3.10 Absorption spectra of BCTA by TDCAM-B3LYP/6-31G(d,p) level in CH_2Cl_2 solvent (C-PCM model)

3.1.2.5 Fluorescence energies

The geometries at the first excited state (S_1) were optimized at the CIS/6-31G (d,p) level of theory. The important inter-ring distance and dihedral angle parameters are listed in Table 3.8. The emission wavelengths are also calculated by TDDFT method on the basis of optimized excited-state geometries by B3LYP/6-31G (d,p) level. The calculated values of the fluorescence spectra in the gas of NT and NTBT2A are found to be 635 and 558 nm respectively, the fluorescence spectra as shown in Figure 3.11. From the results indicate that are emission-wavelength are red-shifted with a enhancing of π -conjugation length.

Table 3.8 Fluorescence energies (E_{fl}) naphthimide derivatives

Molecules	λ_{em} (nm) ^a	f	λ_{em} (nm) ^b
NT	492	0.7174	590
NTB2T	558	1.3825	596

^aCalculated by TDDFT method

^bWavelength emission (λ_{em}) measured according to emission spectra in solution

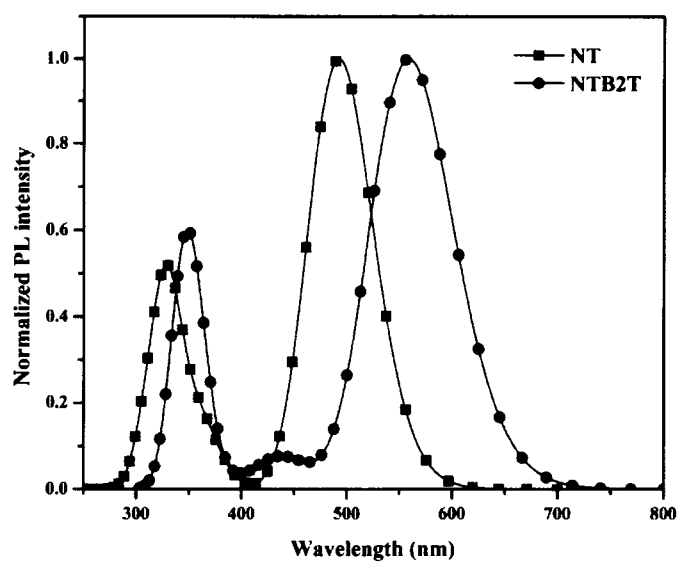


Figure 3.11 Emission spectra of BCTA by TDCAM-B3LYP/6-31G(d,p) level in CH_2Cl_2 solvent (C-PCM model)

CHAPTER 4

THEORETICAL INVESTIGATION OF ORGANIC COMPOUND FOR DSCs APPLICATION

4.1 Porphyrin derivatives for DSCs

For further development of highly efficient porphyrins dye in DSCs has attracted much interest as alternative sensitizer in dye-sensitized solar cells due to their light harvesting ability. The photophysical properties can be modify and tune via optimizing the β -or *meso*-substituents of the porphyrin core. The efficient porphyrin-based sensitizer is the **YD2-oC8**, co-sensitized with an organic dye (**Y123**) on a TiO₂ film using a cobalt-based electrolyte to enhance photovoltage of the device, which shows an overall conversion efficiency of 12.3% under standard AM 1.5 one-sun irradiation. The combination of push-pull porphyrin dye and cobalt redox mediators is an effective way to achieve high-efficiency DSCs. The performance of panchromatic sensitizer SM315 reach to 13.0% at full sun illumination without the requirement of a co-sensitizer [26]. Thus, Zinc porphyrin with push-pull system has considerable attention because of their light harvesting ability which can enhance the power conversion efficiency of DSSCs. The push-pull porphyrin dyes were designed and sensitized with containing a strongly electron-donating such as diphenylamine or triphenylamine moiety as the electron donor [27]. With the employing strong electron donating group, the light-harvesting properties of porphyrin dye possess better in terms of significantly red-shifted and high intensity of Q-band absorption. The conversion efficiencies for push-pull porphyrin dyes are increasing owing to large J_{SC} . Additionally, the porphyrin sensitizers functionalized with various π -spacers were developed to enhanced charge transfer character from the porphyrin ring to the anchoring group [28,29]. The push-pull porphyrin with the strong electron withdrawing moiety can be adsorbed on the TiO₂ surface with the strong electronic coupling and would be more favorable for electron injection into the TiO₂ surface [30-33].

The novel porphyrin dyes were designed and sensitized by introducing of strong donating and strong withdrawing to compose the D- π -A structure. These sensitizer showed significant near-infrared absorption resulting in the highest efficiency of 10% [34]. Therefore, the effect of donor and π -spacer length significantly to improve the efficiency in push-pull ability of porphyrin dye which are very useful to increase efficient for the future development DSSCs. The computational chemistry techniques and especially quantum chemistry offer a competitive alternative for the interpretation of the experimental information [29, 35-37]. So the theoretical investigations of the physical properties of dye sensitizers are very important in order to disclose the relationship among the performance structures and the electronic properties, it is also helpful to design and synthesis novel dye sensitizers with higher performance. Therefore, the aim of this work is to study a series of porphyrin dyes with different electron-donating group (EDG) attached at a *meso*-position for **DPP2**, **TPAP1** and **TPAP2** molecules that compare to **DPP1** dye. Typical electron donors are represented by the substituents with strong electron donating group such as diphenylamine and triphenylamine. The strong electron withdrawing group, benzothiadiazole, is introduced for improve light harvesting efficiency of porphyrin dyes. Furthermore, carboxylic acid and cyanoacrylic acid have been used as anchoring groups in porphyrin sensitizers. Both theoretical calculation and experimental synthesis were reasonably combined to explain more details of the sensitizers, especially electronic structures and excited-state properties.

4.1.1 Computational details

The geometries and electronic structures of porphyrin analogues were theoretical studied based on DFT. Beck's three parameter gradient-corrected hybrid functional and Lee-Yang-Parr correlation functional (B3LYP) with a 6-31G (d,p) basis set were used for fully geometry optimization. The excitation energies for the 20 lowest singlet-singlet transitions were investigated using TDDFT on PBE0 functional. The solvent effect as well as the electrostatic solute-solvent interactions in dichloromethane (CH_2Cl_2) solvent was evaluated using C-PCM. All DFT and TDDFT calculations were carried out using Gaussian09 program package. The UV/Vis absorption spectra were simulated using gausssum program. Electron injection from dye to the conduction band of a metal oxide semiconductor is important for DSSC

performance. The efficiency of the injection process depends on the electronic coupling between the dye and the metal-oxide surface. The adsorption of dyes on the $(\text{TiO}_2)_{38}$ clusters was performed with DFT calculations using DMol³ software.

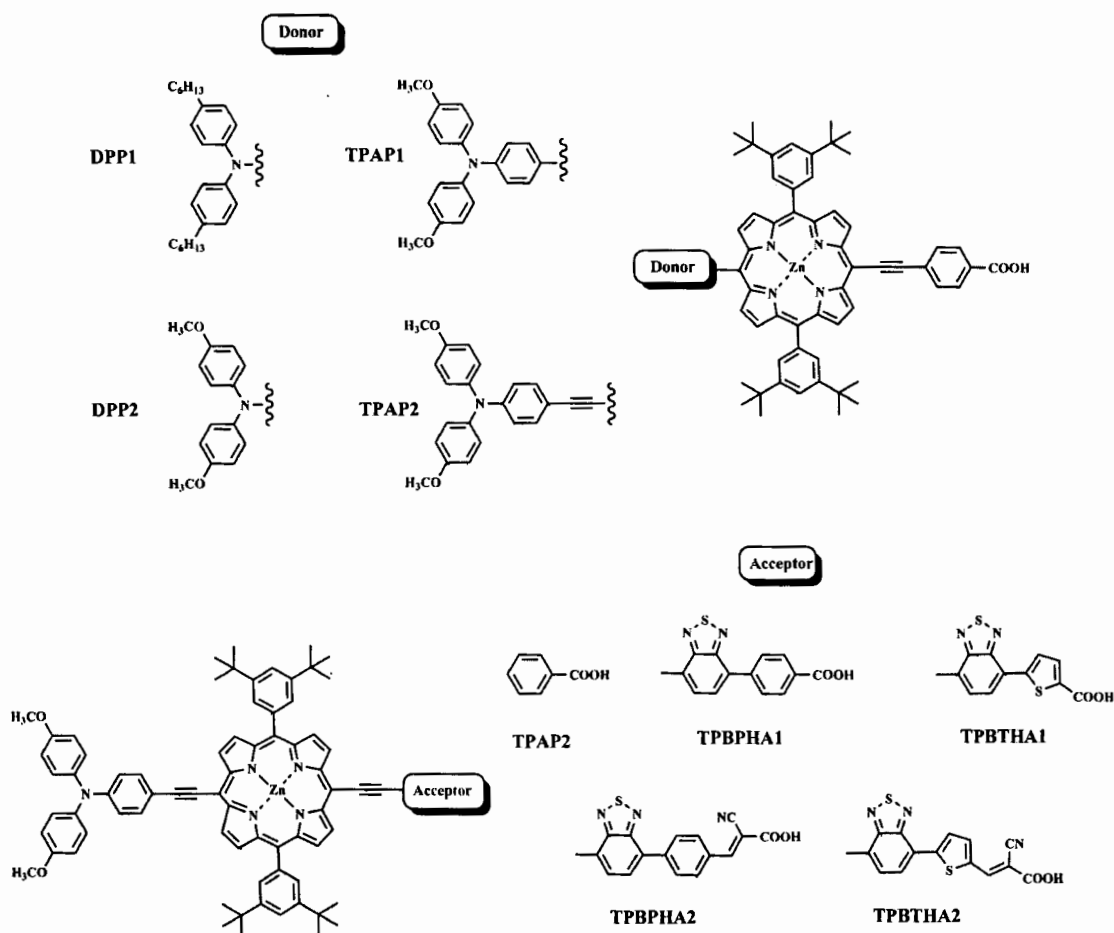


Figure 4.1 Sketch map of porphyrin derivatives

4.1.2 Results and discussion

4.1.2.1 Ground-state geometries of porphyrin derivative

To obtain dyes with improved push-pull performance of porphyrin dye, the molecular structure of porphyrin dye were modified by introducing different donor and acceptor group. The optimized geometries of in their ground-state configurations were calculated by B3LYP/6-31G(d,p) displayed in Figure 4.2.

Table 4.1 The selected important inter-ring distances (r , Å) and dihedral angle (Φ , °) of porphyrin dye calculated by B3LYP/6-31G(d,p) calculations

Molecule		D-P	P-Tr	Tr-Ph	Ph-A1		
DPP1	(Φ)	-70.25	7.56	23.55	0.11		
	(r)	1.43	1.42	1.42	1.48		
DPP2	(Φ)	-68.20	72.59	-58.68	0.09		
	(r)	1.43	1.42	1.42	1.48		
TPAP1	(Φ)	-62.88	68.40	-56.90	-0.03		
	(r)	1.41	1.42	1.42	1.48		
TPAP2	(Φ)	45.15	-73.59	38.66	-0.05		
	(r)	1.40	1.42	1.42	1.42		
		D-P	P-Tr	Tr-BT	BT-Ar	Ar-A1	Ar-A2
TPBPHA1	(Φ)	-48.92	5.71	-3.97	-35.41	-0.39	-
	(r)	1.42	1.41	1.40	1.47	1.48	-
TPBTHA1	(Φ)	-99.19	-7.25	4.92	-1.49	0.05	-
	(r)	1.42	1.41	1.40	1.47	1.48	-
TPBPHA2	(Φ)	-31.26	-1.85	-0.20	-30.85	-	0.81
	(r)	1.42	1.41	1.40	1.47	-	1.48
TPBTHA2	(Φ)	-69.59	-2.11	-0.27	-0.88	-	0.04
	(r)	1.42	1.41	1.40	1.47	-	1.48

D = Donor, P = Porphyrin, Tr = Triple bond, BT = Benzoethiadiazole,

Ar = Benzene or Thiophene, A1 = Carboxylic acid, A2 = Cyanoacrylic acid

Firstly, the replacement of alkyl group by alkoxy group is considered to increasing the donating ability of diphenylamine donor for **DPP2** compound. Moreover, the improving of charge separation between porphyrin and TiO₂ by extending the conjugation length at donor part, triaryl amino group and triple bond were introduced to construct the compound **TPAP1** and **TPAP2**. From the calculation results, we found that adding of bulky donor connected to macrocycle twist the dihedral angle between donor moieties and phenyl ring at *meso*-position of porphyrin which were calculated to be -63.02 and 45.15 degrees for **TPAP1** and **TPAP2**,

respectively. The dihedral angle of donor and porphyrin core of **TPAP1** was decreased when modifying triple bond between TPA donor and macrocycle. The results imply that the adding of different electron donating group connected at *meso*-position in porphyrin analogues twisted the geometric structure of porphyrin core which can be modified to be coplanar structure by adding triple bond between donor and porphyrin core. Our results show that **TPAP2** with modified triple bond is performed stronger ICT than that **TPAP1** compound. The **TPAP2** was selected to explore the influence of the strong electron withdrawing group on photophysical and electronic properties of porphyrin sensitizers.

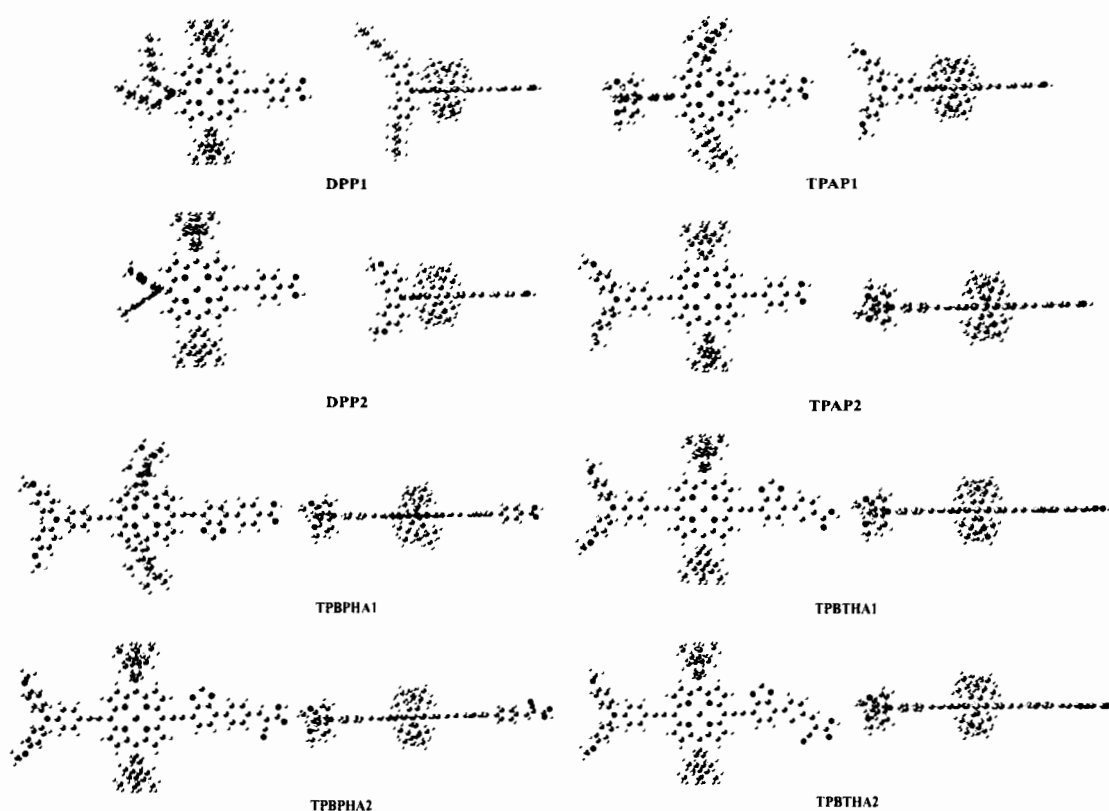


Figure 4.2 Optimized structures of porphyrin target molecule

The push-pull porphyrin was modified by introduced the strong electron withdrawing group to create **TPBPHA1**, **TPBTHA1**, **TPBPHA2** and **TPBTHA2**. The dihedral angle between BTB and benzenoic acid of **TPBPHA1** compound presents twist angle about -35.41 degrees. The twist geometry of porphyrin dye can be reduced by replacing benzene ring with thiophene ring. It was found that the dihedral angle between BTB and thiophene ring was calculated to be 0.81 degrees

which implying that the optimized geometry of **TPBTHA1** dye is more coplanar than **TPBPHA1** dye. The designed porphyrin dye with cyanoacrylic acid, **TPBPHA2** and **TPBTHA2** compound, were also calculated. The structural of **TPBPHA2** and **TPBTHA2** reveal the coplanar geometry when replacing benzene ring with thiophene ring which is the same result with **TPBPHA1** and **TPBTHA1** compound. From the calculation results, the optimized structure of porphyrin dye can be modified by using strong electron donating group and strong electron withdrawing group.

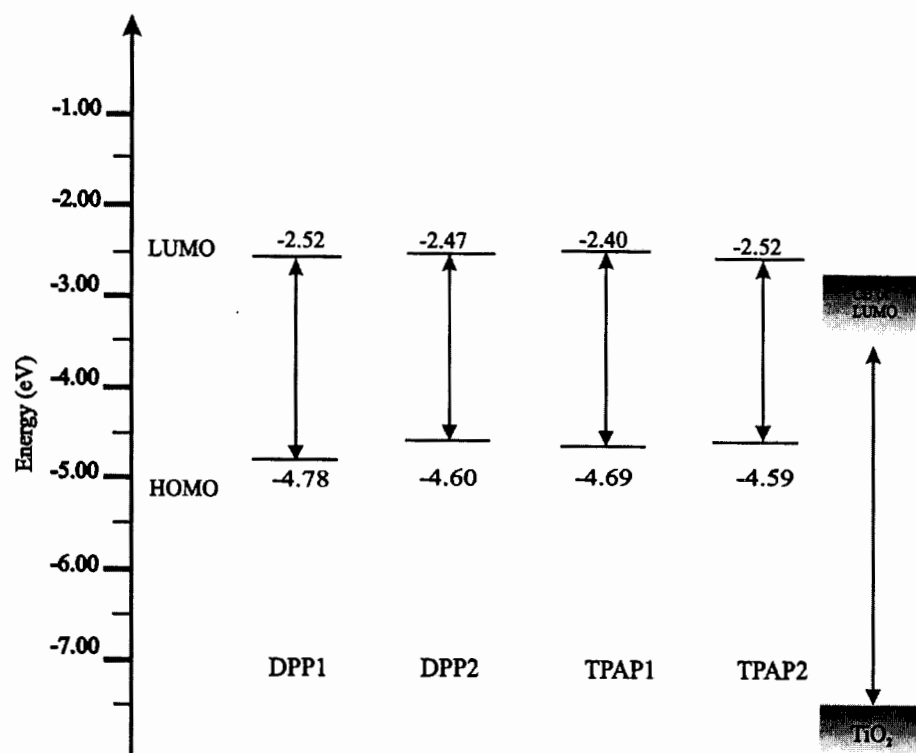
4.1.2.2 Electronic properties of porphyrin derivative

The small torsion angle of donor and acceptor at *meso*-position of porphyrin affect to electronic properties of porphyrin dye which can improve intramolecular charge transfer (ICT). The HOMO-LUMO energy level of all porphyrin sensitizers were computed using B3LYP/6-31G(d,p) level of theory. The molecular orbital diagram is shown in Figure 4.3. The calculated HOMO-LUMO gaps of **DPP1**, **DPP2**, **TPAP1** and **TPAP2** are 2.26, 2.13, 2.29 and 2.07 eV respectively. It is found that adding of electron donating group in **DPP2**, **TPAP1** and **TPAP2** decrease the HOMO-LUMO gap compared with **DPP1**. From the calculated results show that substitution of electron donating group in **DPP2-TPAP2** can destabilize HOMO level. We have also examined the effects of substituents different linker and acceptor on the electronic properties of porphyrin sensitizer. The LUMO energy levels of porphyrin dyes with strong electron withdrawing group, **TPBPHA1-TPBTHA2**, are lower than **TPAP2** reference dye without strong electron withdrawing group.

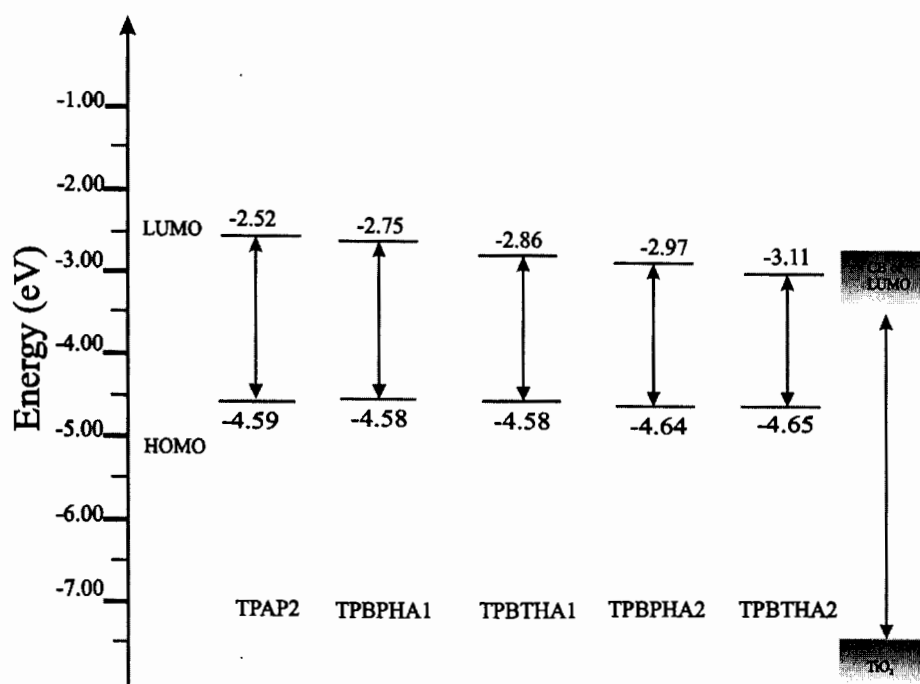
As mention above, for a high-efficiency sensitizer of DSSCs, the LUMO energies of dyes must be slightly placed above the conduction band of TiO₂ and the HOMO energies of dyes must be properly located under the redox couple of I⁻/I₃⁻ electrolyte. The energy level diagram of demonstrates that the HOMO energies of all analogues are closed to the redox couple of I⁻/I₃⁻ and LUMO lied above CB of TiO₂ which is effective electron regenerations of the oxidized porphyrin dyes in DSSC devices. Furthermore, the LUMO energy levels of the designed porphyrins are lower than the CB of TiO₂, leading to provide the driving force for electron injection from the excited state of the porphyrin dye into the CB of semiconductor. The frontier molecular orbitals of the porphyrin dyes are shown in Figure 4.3. The calculated the HOMOs level, the LUMOs level and percentage contribution of frontier molecular

orbital of all target molecule are list in Table 4.2. For porphyrin dye with different donor, It can be seen that the HOMOs level is a delocalized π orbital over the donor group and porphyrin macrocycle, whereas the LUMOs level is π^* orbital which π -electron is localized on porphyrin core and anchoring group. Therefore, this distribution of the HOMO and LUMO is separated in the donor and acceptor part of compounds, indicating that the HOMO \rightarrow LUMO transition can be considered as an intramolecular charge transfer (ICT) transition and π - π^* transition.

Obviously, the charge separation, the electron density of each part was shown in Table 4.2. Electron density distribution of HOMO state for **DPP2-TPAP2** is mainly located at the donor group which is calculated to be 63%, 70% and 57% and the porphyrin core calculated to be 32%, 25% and 37%, respectively. These results indicate that the electron density of HOMO is mainly located on donor and porphyrin core. For the LUMOs level, the macrocycle calculated to be 77%, 76% and 72% and the percentage contributions of linker and acceptor part are calculated to be 20%, 22% and 17% in for in **DPP2-TPAP2** respectively, which is mainly delocalized on macrocycle part. From these results, the excited electrons move from the electron donor moiety to the electron acceptor unit. It is note that electron contributions are mostly delocalized on the macrocycle implying that the single excited state of these molecules could be considered as an intramolecular charge transfer (ICT) transition and π - π^* transition from donor to acceptor along through porphyrin core and the π -conjugated bridge.



(a)



(b)

Figure 4.3 Molecular orbital energy diagram of porphyrin target molecule

Table 4.2 Summarizes the Energies and Character of Frontier Orbitals of porphyrin dye Calculated by B3LYP/6-31G (d, p)

Molecule	Molecular orbital	Energy (eV)	E_{gab}	Percentage composition		
				Donor	Porphyrin	Linker-acceptor
DPP1	LUMO	-2.52	2.26	3	77	20
	HOMO	-4.78		48	44	8
DPP2	LUMO	-2.47	2.13	3	77	20
	HOMO	-4.60		63	32	5
TPAP1	LUMO	-2.4	2.29	2	76	22
	HOMO	-4.69		70	25	5
TPAP2	LUMO	-2.52	2.07	10	72	17
	HOMO	-4.59		57	37	6
TPBPHA1	LUMO	-2.75	1.83	5	32	64
	HOMO	-4.58		54	37	8
TPBTHA1	LUMO	-2.86	1.72	14	24	72
	HOMO	-4.58		51	39	10
TPBPHA2	LUMO	-2.97	1.67	3	20	78
	HOMO	-4.64		57	35	8
TPBTHA2	LUMO	-3.11	1.54	2	16	81
	HOMO	-4.65		56	34	9

All values are reported in eV.

^aCalculations are performed with B3LYP/6-31G (d,p) in

For the series of different π -spacer and acceptor, the HOMOs level are a delocalized π orbital over the donor and porphyrin ring, while the LUMOs level are π^* orbital that localized in π -spacer and acceptor part. The percentage contributions of donor are calculated to be 54% and 51% and the electron density of linker are calculated to be 37% and 39% for in **TPBPHA1** and **TPBTHA1** respectively. For the LUMOs level, the percentage contributions of linker, **TPBPHA1**

and TPBTHA1 compound, are calculated to be 64% and 72% for porphyrin dye with BTD unit. Obviously, the electron contribution of TPBPHA2 and TPBTHA2 dye are 56-57% for donor part and 34-35% for porphyrin core. The percentage contributions of BTD and acceptor are calculated to be 78% and 81% are with respect to TPBPHA1 and TPBTHA1. It was found that the excited electrons transfer from the electron donor to the electron acceptor unit indicating that the excited state of these organic dyes could be considered as the ICT transition. These results suggesting that the ICT properties of porphyrin dye occur by introducing BTD unit. Therefore, it is suggesting that the strong electron withdrawing group is useful for improving intramolecular charge transfer of our dye molecules. Furthermore, carboxylic acid acceptor is replaced by cyanoacrylic acid can pull electron from the donor and porphyrin core that can increase electron injection from porphyrin dye to TiO₂ surface. The power conversion efficiency of porphyrin dye can enhance by adding strong electron withdrawing group due to their good push-pull ability.

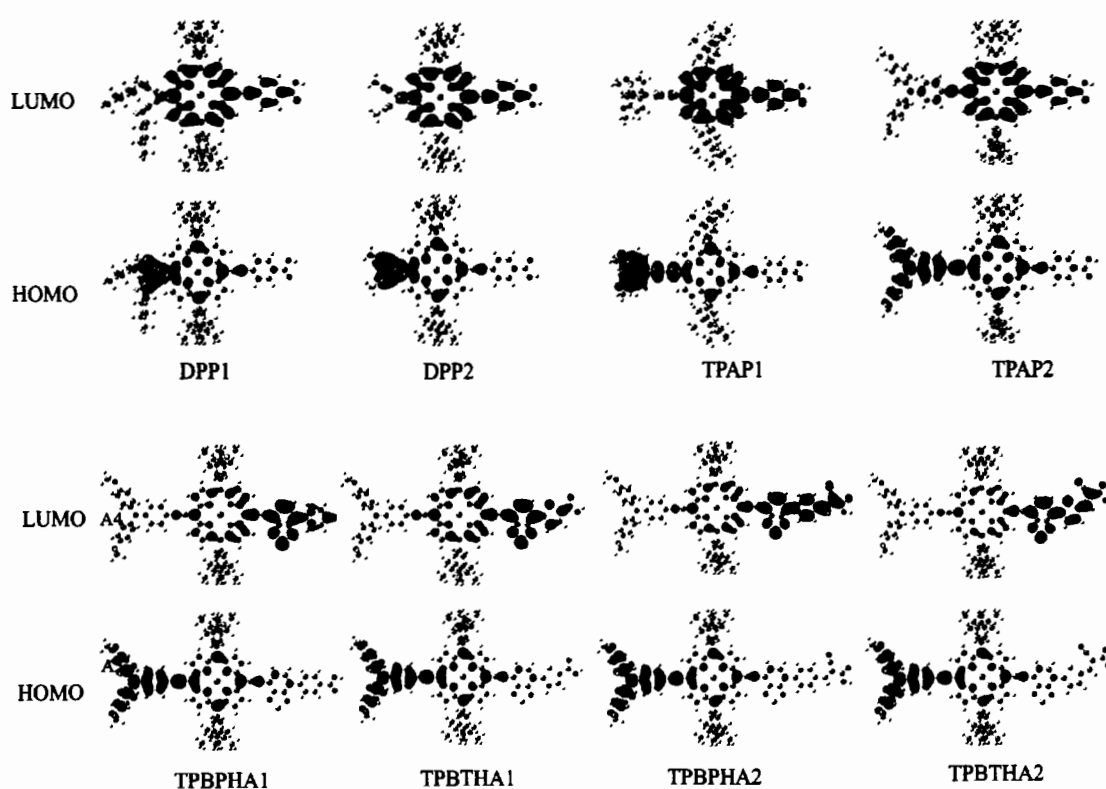


Figure 4.4 Frontier molecular orbital of porphyrin target molecule

4.1.2.3 Absorption spectra of organic sensitizers

The light-harvesting efficiency and absorption coverage is an important parameter that affect to the generated photocurrent. We performed TDDFT calculations to determine the optical properties of porphyrin dye. The calculated maximum absorption wavelengths (λ_{\max}), oscillator strengths (f), and electronic transitions for porphyrin dyes are listed in Table 4.3. The porphyrin macrocycle is connected with an electron donor (D) and an electron acceptor (A) at *meso*-position represent of the push-pull systems. The porphyrins molecule exhibit typical metalloporphyrin features which are high intensity called soret-band and the low intensity called Q-band. The UV/Vis absorption spectra of studied porphyrin dyes are shown in Figure 4.5.

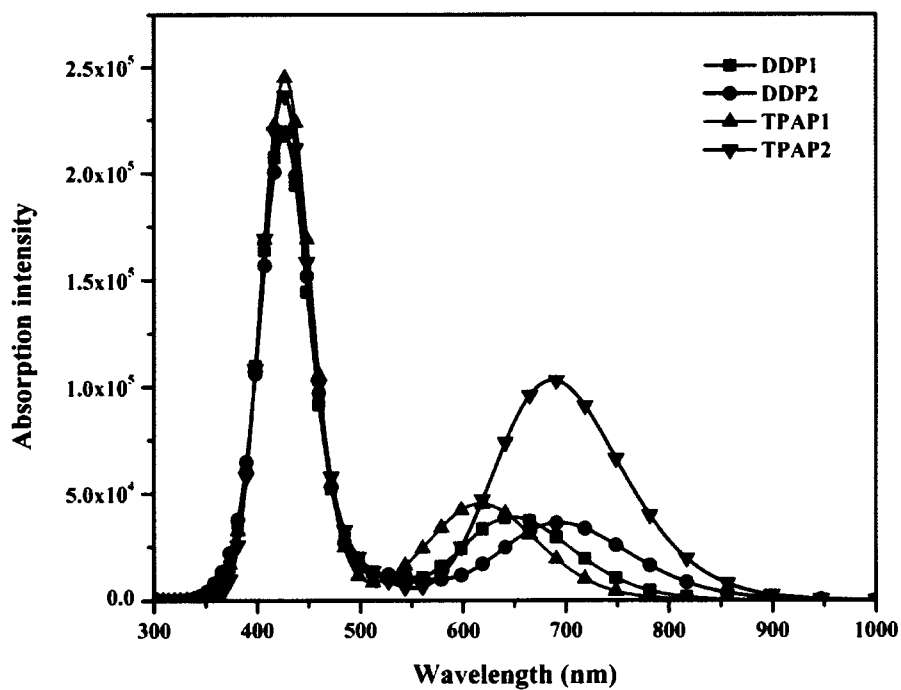
The absorption spectra of **DPP1**, **DPP2** **TPAP1** and **TPAP2** molecules are about 649-687 nm that could be attributed to mixed transition between intramolecular charge transfer (ICT) and π - π^* transition. The strong absorption peak of porphyrin dye with different donor are about 427-430 nm which are attributed to π - π^* transition. The absorption of **TPAP2** is the most red-shifted which is compared to the other porphyrin dye. Therefore, the results assume that the introduction of triple bond link between triphenylamine donor and porphyrin core can increases the π -conjugation length of porphyrin dye. Among these photosensitizes with strong electron donating ability of triphenylamine unit, the **TPAP2** dye presents the longest maximum absorption wavelength which is an advantageous spectral property for light harvesting of the solar spectrum.

To enhance the push-pull ability of porphyrin dye, **TPAP2** molecule was modified by introducing the strong electron withdrawing group. The absorption spectra of **TPBPHA1-TPBTHA2** molecules are about of 698-856 nm that could be attributed intramolecular charge transfer (ICT) transition. The strong absorption peak of porphyrin dye with different donor are about 421-493 nm which are attributed to π - π^* transition It was found that the soret-band and the Q-band of the design dye are more red-shifted than the referent dye (**TPAP2**). The result indicating that absorption the series of different π -spacer and acceptor can harvest sun light in the range of UV to near-IR region that are matching with high photon flux of solar

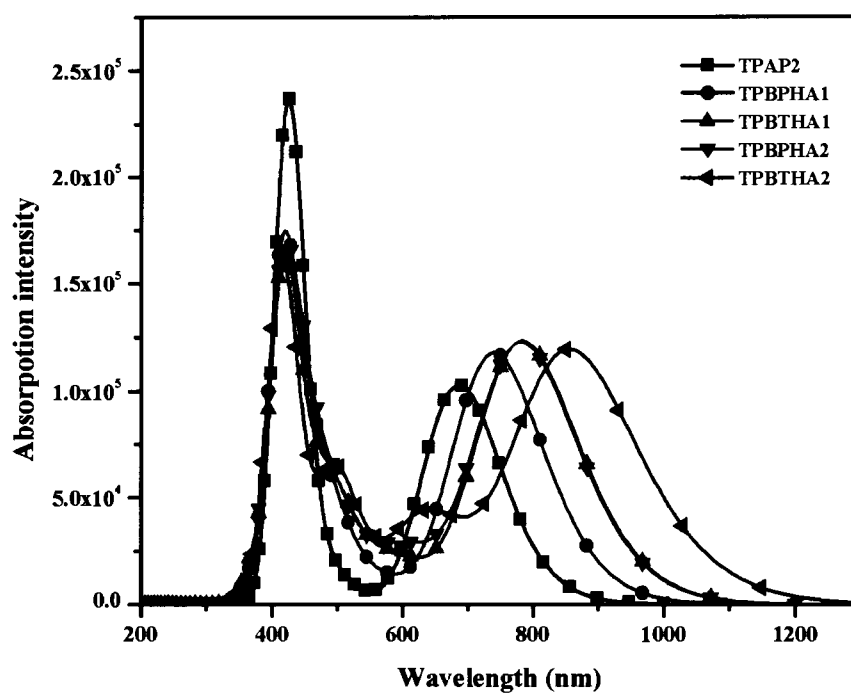
spectrum. From this reason, **TPBTHA2** compound is expected to be the efficient sensitizer for DSCs application.

Table 4.3 The excitation energies, oscillator strengths, and molecular compositions for the 2 lowest states of porphyrin by PBE0/6-31G(d,p)

Dyes	State	Excitation			Assignment	Exp (nm)
			energy (eV, nm)	<i>f</i>		
DDP1	S ₀ →S ₁	Q	1.91 (649)	0.5305	HOMO→LUMO (0.67)	648
	S ₀ →S ₅	B	2.90 (428)	1.8577	H-1→L+1 (-0.52)	444
DDP2	S ₀ →S ₁	Q	1.78 (695)	0.4905	HOMO→LUMO (0.68)	664
	S ₀ →S ₅	B	2.88 (430)	1.6361	H-2→L+1 (0.51)	440
TPAP1	S ₀ →S ₁	Q	1.99 (622)	0.5842	HOMO→LUMO (0.67)	628
	S ₀ →S ₅	B	2.90 (428)	1.9771	H-2→L+1 (0.57)	443
TPAP2	S ₀ →S ₁	Q	1.80 (687)	1.4206	HOMO→LUMO (0.68)	672
	S ₀ →S ₅	B	2.91 (427)	1.6269	H-2→L+1 (0.55)	449
TPBPHA1	S ₀ →S ₁	Q	1.67 (740)	1.6273	HOMO→LUMO (0.68)	N.A.
	S ₀ →S ₉	B	2.98 (417)	1.0789	H-2→L+1 (0.52)	
TPBTHA1	S ₀ →S ₁	Q	1.58 (784)	1.7003	HOMO→LUMO (0.69)	N.A
	S ₀ →S ₉	B	2.94 (421)	1.0725	H-2→L+1 (0.50)	
TPBPHA2	S ₀ →S ₁	Q	1.59 (782)	1.6924	HOMO→LUMO (0.68)	N.A
	S ₀ →S ₁₁	B	2.73 (421)	0.8041	H-1→L+2 (0.49)	
TPBTHA2	S ₀ →S ₁	Q	1.45 (856)	1.6452	HOMO→LUMO (0.69)	N.A
	S ₀ →S ₁₁	B	2.95 (421)	1.1065	H-2→L+1 (0.49)	



(a)



(b)

Figure 4.5 Absorption spectra of porphyrin target molecule

4.1.2.4 The dye adsorption and electron injection

Dye structures were adsorbed on $(\text{TiO}_2)_{38}$ clusters under vacuum and optimized using the Dmol₃ software program. Optimization geometry was calculated using the single point TD-DFT method, For TiO_2 semiconductor surface, we used $(\text{TiO}_2)_{38}$ clusters obtained by cutting an anatase 101 surface; this surface is the most stable and most typically observed surface for this material.

On the titanium-oxide surface, bidentate chemisorption of the dye arises from acidic dissociation of carboxylic acid anchoring groups. In this adsorption mode, a proton transfers from the carboxylic acid to the metal oxide surface, and bond formation occurs between carboxylate oxygen atoms and the surface titanium atoms. The $(\text{TiO}_2)_{38}$ configurations were fully optimized using the generalized gradient-corrected approximation (GGA) method. The Perdew-Burke-Ernzerhof (PBE) functional was used with the DNP basis set to account for exchange-correlation effects. The adsorption energies (E_{ads}) of dyes on the $(\text{TiO}_2)_{38}$ clusters were calculated by using Equation 3

$$E_{\text{ads}} = E_{\text{dye}} + E_{\text{TiO}_2} - E_{\text{dye} + \text{TiO}_2} \quad (3)$$

Where E_{dye} is the total energy of isolated dye, E_{TiO_2} is the total energy of the $(\text{TiO}_2)_{38}$ cluster, and $E_{\text{dye} + \text{TiO}_2}$ is the total energy of the dye- $(\text{TiO}_2)_{38}$ complex.

A positive value for E_{ads} indicates that stable adsorption of porphyrin on TiO_2 surface. Bond lengths and adsorption energies (E_{ads}) for the TiO_2 -coumarin dye complexes were determined. The Ti-O bond distances were calculated to be 2.12-2.15 Å. The adsorption energies (E_{ads}) of all porphyrin-based dyes were found to be in the range of 17.05-17.66 kcal/mol suggesting strong coupling between porphyrin dye and the TiO_2 surface. For improved the electron injection transfer from dye to the conduction bands of TiO_2 , the orientation of the adsorbed porphyrin dye relative to the TiO_2 surface should be perpendicular with respect to metal oxide surface. The previous research suggested that the *para*-carboxyphenyl substituent the porphyrin -system orthogonal to the TiO_2 surface which is contributes to the increase of photocurrent and power conversion efficiency. The *para* porphyrin derivative with the long edge-to-edge distance between porphyrin-core and the TiO_2 surface revealed

the slow charge recombination [38]. Thus, the edge-to-edge distance between porphyrin-core and the TiO_2 surface was measured to understand the electron transfer between the edge of the porphyrin core and the TiO_2 surface [39]. As present in Figure 4.5., the distance between the edge of the porphyrin core and the surface was calculate to be 12 and 15 Å for **TPBTHA1** and **TPBTHA2** compound, respectively. The dye- TiO_2 -distanc of porphyrin dye with cyanoacrylic acid, **TPBTHA2** compound, is longer than the porphyrin dye without cyanoacrylic acid, **TPBTHA1** compound. From this reason, **TPBTHA2** compound should be slow recombination that can enhance the efficiency of DSSCs device.

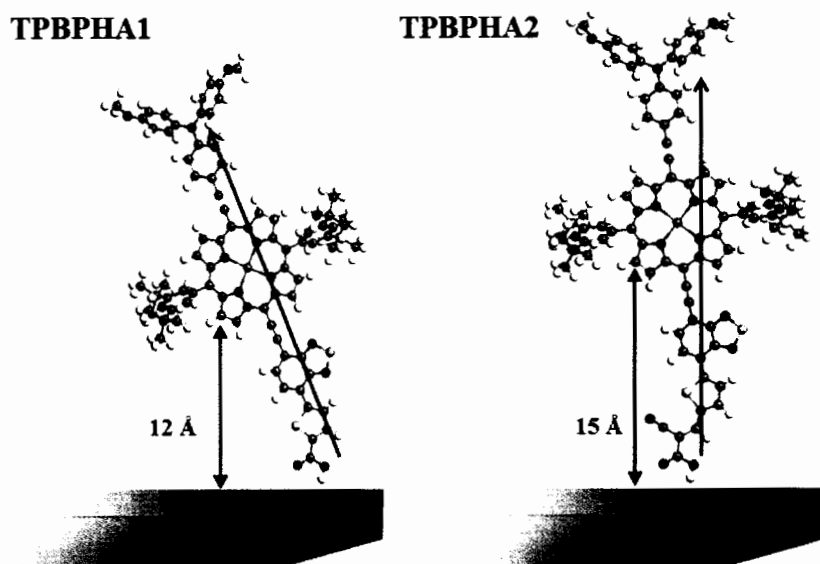


Figure 4.6 The distance between the edge of the porphyrin core and the surface

Additionally, we calculated excited state properties using TDCAM-B3LYP with the 6-31G(d,p) basis set, we chose the **TPBTHA1@TiO₂** and **TPBTHA2@TiO₂** complexes are chosen to display the effect of different anchoring group for push-pull porphyrin system. Comparison of the electronics excitation energy between **TPBTHA1@TiO₂** and **TPBTHA2@TiO₂**, we found that **TPBTHA2@TiO₂** display red-shift of spectra wavelength in the ICT peak. The strong ICT absorption band can improve the light-harvesting properties of the push-pull porphyrin dye, which can provide higher efficiency for this porphyrin sensitizer.

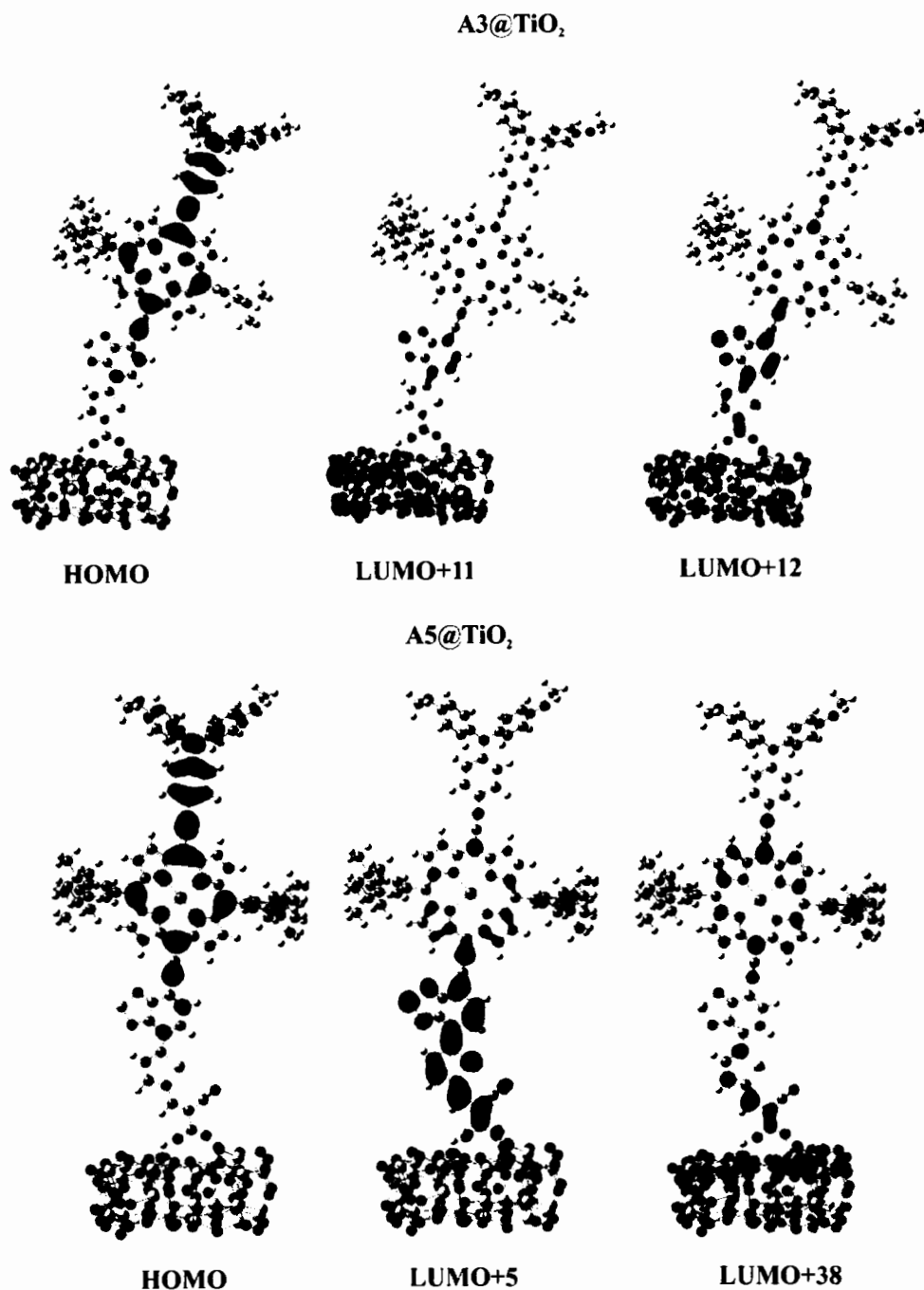


Figure 4.7 Frontier molecular orbital of porphyrin dye adsorbed on TiO₂ in gas phase calculated by CAM-B3LYP/6-31G(d,p) on Dmol₃ geometry

The electron injection from dye to TiO₂ surface display in Figure 4.6 which is the most relevant to the transitions represented. The strongest transition in the dyes is a linear combination of electronic configurations; the greatest oscillator

strength for **TPBTHA1@TiO₂** is a linear combination of 0.25(H→L+11), 0.36(H→L+12) and the excitation of **TPBTHA2@TiO₂** arises from the 0.53(H→L+5), -0.16(H→L+38) linear combination. Applying the TDDFT approach reveals that the lowest excited state with the greatest oscillator strength arises from orbitals on the donor and porphyrin core to orbitals delocalized over the acceptor (A) and the (TiO₂)₃₈ clusters. Thus, electron excitation in this system directly induces electron injection from the dye into the conduction band of TiO₂. Due to the orientation of porphyrin dye on TiO₂ surface of **TPBTHA2@TiO₂** is slightly tilted, the electron injection pathway is more effective than **TPBTHA1@TiO₂**. Our theoretical study suggests that cyanoacrylic acid is suitable for push-pull porphyrin system which can decrease recombination and increase electron transfer from dye to TiO₂ surface.

4.2 Coumarin derivatives for DSCs

Coumarin dyes are strong metal-free organic dye candidates because of their excellent photoelectric conversion efficiency [40] and coumarin-dye-based DSCs were first reported by Hara et al in 2001.[41] The group inserted a methine bridge (-CH=CH-) into coumarin C343 (%PCE = 0.9%) to form two new dyes: **NKX-2510** and **NKX-2311**. The absorption spectra for these dyes are appreciably red-shifted compared to **C343** and appear in the visible region, providing conversion efficiency of 4.7% and 5.6%, respectively.[42] Introduction of bulky substituents to prevent aggregation increases efficiency to 6.7% for **NKX-2753**.[43] Hara et al. extended the π -conjugation system using a thiophene moiety to provide a conversion efficiency of 7.7% for **NKX-2677**.[44] These reports suggest that further chemical modification of these coumarin-based dyes could provide even greater conversion efficiencies. Thus, a theoretical analysis of the electronic structure, photophysical properties, and electron injection mechanism for this series of dyes will facilitate further development in this area. Current molecular modeling techniques and quantum chemistry calculations in particular, offer a competitive alternative to empirical research for the interpretation of experimental data. Theoretical investigations into the physical properties of dye sensitizers are very important to determine relationships between performance, structure, and properties, and are helpful in the design and synthesis of novel high-performance dye sensitizers. We used DFT and TDDFT method to investigate the

ground-state and excited-state electronic structures including optical properties of dye sensitizers. Our theoretical prediction will be useful and helpful for the design and synthesis of new novel molecular materials [45-47].

Our aim in this study was to enhance the light-harvesting performance of coumarin-based sensitizers, using the **NKX-2510** dye as the reference material for comparison. Figure 4.6 shows the chemical structures of coumarin-based sensitizers incorporating thiophene or benzothiadiazole (BTD) moieties used in this study. Generally, D- π -A molecules possessing short π -conjugated chains only absorb at short wavelengths, while longer π -conjugated dye molecules tend to undergo unfavorable π -stacking.[42, 48-50]. The Incorporation of an additional electron-withdrawing unit extends the length of the π -conjugated system [51, 52]. However, the extended system possesses a D-A- π -A configuration, which does not undergo unfavorable π -stacking. Additionally, the extended π -system absorbs at longer wavelengths than the unmodified D- π -A systems does, resulting in improved electron transfer and greatly enhanced light harvesting properties. Consequently, we used DFT and TDDFT to design two novel D-A- π -A dyes: **NCBTA** and **NCBT2A**, and a D- π -A- π -A dye, **NCTBTA**. We investigated the effects of BTD on photophysical and photovoltaic properties, intramolecular charge transfer rates, optical properties, and differences in the energy gaps between the organic sensitizers.

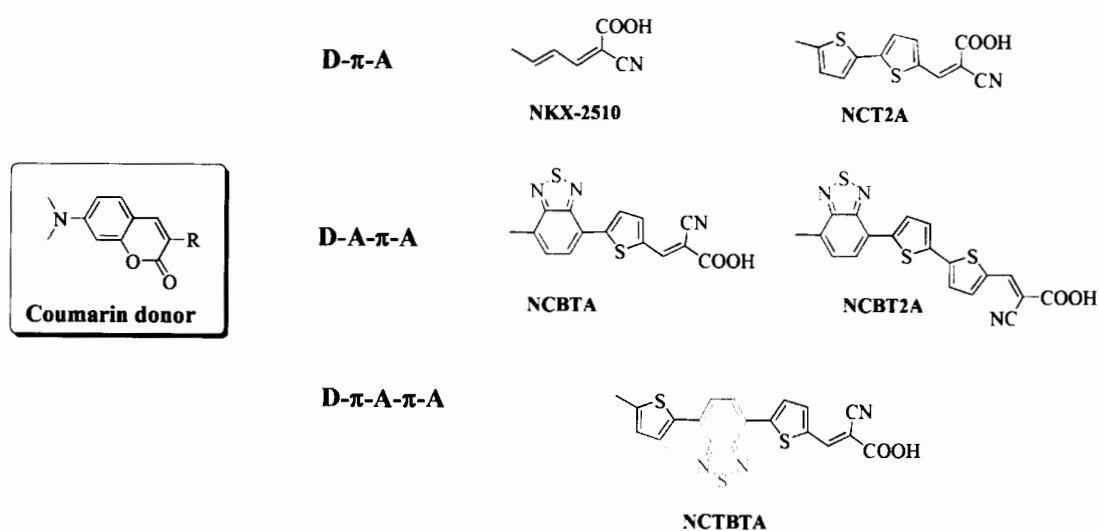


Figure 4.8 Structures of the D- π -A, D-A- π -A, and D- π -A- π -A dyes

4.2.1 Computational details

DFT and TDDFT calculations were performed to optimize organic dye ground state structures by using the Gaussian 09 software program [53]. The ground state structures of all target molecules were calculated by DFT, using the B3LYP exchange–correlation function, with the 6-31G (d,p) basis set [54]. HOMO and LUMO electronic populations were calculated to show localized electron populations and to construct molecular orbital energy diagrams. The optimized structures were employed to estimate the photo-physical properties of the organic sensitizers at the same level of theory. Theoretical calculations were performed to determine allowed excitation and oscillator strengths using TDDFT, with a range-separated CAM-B3LYP functional [55, 56]. Absorption spectra were calculated for all organic dyes using the the GausSum program [57] and the results of reference dye, **NKX-2510**, was compared with experimental data. Solvation effects for dichloromethane were included by applying the C-PCM [46, 58-61]. This computational approach provides a detailed assignment of the excited state associated with a given absorption process. The electron densities of all molecules (for both the ground and the excited states) were generated on a grid of points using the cubegen utility provided by the Gaussian package. For the electron injection capability of dyes, the adsorption of coumarin dyes on the $(\text{TiO}_2)_{38}$ cluster was optimized by DFT calculations using DMol³ program [62] in Materials Studio version 5.5. We used $(\text{TiO}_2)_{38}$ clusters obtained by cutting an anatase 101 surface this surface is the most stable and most typically observed surface for this material.

4.2.2 Results and discussion

4.2.2.1 Ground-state geometries of coumarin derivative

The optimized structures for the gas-phase coumarin-based dyes, and Table 4.4 lists selected bond distances (r) and dihedral angles (ϕ). Calculations reveal planar geometries for the D- π -A configuration **NKX-2510** and **NCT2A** optimized structures. Calculated dihedral angles for these dyes are all less than 1 degree for the entire backbone. Therefore, a thiophene moiety, which is a small and rigid unit, connected to the planar coumarin dye donor can maintain a planar conformation. Planarity increases the π -conjugation length, and facilitates charge-transfer between donor and acceptor groups.

Table 4.4 Selected bond distances (r , Angstroms) and dihedral angles (Φ , degrees) for Coumarin dyes, calculated using B3LYP/6-31G(d,p)

D-π-A		D-π		π_1-π_2	π-A
NKX-2510	Dihedral (Φ)	-0.01	-	-	0.00
	Distance (r)	1.46	-	-	1.42
NCT2A	Dihedral (Φ)	0.34	-	-0.33	0.01
	Distance (r)	1.46	-	1.44	1.42
D-A-π-A		D-A_1	A_1-π_1	π_1-π_2	π-A
NCBTA	Dihedral (Φ)	23.08	0.23	-	-0.03
	Distance (r)	1.47	1.46	-	1.43
NCBT2A	Dihedral (Φ)	22.66	4.51	-1.11	0.09
	Distance (r)	1.47	1.45	1.43	1.42
D-π-A-π-A		D-π_1	π_1-A_1	A_1-π_2	π_2-A
NCTBTA	Dihedral (Φ)	-0.12	0.11	0.22	-0.01
	Distance (r)	1.47	1.45	1.43	1.42

To modify the D-A- π -A dye structure, we incorporated a BTB moiety as an auxiliary acceptor in a π -bridged segment between the coumarin donor and the thiophene linker to form the NCBTA and NCBT2A dyes. The side views of NCBTA and NCBT2A show that the BTB auxiliary acceptor disrupts the planarity present in the D- π -A molecules; the calculated dihedral angles between the coumarin donor and BTB (D- A_1) for NCBTA and NCBT2A are approximately 23 degrees. In contrast to thiophene, our calculated results reveal that the larger BTB moiety disrupts molecular planarity when connected directly to the coumarin donor. Interestingly, positioning BTB at the center, between thiophene and the thiophene ring to form NCTBTA, provides the D- π -A- π -A architecture, which exhibits an almost perfect coplanar conformation; all dihedral angles along the NCTBTA spine are close to zero. Thus, the positioning of BTB within the molecule has a profound effect on the planarity of these dye molecules. The almost perfect planarity calculated for the NCTBTA molecule extends the π -conjugation system across the entire molecule, and thus will improve the light harvesting efficiency of this organic dye

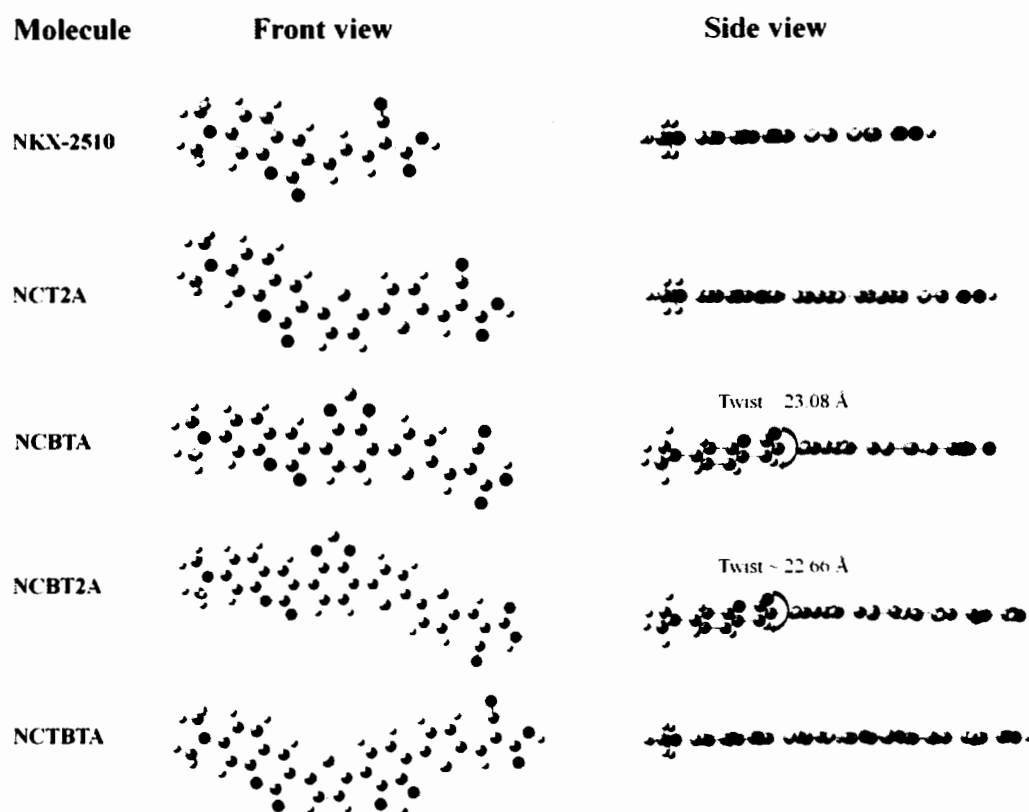


Figure 4.9 Optimized structures of the D- π -A, D-A- π -A, and D- π -A- π -A dyes

3.2.2.2 Electronic properties of triphenylamine derivative

We performed DFT and TD-DFT calculations to determine the electronic properties of coumarin-based dyes. Figure 4.7 shows calculated HOMO and LUMO orbitals for these dyes. Alignment of the HOMO and LUMO energy levels is a crucial factor for an efficient DSSC dye. To ensure effective electron injection from the excited dye into the TiO₂ conduction band (CB), the LUMO energy level of the dye must be greater than that of the conduction band edge. Additionally, the HOMO energy level of the dye should be less than the redox potential of I⁻/I₃⁻ redox couple for efficient regeneration of the oxidized dye following photo-induced electron injection into the TiO₂ film. Table 4.5 lists the calculated HOMO-LUMO energies for the coumarin-based dyes used in this study, and Figure 4.9 illustrates the dye HOMO-LUMO energy levels. The figure shows that HOMO levels of all dyes are below the redox potential of the electrolyte (-4.8 eV).[63]

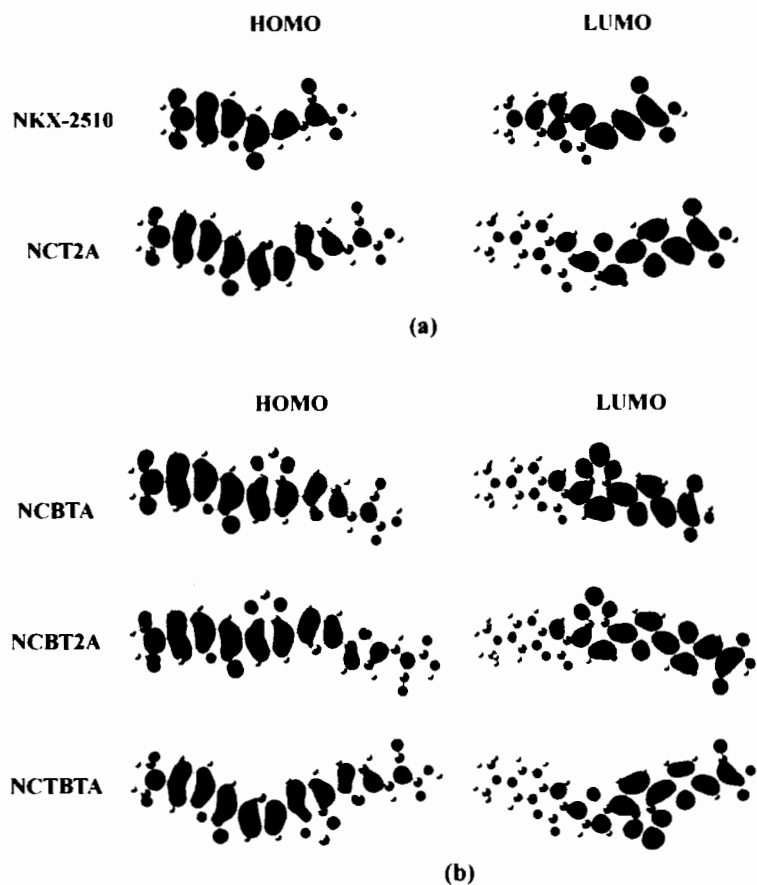


Figure 4.10 Frontier molecular orbitals for (a) D- π -A and (b) D-A- π -A calculated using CAM-B3LYP/6-31G(d,p)

Table 4.5 Calculated HOMO, LUMO, and HOMO-LUMO orbital energies, and energy gap (Δ_{H-L}) for coumarin dyes

Dyes	HOMO ^[a]	LUMO ^[a]	Δ_{H-L} ^[a]
NKX-2510	-5.62	-2.80	2.82
NCT2A	-5.27	-2.79	2.48
NCBTA	-5.47	-3.13	2.34
NCBT2A	-5.32	-3.07	2.25
NCTBTA	-5.19	-3.12	2.07

[a] Δ_{H-L} values were calculated by B3LYP/6-31G(d), under vacuum

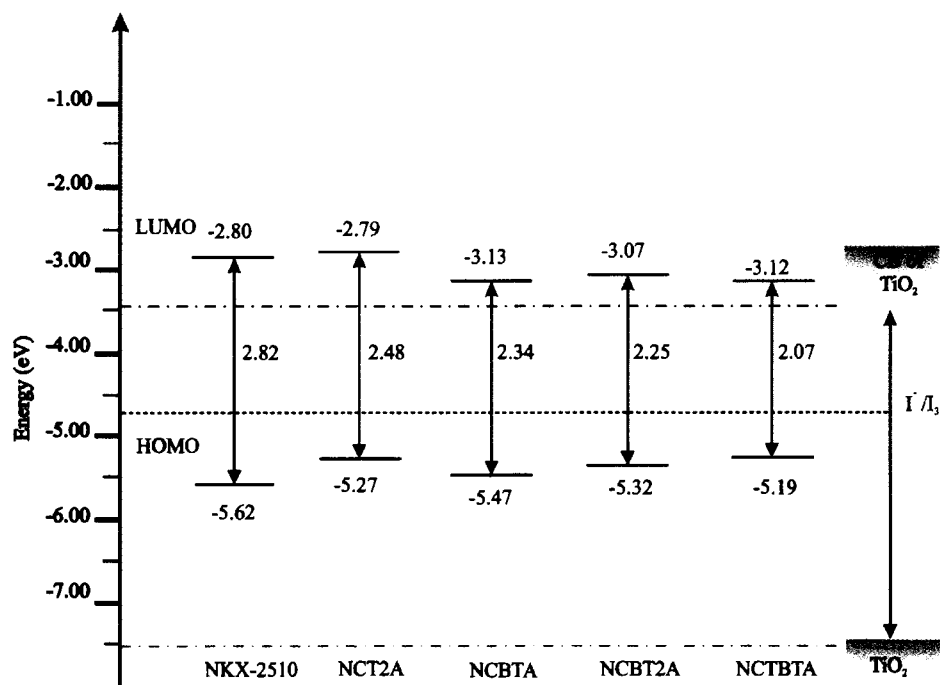


Figure 4.11 HOMO and LUMO of D- π -A and D-A- π -A calculated using B3LYP/6-31G(d,p)

These results suggest efficient electron regeneration of the oxidized dye by the electrolyte system. For the D- π -A system, the HOMO-LUMO gap (Δ_{H-L}) of **NKX-2510** and **NCT2A** dye were calculated as 2.82 and 2.48 eV, respectively. This indicates that replacing the thiophene moiety at the methine (-CH=CH-) position in **NKX-2510**, the HOMO level, close to that of I^-/I_3^- redox couple, improving the regeneration efficiency of the oxidized **NCT2A** dye. Positioning the BTB moiety between the coumarin donor and thiophene forms the conjugated **D-A- π -A** structure present in **NCBTA** and **NCBT2A**, while incorporating BTB between thiophene and the thiophene ring provides the D- π -A- π -A system seen for **NCTBTA**. These three dyes show the trend of decreasing HOMO-LUMO gap in the order of, **NCBTA** (2.34 eV) > **NCBT2A** (2.25 eV) > **NCTBTA** (2.07 eV). Moreover, the LUMOs of **NKX-2510** and **NCT2A**, which lack BTB, are significantly further from the TiO_2 conduction band than the LUMOs of dyes with BTB (**NCBTA**, **NCBT2A**, and **NCTBTA**), leading to a more favorable electron injection process from the excited dye molecule to the TiO_2 conduction band for the BTB-containing molecules [64]. **NCTBTA** with its narrow energy gap is predicted to be the most efficient sensitizer in

this study. As a consequence of the above, it is suggesting that the D- π -A- π -A dye have desired properties of dyes through reasonable molecular design which is the promising candidates of DSC.

3.2.2.3 Absorption spectra of organic sensitizers

Key factors that influence photocurrent are light-harvesting efficiency and absorption coverage. We performed TD-DFT calculations in the C-PCM model using dichloromethane solvent were performed with CAM-B3LYP functional to determine dye absorption properties [65-67]. Figure 4.10 shows UV-Vis absorption spectra for the dyes investigated in this study. In the TD-DFT calculations of absorption spectra, the 101 lowest singlet-singlet transitions were taken into account. Within the considered energy range, we calculated transitions of sizable intensity (a few highest oscillator strengths) [68] Calculated maximum absorption wavelengths (λ_{\max}), oscillator strengths (f), and composition in terms of molecular orbital contributions of coumarin dyes are listed in Table 4.6.

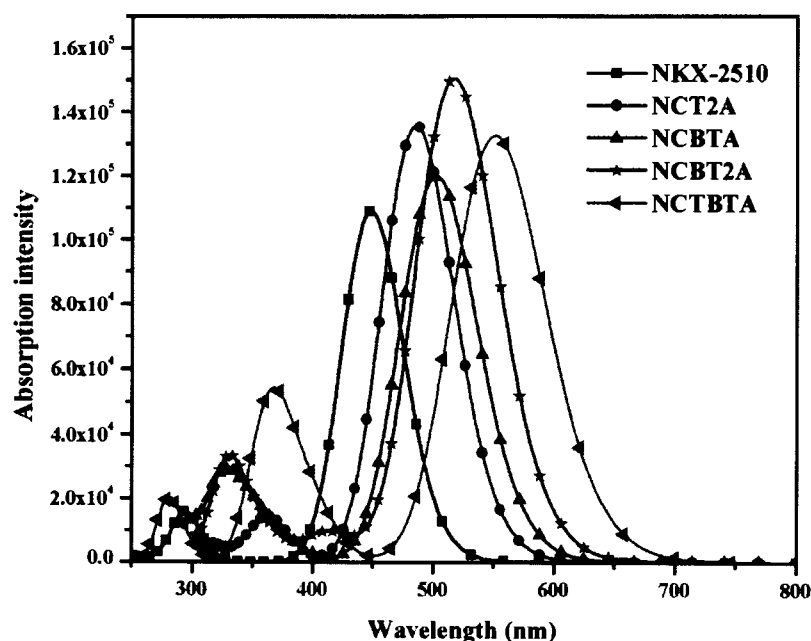


Figure 4.12 Calculated absorption spectra of D- π -A and D-A- π -A calculated using TDCAM-B3LYP/6-31G(d,p)

All of the coumarin dyes show two absorption regions, a short wavelength, high-energy region, and a long wavelength, low energy region. For the

absorption spectra of **D- π -A** molecules **NKX2510** and **NCT2A**, we assigned the calculated high energy absorption bands at 296 and 362 nm to π - π^* transitions, and the low energy absorption bands at 448 and 484 nm to intramolecular charge transfer (ICT) transitions, consistent with transition from the ground state to the first excited state. Substituting a thiophene moiety at the methane (-CH=CH-) position extends the π -conjugation length and increases (red shifts) the maximum absorption wavelength by approximately 36 nm. In the absorption spectra of D-A- π -A sensitizers **NCBTA** and **NCBT2A**, the maximum absorption bands appear at 502 and 516 nm respectively. The maximum absorption band for **NCTBTA**, with its D- π -A- π -A structure, appears at the much longer wavelength of 549 nm. All absorption spectra arise from the electronic transition from S_0 to S_1 , which represents promotion from the HOMO to the LUMO. Among these sensitizer dyes, the **NCTBTA** dye exhibits the longest maximum absorption wavelength as a result of the strongly electron withdrawing BTM moiety located between two thiophene linkers, and the coplanar structure of the molecule. These two factors extend the length of the π -conjugation system, and red shift the absorption spectrum to near IR wavelengths, a desirable property for an efficient light harvesting sensitizer.

Table 4.6 Excitation energy, oscillator strength, and molecular composition for various electronic coumarin dye transition states by TDCAM-B3LYP/6-31G(d,p) (C-PCM model)

Dyes	State	(λ_{\max}) eV, (nm)	f	Character	Assignment
NKX-2510	$S_0 \rightarrow S_1$	2.77 (448)	1.5044	ICT	(0.67) HOMO→LUMO, (-0.12) H-1→LUMO
	$S_0 \rightarrow S_3$	4.19 (296)	0.167	ICT, π - π^*	(-0.37) H-2→LUMO, (0.48) HOMO→L+1,
NCT2A	$S_0 \rightarrow S_1$	2.55 (484)	1.8721	ICT, π - π^*	(-0.23) H-1→LUMO, (0.62) HOMO→LUMO
	$S_0 \rightarrow S_2$	3.42 (362)	0.1973	ICT, π - π^*	(-0.39) H-1→LUMO, (0.55) HOMO→L+1,
NCBTA	$S_0 \rightarrow S_1$	2.47 (502)	1.6541	ICT, π - π^*	(-0.25) H-1→LUMO, (0.62) HOMO→LUMO
	$S_0 \rightarrow S_3$	3.58 (346)	0.2027	ICT, π - π^*	(0.33) H-1→LUMO, (-0.33) HOMO→L+2, (0.33) HOMO→L+1,
	$S_0 \rightarrow S_4$	3.84 (322)	0.3329	ICT, π - π^*	(0.24) H-1→LUMO, (0.56) HOMO→L+2
NCBT2A	$S_0 \rightarrow S_1$	2.40 (516)	2.073	ICT, π - π^*	(-0.25) H-1→LUMO, (0.59) HOMO→LUMO
	$S_0 \rightarrow S_3$	3.47 (356)	0.1426	ICT, π - π^*	(0.33) H-1→LUMO, (-0.32) H-1→L+1,
	$S_0 \rightarrow S_4$	3.77 (328)	0.434	ICT, π - π^*	(0.21) H-1→LUMO, (0.54) HOMO→L+2
NCTBTA	$S_0 \rightarrow S_1$	2.26 (551)	1.8280	ICT, π - π^*	(-0.27) H-1→LUMO, (0.62) HOMO→LUMO,
	$S_0 \rightarrow S_2$	3.13 (396)	0.2617	ICT, π - π^*	(0.48) H-1→LUMO, (0.46) HOMO→L+2,
	$S_0 \rightarrow S_3$	3.37 (367)	0.6292	ICT, π - π^*	(0.34) H-1→L+1, (-0.31) HOMO→L+1, (-0.46) HOMO→L+2,

4.2.2.4 The dye adsorption and electron injection

Electron injection from dye to the conduction band of a metal oxide semiconductor is important for DSC performance. The efficiency of the injection process depends on the electronic coupling between the dye and the metal-oxide surface. The adsorption of dyes on the $(\text{TiO}_2)_{38}$ clusters was performed with DFT calculations using DMol³ software. On the titanium-oxide surface, bidentate chemisorption of the dye arises from acidic dissociation of carboxylic acid anchoring groups. In this adsorption mode, a proton transfers from the carboxylic acid to the metal oxide surface, and bond formation occurs between carboxylate oxygen atoms and the surface titanium atoms.

Table 4.7 Selected bond lengths (Å) and adsorption energies (kcal/mol) of coumarin complexes calculated using Dmol³

Dyes	Ti-O ₁	Ti-O ₂	E _{ads} (kcal/mol)
NKX-2510	2.03	2.16	-16.01
NCT2A	2.05	2.14	-16.63
NCBTA	2.04	2.16	-16.75
NCBT2A	2.04	2.18	-16.81
NCTBTA	2.05	2.16	-16.87

Table 4.7 lists important optimized bond lengths and adsorption energies (E_{ads}) for the TiO_2 -coumarin dye complexes. The Ti-O bond distances were calculated to be 2.03-2.18 Å. The adsorption energies (E_{ads}) of all coumarin-based dyes were found to be in the range of 16.01–16.87 kcal/mol, suggesting strong coupling between D- π -A and D-A- π -A dyes and the TiO_2 surface. Additionally, we calculated excited state properties using TD-CAM-B3LYP with the 6-31G(d,p) basis set; we chose the **NKX-2510@TiO₂** and **NCTBTA@TiO₂** complexes to represent the D- π -A and D- π -A- π -A systems, respectively, and perform the electron injection process. Figure 4.10 shows calculated ICT peaks for the **NKX-2510@TiO₂** and **NCTBTA@TiO₂** dye complexes, which exhibit the greatest oscillator strengths. The absorption maxima are calculated to be 448 and 576 nm, respectively. Comparison of the two spectra reveals a very large bathochromic shift in the ICT peak. In addition,

a new absorption band appears at approximately 390 nm for the **NCTBTA@TiO₂** complex (D- π -A- π -A) that is not present for the **NKX-2510@TiO₂** complex (D- π -A). The emergence of a new absorption band will improve the light-harvesting properties of the D- π -A- π -A dye over those of D- π -A, which may provide greater efficiency for this organic sensitizer.

The strongest transition in the dyes is a linear combination of electronic configurations; the greatest oscillator strength for **NKX-2510@TiO₂** is a linear combination of 0.47(H \rightarrow L+9)-0.26(H \rightarrow L+11). The **NCTBTA@TiO₂** excitation arises from the 0.51(H \rightarrow L+3)-0.37(H \rightarrow L+4) linear combination. Applying the TDDFT functional, reveals that the transition with the greatest oscillator strength arises from orbitals on the donor-linker (D- π) to orbitals delocalized over the acceptor (A) and the (TiO₂)₃₈ cluster. The former orbitals are similar to the HOMOs of dye, and the latter orbitals correspond to interacting orbitals between LUMOs of the dyes and the conduction band of TiO₂. Thus, electron excitation in this system directly induces electron injection from the dye into the conduction band of TiO₂. Note that the latter orbitals are firstly embedded in the conduction band of TiO₂ and then the injected electron is transferred to the conduction bands of TiO₂. Interestingly, the **NKX-2510** and **NCTBTA** LUMOs are distinctly different. For **NKX-2510**, there is some electron distribution within the donor section of dye, while there is an absence of electron density in the donor component on **NCTBTA**, indicating that the injected electron completely transfers from the donor on **NCTBTA**, to the TiO₂ surface

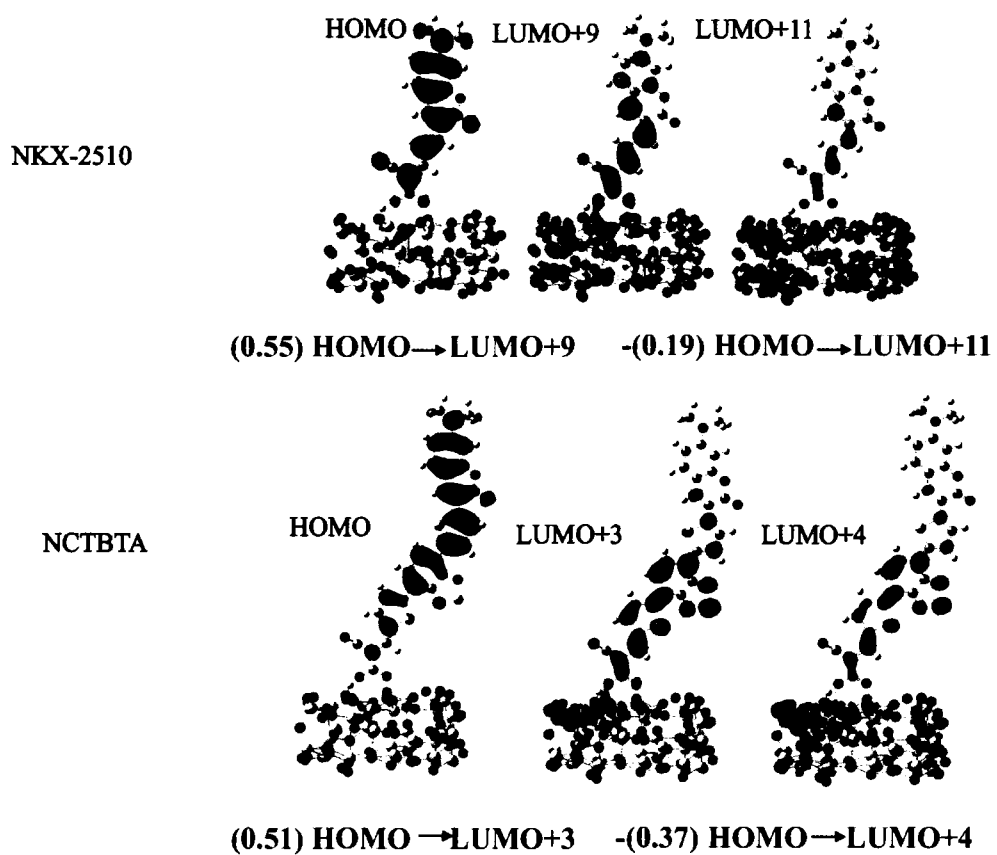


Figure 4.13 Frontier molecular orbitals for NKX-2510@TiO₂ and NCTBTA@TiO₂ in the gas phase, calculated by CAM-B3LYP/6-31G(d,p) using Dmol³

CHAPTER 5

CONCLUSION

The theoretical studies of the structure and energetic properties of sensitizer for dye-sensitized solar cells were successfully investigated by DFT, TDDFT calculation were carried out by mean of the theoretical calculation. A series of new organic materials based on triphenylamine and naphthalimide derivative were investigated. The structural, energy level, absorption and emission properties as well as the change of absorption and emission wavelengths had been calculated by using density functional theory (DFT) and time-dependent DFT (TD-DFT) method as implemented in Gaussian 09. According to the calculated results, the $S_1 \leftarrow S_0$ electronic transition involves primarily the promotion of an electron from the HOMO to the LUMO. Excitation energies are red-shifted, when adding the strong electron withdrawing group. The maximal absorption spectra are excellently agreement with experimental data. It has, therefore, been demonstrated that TDDFT provides an accurate performance and can be one of the useful and affordable methods for future studies involving conjugated organic materials in OLEDs. The results strongly showed that the molecules can be used as multifunctional properties as the hole-transporting and emitting materials for application in OLEDs device.

The conformations, electronic and optical properties of porphyrin and coumarin dyes have been investigated by DFT and TDDFT calculation. The effects of different donors, different linkers and different acceptors have been performed on the porphyrin and coumarin derivatives. The ground state structures were optimized at the B3LYP/6-31G (d,p) level of theory. The intramolecular charge transfer (ICT) properties were evaluated by single point energy calculation using TDDFT at the same basis set. This study investigated the effects of incorporating benzoethiadiazole (BTD) on the geometrical, photophysical, and electronic properties of organic dyes. The new D-A- π -A and D- π -A- π -A structures have lower energy LUMOs and smaller energy gaps than the pristine dyes, resulting in significantly red-shifted absorption spectra.

The substituted dyes may have application in improved light-harvesting ability. The delocalized ring systems present on BTB increase charge-transfer distances and provide a greater dipole moment, resulting in improvements to charge transfer properties over those of the unmodified dye.

REFERENCES

REFERENCES

- [1] Tang, CW, Van Slyke, SA. "Organic electroluminescent diodes", **Applied Physics Letters**. 51(12): 913-915; July, 1987.
- [2] Lee, CW. and et al. "Organic materials for organic electronic devices", **Journal of Industrial and Engineering Chemistry**. 20(4): 1198-1208; July, 2014.
- [3] Thejo kalyani, N, Dhoble, SJ. "Novel approaches for energy efficient solid state lighting by RGB organic light emitting diodes – A review", **Renewable and Sustainable Energy Reviews**. 32: 448-467; April, 2014.
- [4] Thejo Kalyani, N, Dhoble, SJ. "Organic light emitting diodes: Energy saving lighting technology-A review", **Renewable and Sustainable Energy Reviews**. 16(5): 2696-2723; June, 2012.
- [5] Nazeeruddin, MK. and et al. "Combined Experimental and DFT-TDDFT Computational Study of Photoelectrochemical Cell Ruthenium Sensitizers", **Journal of the American Chemical Society**. 127(48): 16835-16847; December, 2005.
- [6] Yella, A. and et al. "Molecular Engineering of Push-Pull Porphyrin Dyes for Highly Efficient Dye-Sensitized Solar Cells: The Role of Benzene Spacers", **Angewandte Chemie International Edition**. 53(11): 2973-2977; February, 2014.
- [7] Dreuw, A, Head-Gordon, M. "Single-Reference ab Initio Methods for the Calculation of Excited States of Large Molecules", **Chemical Reviews**. 105(11): 4009-4037; November, 2005.
- [8] Singh, G. and et al. "Carbazole end-capped and triphenylamine-centered starburst derivative for hole-transport in electroluminescent devices", **Optical Materials**. 46: 82-87; August, 2015.
- [9] Karthik, D. and et al. "Synthesis, characterization and electroluminescence of carbazole-benzimidazole hybrids with thiophene/phenyl linker", **Dyes and Pigments**. 133: 132-142; October, 2016.

REFERENCES (CONTINUED)

- [10] Wang, C. and et al. "Highly Efficient Nondoped Green Organic Light-Emitting Diodes with Combination of High Photoluminescence and High Exciton Utilization", **ACS Applied Materials & Interfaces**. 8(5): 3041-3049; February, 2016.
- [11] Khanasa, T. and et al. "Bis(carbazol-9-ylphenyl)aniline End-Capped Oligoarylenes as Solution-Processed Nondoped Emitters for Full-Emission Color Tuning Organic Light-Emitting Diodes", **The Journal of Organic Chemistry**. 78(13): 6702-6713; July, 2013.
- [12] Gudeika, D. and et al. "Structure Properties Relationship of Donor-Acceptor Derivatives of Triphenylamine and 1,8-Naphthalimide", **The Journal of Physical Chemistry C**. 116(28): 14811-14819; July, 2012.
- [13] Sun, F, Jin, R. "Optical and charge transport properties of N-butyl-1,8-naphthalimide derivatives as organic light-emitting materials: A theoretical study", **Journal of Luminescence**. 149: 125-132; May, 2014.
- [14] Jin, R, Ahmad, I. "Theoretical study on photophysical properties of multifunctional star-shaped molecules with 1,8-naphthalimide core for organic light-emitting diode and organic solar cell application", **Theoretical Chemistry Accounts**. 134(7): 89; July, 2015.
- [15] Luo, S. and et al. "Novel 1,8-naphthalimide derivatives for standard-red organic light-emitting device applications", **Journal of Materials Chemistry C**. 3(20): 5259-5267; April, 2015.
- [16] Chai, W, Jin, R. "Theoretical investigations into optical and charge transfer properties of donor-acceptor 1,8-naphthalimide derivatives as possible organic light-emitting materials", **Journal of Molecular Structure**. 1103: 177-182; May, 2016.
- [17] Hsieh, C-P. and et al. "Synthesis and characterization of porphyrin sensitizers with various electron-donating substituents for highly efficient dye-sensitized solar cells", **Journal of Materials Chemistry**. 20(6): 1127-1134; February, 2010.

REFERENCES (CONTINUED)

- [18] Chou, H-H. and et al. "Influence of Phenylethynylene of Push-Pull Zinc Porphyrins on the Photovoltaic Performance", **ACS Applied Materials & Interfaces**. 8(5): 3418-3427; February, 2016.
- [19] Arooj, Q. and et al. "Shifting UV-vis absorption spectrum through rational structural modifications of zinc porphyrin photoactive compounds", **RSC Advances**. 6(19): 15345-15353; January, 2016.
- [20] Qian, X. and et al. "Phenothiazine-functionalized push-pull Zn porphyrin photosensitizers for efficient dye-sensitized solar cells", **RSC Advances**. 6(11): 9057-9065; January, 2016.
- [21] Krishna, NV. and et al. "Donor- π -Acceptor Based Stable Porphyrin Sensitizers for Dye-Sensitized Solar Cells: Effect of π -Conjugated Spacers", **The Journal of Physical Chemistry C**. 121(12): 6464-6477; March, 2017.
- [22] Hara, K. and et al. "Molecular Design of Coumarin Dyes for Efficient Dye-Sensitized Solar Cells", **The Journal of Physical Chemistry B**. 107(2): 597-606; January, 2003.
- [23] Soto-Rojo, R. and et al. "Study of chemical reactivity in relation to experimental parameters of efficiency in coumarin derivatives for dye sensitized solar cells using DFT", **Physical Chemistry Chemical Physics**. 17(21): 14122-14129; April, 2015.
- [24] Song, X. and et al. "Influence of ethynyl position on benzothiadiazole based D-A- π -A dye-sensitized solar cells: spectral response and photovoltage performance", **Journal of Materials Chemistry C**. 4(39): 9203-9211; October, 2016.
- [25] Khanasa, T. and et al. "The design, synthesis, and characterization of D- π -A- π -A type organic dyes as sensitizers for dye-sensitized solar cells (DSSCs)", **Tetrahedron Letters**. 55(21): 3244-3248; May, 2014.
- [26] Yella, A. and et al. "Porphyrin-Sensitized Solar Cells with Cobalt (II/III) Based Redox Electrolyte Exceed 12 Percent Efficiency", **Science**. 334(6056): 629-634; November, 2011.

REFERENCES (CONTINUED)

- [27] Tang, Y. and et al. "Porphyrins Containing a Triphenylamine Donor and up to Eight Alkoxy Chains for Dye-Sensitized Solar Cells: A High Efficiency of 10.9%", **ACS Applied Materials & Interfaces**. 7(50): 27976-27985; December, 2015.
- [28] Karthikeyan, S, Lee, JY. "Zinc-Porphyrin Based Dyes for Dye-Sensitized Solar Cells", **The Journal of Physical Chemistry A**. 117(42): 10973-10979; October, 2013.
- [29] Lu, J. and et al. "Novel porphyrin-preparation, characterization, and applications in solar energy conversion", **Physical Chemistry Chemical Physics**. 18(9): 6885-6892; February, 2016.
- [30] Guo, M. and et al. "Electron-Deficient Pyrimidine Adopted in Porphyrin Sensitizers: A Theoretical Interpretation of π -Spacers Leading to Highly Efficient Photo-to-Electric Conversion Performances in Dye-Sensitized Solar Cells", **The Journal of Physical Chemistry C**. 116(16): 9166-9179; April, 2012.
- [31] Paredes-Gil, K. and et al. "Electronic structure and optical properties calculation of Zn-porphyrin with N-annulated perylene adsorbed on TiO₂ model for dye-sensitized solar cell applications: A DFT/TD-DFT study", **Computational Materials Science**. 126: 514-527; January, 2017.
- [32] Kang, G-J. and et al. "Theoretical study of zinc porphyrin-based dyes for dye-sensitized solar cells", **Journal of Photochemistry and Photobiology A: Chemistry**. 333: 200-207; January, 2017.
- [33] Keawin, T. and et al. "Anchoring number-performance relationship of zinc-porphyrin sensitizers for dye-sensitized solar cells: A combined experimental and theoretical study", **Dyes and Pigments**. 136: 697-706; January, 2017.
- [34] Ye, S. and et al. "Role of Adsorption Structures of Zn-Porphyrin on TiO₂ in Dye-Sensitized Solar Cells Studied by Sum Frequency Generation Vibrational Spectroscopy and Ultrafast Spectroscopy", **The Journal of Physical Chemistry C**. 117(12): 6066-6080; March, 2013.

REFERENCES (CONTINUED)

- [35] Rehm, JM. and et al. "Femtosecond Electron-Transfer Dynamics at a Sensitizing Dye-Semiconductor (TiO₂) Interface", **The Journal of Physical Chemistry**. 100(23): 9577-9578; January, 1996.
- [36] Hara, K. and et al. "A coumarin-derivative dye sensitized nanocrystalline TiO₂ solar cell having a high solar-energy conversion efficiency up to 5.6%", **Chemical Communications**. (6): 569-570; March, 2001.
- [37] Hara, K. and et al. "Molecular Design of Coumarin Dyes for Efficient Dye-Sensitized Solar Cells", **The Journal of Physical Chemistry B**. 107(2): 597-606; September, 2002.
- [38] Wang, Z-S. and et al. "Photophysical and (Photo)electrochemical Properties of a Coumarin Dye", **The Journal of Physical Chemistry B**. 109(9): 3907-3914; March, 2005.
- [39] Hara, K. and et al. "Design of new coumarin dyes having thiophene moieties for highly efficient organic-dye-sensitized solar cells", **New Journal of Chemistry**. 27(5): 783-785; April, 2003.
- [40] Yella, A. and et al. "Molecular Engineering of a Fluorene Donor for Dye-Sensitized Solar Cells", **Chemistry of Materials**. 25(13): 2733-2739; September, 2013.
- [41] Zhang, J. and et al. "Modification on C219 by coumarin donor toward efficient sensitizer for dye sensitized solar cells: A theoretical study", **Dyes and Pigments**. 99(1): 127-135; May, 2013.
- [42] Han, L. and et al. "Synthesis and density functional theory study of novel coumarin-type dyes for dye sensitized solar cells", **Journal of Photochemistry and Photobiology A: Chemistry**. 290(0): 54-62; June, 2014.
- [43] Hara, K. and et al. "Dye-sensitized nanocrystalline TiO₂ solar cells based on novel coumarin dyes", **Solar Energy Materials and Solar Cells**. 77(1): 89-103; February, 2003.
- [44] Hara, K. and et al. "Electron Transport in Coumarin-Dye-Sensitized Nanocrystalline TiO₂ Electrodes", **The Journal of Physical Chemistry B**. 109(50): 23776-23778; September, 2005.

REFERENCES (CONTINUED)

- [53] Jungsuttiwong, S. and et al. "Theoretical study on novel double donor-based dyes used in high efficient dye-sensitized solar cells: The application of TDDFT study to the electron injection process", **Organic Electronics**. 14(3): 711-722; March, 2013.
- [54] Wu, C-G. and et al. "Molecular engineering of cyclopentadithiophene-containing organic dyes for dye-sensitized solar cell: Experimental results vs theoretical calculation", **Dyes and Pigments**. 99(3): 1091-1100; December, 2013.
- [55] Chiu, KY. and et al. "DPP containing D- π -A organic dyes toward highly efficient dye-sensitized solar cells", **Dyes and Pigments**. 125: 27-35; February, 2016.
- [56] Delley, B, Ellis, DE. "Efficient and accurate expansion methods for molecules in local density models", **The Journal of Chemical Physics**. 76(4): 1949-1960; October, 1982.
- [57] De Angelis, F. and et al. "Time-Dependent Density Functional Theory Investigations on the Excited States of Ru(II)-Dye-Sensitized TiO₂ Nanoparticles: The Role of Sensitizer Protonation", **Journal of the American Chemical Society**. 129(46): 14156-14157; November, 2007.
- [58] Pastore, M. and et al. "Modeling Excited States and Alignment of Energy Levels in Dye-Sensitized Solar Cells: Successes, Failures, and Challenges", **The Journal of Physical Chemistry C**. 117(8): 3685-3700; September, 2013.
- [59] Jungsuttiwong, S. and et al. "The effect of conjugated spacer on novel carbazole derivatives for dye-sensitized solar cells: Density functional theory/time-dependent density functional theory study", **Journal of Computational Chemistry**. 33(17): 1517-1523; April, 2012.
- [60] Xia, H-Q. and et al. "Design of D-A- π -A organic dyes with different acceptor and auxiliary acceptor for highly efficient dye-sensitized solar cells: a computational study", **RSC Advances**. 4(92): 50338-50350; October, 2014.

CURRICULUM VITAE

NAME Miss Rattanawalee Rattanawan

DATE OF BIRTH 28th April 1988

BIRTH PLACE Si-Sa-Ket, Thailand

EDUCATION B.Sc. (Chemistry), Ubon Ratchathani University, Ubon Ratchathani, Thailand (2010)
M.Sc. (Chemistry), Ubon Ratchathani University, Ubon Ratchathani, Thailand (2012)

ADDRESS 112/3 Moo.5, Tambon Nongkrok, Amphor Mueng, Si-Sa-Ket, Thailand, 33000

SCHOLARSHIP Thailand Graduate Institute of Science and Technology (TGIST), National science and technology development agency Thailand (NSTDA)

